UNIVERSITÀ DEGLI STUDI DI BARI

DIPARTIMENTO INTERATENEO DI FISICA

"Michelangelo Merlin"

Corso di Laurea Magistrale in Fisica Teorica

Axion emissivity from photon conversions in the solar magnetic field

Laureanda: Ersilia Guarini

Relatore: Prof. Alessandro Mirizzi

ANNO ACCADEMICO 2019-2020

Contents

Introduction

The *axion* is an hypothetical particle postulated by Wilczek and Winberg in relation to the Peccei-Quinn (PQ) mechanism introduced to solve the so called *strong CP problem* of Quantum Chromodynamics. Moreover, typically Beyond Standard Model (BSM) theories, like four-dimensional ordinary and supersymmetric models and the string theory, present particles, called *axion-like particles* (ALPs), which are originated through a spontaneous simmetry breaking and have properties similiar to the ones of the QCD axion. ALPs can be either scalar or pseudoscalar and may interact with all the Standard Model particles. Neverthless, in general the main interest is in the ALP-photon interaction, since it is important for direct detection and for ALPs signatures in astrophysics. While the QCD axion mass is expected to be related to the fundamental scale of the theory and then to the photon coupling, for ALP there is no relation between the mass and the photon coupling. In particular, the mass spectrum of ALPs can range from ultra-light ($m_a \ll$ eV) to heavy ($m_a >$ keV). The ALP parameter space can be constrained through experimental, astrophysical and cosmological arguments, setting bounds on the value of the photon-ALP coupling in a wide mass range.
An important and well-studied astrophysical source of ALPs is represented by the Sun, where they are mainly produced through the Primakoff effect, consisting in the production of ALPs in a hot thermal plasma due to the fluctuating electric and magnetic fields. The solar ALP flux, produced by the Primakoff process, has been searched by the CAST experiment at CERN setting the best direct limit on ALP-photon coupling for $m_a < 10^{-2}$ eV. Moreover, in the Sun are also possible large magnetic fields that can catalyze an ALP production via a coeherent conversion of thermal photons. This contribution has been typically neglected in previous investigations and it is the subject of the current Thesis. In order to characterize this flux, we will solve

the kinetic equations of the photon-ALP system in large-scale solar B-fields. Moreover, we will explore bounds and perspectives of this new ALP flux at future helioscope experiments.
The Thesis is organized as follows:

- In Chapter 1 we introduce the QCD axion and axion-like particles which emerge in theories beyond the Standard Model of particle physics. We will present the current bounds on ALP parameter space.

- In Chapter 2 we discuss axion emission from the Sun through the Primakoff effect and their possible detection through helioscope experiments. In particular, we use the Standard Solar Model to characterize the expected flux at Earth from the Primakoff effect and we discuss the results obtained at the CAST experiment at CERN.

- In Chapter 3 we present the propagation of electromagnetic waves in a plasma and the phenomenon of axion-photon mixing. We first discuss the magnetohydrodynamics equations and then we consider the photon-ALP ensemble in a magnetized plasma, deriving the kinetic equations for such a system.

- In Chapter 4 we discuss the ALPs production in the Sun from photon conversions in the solar magnetic fields. We compute the expected ALP flux expected at Earth from processes of photon conversions. Finally, we set a bound on the ALP emissivity from the energy-loss argument in the Sun and we discuss possible perspectives of detection of ALPs.

Chapter 1

Axions and Axion Like Particles

In this Chapter we introduce axions and axion-like particles which emerge in theories beyond the Standard Model of particle physics. In Section 1.1 we discuss the Strong CP problem of QCD. In Section 1.2 we introduce a possible solution of this puzzle in terms of the Peccei-Quinn mechanism, from which axions emerge. In Section 1.3 axions and their different models are introduced. In Section 1.4 we introduce axion-like particles that emerge in some beyond the Standard Model theories. In Section 1.5 we present the current bounds on the axion-like particles parameter space and discuss the sensitivity of future experiments.

1.1 The Strong CP-Problem

The QCD is a $SU(3)_c$ gauge theory whose Lagrangian [Kak93]

$$\begin{aligned} \mathcal{L}_{\text{QCD}} &= \sum_a \bar{Q}_a (i\not{D} - m_a) Q_a - \frac{1}{2} \operatorname{tr} G^{\mu\nu} G_{\mu\nu} \ ; \\ (D_\mu)_{ij} &= \delta_{ij}\partial_\mu - ig(A_\mu)_{ij}, \ ; \\ A_\mu &= A_\mu^a \frac{\lambda^a}{2} \ ; \end{aligned} \tag{1.1}$$

where

$$Q_a = \begin{pmatrix} q_{a,1} \\ q_{a,2} \\ q_{a,3} \end{pmatrix} \tag{1.2}$$

is the Dirac spinor of the quark field, D_μ is the covariant derivative, $\not{D} = D_\mu \gamma^\mu$, A_μ is the gluon field, $G_{\mu\nu}$ is the colour field strength tensor and λ_a are the Gell-Mann matrices. The quark have two indices: a is the flavor index, while i and j are the colour indices.

If we take into account N flavors and we consider the limit of vanishing quark masses the QCD action has a global simmetry $U(N)_V \otimes U(N)_A$, where the label V stands for *vector* and the label A stands for *axial*. If only the up and down quarks are considered at low energy the limit of vanishing masses stands since $m_u, m_d \ll \Lambda_{\rm QCD}$, where $\Lambda_{\rm QCD} \simeq 218 \pm 24$ MeV is the QCD scale which determines the scale dependence of α_s, i.e. the coupling of strong interactions. Thus the QCD Lagrangian for these quarks has a global simmetry $SU(2)_V \otimes U(1)_V \otimes SU(2)_A \otimes U(1)_A$ in the flavor space. Experimentally, one finds that the vector simmetry $U(2)_V = SU(2)_I \otimes U(1)_B$ is a good simmetry of nature. Indeed, it physically corresponds to the conservation of isospin and baryon number and it is manifested by the existence of nucleon and pion multiplets in the spectrum of hadrons.

Conversely, axial simmetry spontaneously breaks because of quark-antiquark condensation, $\langle q\bar{q} \rangle \neq 0$, which is favored by the attractive force between these kind of pairs [Pec77a,Pec77b,Pec06]. Consequently from the Goldstone theorem one expects to find four Nambu-Goldstone bosons (NGB) associated with the dynamical breakdown of $U(2)_A = SU(2)_A \otimes U_1(A)$, one for each generator of the group. These NGB were supposed to be the three pions π^+, π^-, π^0 and the meson η. Pions are light enough, but η cannot be considered the fourth NGM of the $U(2)_A$ spontaneous simmetry breaking as its mass $m_\eta \gg m_\pi$. This result forces us to conclude that $U(1)_A$ is not a real simmetry of QCD, a problem that Weinberg dubbed the $U(1)_A$ problem. A solution of the latter was provided by 't Hooft assuming that the QCD vacuum has a more complicated structure which involves a phase parameter $\theta_{\rm QCD}$. Moreover, there is an anomalous axial current associated with $U(1)_A$. As a consequence of the anomaly, $U(1)_A$ is just an apparent QCD simmetry. The resolution of the problem consists in adding an extra term to the QCD Lagrangian

$$\mathcal{L}_{\theta_{\rm QCD}} = \theta_{\rm QCD} \frac{\alpha_s}{8\pi} \,{\rm tr}\, G^{\mu\nu} \tilde{G}_{\mu\nu} \; ; \tag{1.3}$$

where $\alpha_s = g^2/4\pi$ is the fine-structure constant of strong interactions, ${\rm tr}\, G^{\mu\nu}\tilde{G}_{\mu\nu} = G^{a\mu\nu}\tilde{G}_{a\mu\nu}$ and $\tilde{G^{\mu\nu}} = 1/2\epsilon^{\mu\nu\rho\sigma}G_{\rho\sigma}$ is the dual tensor of $G^{\mu\nu}$. Definitely the complex structure of the QCD vacuum acts as an extra self-interaction of

the gluon field. We easily observe that Eq. (1.3) has the structure of the scalar product of a polar with an axial vector, i.e. $\mathbf{E}_{\text{color}} \cdot \mathbf{B}_{\text{color}}$, which is CP-odd. Thus if we combine the action of charge conjugation (C) and a parity transormation (P) the Lagrangian Eq. (1.3) changes sign, that is the QCD Lagrangian Eq. (1.1) is not CP invariant. Moreover, we need to make real and diagonal the quark mass matrix M_q, which is actually complex because quarks are not massless. This consists in a global chiral phase transformation such that in the end the total CP-violating term is

$$\bar{\theta}_{\text{QCD}} = \theta_{\text{QCD}} + \arg\det M_q \, . \tag{1.4}$$

An experimental bound on the term in Eq. (1.4) comes from the constraint on the electric dipole moment [Abe20]

$$|d_n| < 2.9 \times 10^{-26} \; e \text{ cm} \; ; \tag{1.5}$$

since $|d_n| \approx 4.5 \times 10^{-15} \bar{\theta}$ [Kim08]. Then

$$|\bar{\theta}_{\text{QCD}}| < 0.7 \times 10^{-11} \, . \tag{1.6}$$

The Eq. (1.6) is satisfied either both θ_{QCD} and $\arg\det M_q$ are small or they cancel each other. Neverthless, these are unrelated quantities, thus the smallness of θ_{QCD} is known as the *strong CP-Problem* which can be elegantly explained by the Peccei-Quinn Mechanism that we will describe in the next Section.

1.2 The Peccei-Quinn Mechanism and the QCD axion

The most elegant and efficient explanation to the strong CP-problem is given by the Peccei-Quinn Mechanism which consists in postulating a new simmetry group, $U(1)_{\text{PQ}}$ [Pec77b, Pec77a, Wei78, Wil78]. This is a global simmetry and it is not experienced, thus it must be spontaneously broken at the fundamental scale of axion physics f_a, the so called Peccei-Quinn scale. From Goldstone theorem one expects a massless NGB corresponding to this spontaneous simmetry breaking, introduced with the name of *axion* field $a(x)$, which under a $U(1)_{PQ}$ tranformations with parameter α transforms as

$$a(x) \to a(x) + \alpha f_a. \tag{1.7}$$

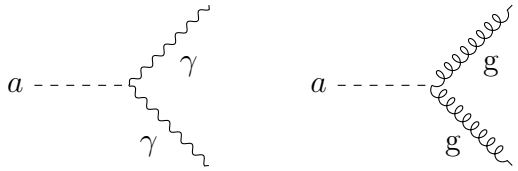

Figure 1.1: On the left, Feynman diagram of axion interaction with photons. On the right, Feynman diagram of axion interaction with gluons.

The Lagrangian of the Standard model $\mathcal{L}_{\rm SM}$ must be made $U(1)_{\rm PQ}$ invariant. To this end axions must be included in the total Lagrangian, which reads [Pec77b, Pec77a]

$$\begin{aligned}\mathcal{L}_{\rm tot} = \mathcal{L}_{\rm SM} - \bar{\theta}_{\rm QCD}\frac{g^2}{32\pi^2}\tilde{G}^a_{\mu\nu}G^{\mu\nu a} - \frac{1}{2}(\partial_\mu a)^2 + \mathcal{L}_{\rm int}[a,\Psi] + \\ \xi\frac{a}{f_a}\frac{g^2}{32\pi^2}\tilde{G}^a_{\mu\nu}G^{\mu\nu a} + \xi_\gamma\frac{a}{f_a}\frac{e^2}{16\pi^2}\tilde{F}_{\mu\nu}F^{\mu\nu}\end{aligned} \; ; \tag{1.8}$$

where again $G_{\mu\nu}$ is the gluon field strenght tensor, $F_{\mu\nu}$ is the photon field strenght tensor, $\mathcal{L}_{\rm int}[a,\Psi]$ describes the interaction of the axion field with a fermion field Ψ and the last two terms describes the coupling of axions with gluons, through the coupling costant ξ, and photons, through the coupling costant ξ_γ. These terms are represented by the Feynman diagrams shown in Fig. (1.1). We note that the interaction of axions with gluons plays the role of an effective potential for the axion field $V_{\rm eff}$ whose minimum occurs for $< a >= -\frac{f_a}{\xi}$

$$< \frac{\partial V_{\rm eff}}{\partial a} >\Big|_{<a>=-\frac{f_a}{\xi}} = -\frac{\xi}{f_a}\frac{g^2}{32\pi^2} < G^{a\mu\nu}\tilde{G}^a_{\mu\nu} >\Big|_{<a>=-\frac{f_a}{\xi}} = 0\ . \tag{1.9}$$

Therefore we can redefine the axion field as the physical field whose vacuum expectation value is zero

$$a_{\rm phys} = a - < a >\ . \tag{1.10}$$

The Lagrangian in Eq. (1.8) rewritten in terms of the field Eq. (1.10) is now CP-invariant, because the $\bar{\theta}_{\rm QCD}$-dependent term is cancelled out.
Therefore the axion field dinamically solves the strong CP-problem.

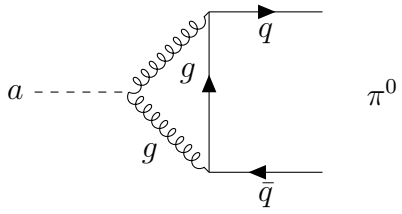

Figure 1.2: $a - \pi^0$ mixing.

1.3 Axions Models

The complete lagrangian for the axion field can be written as [Ira18]

$$\mathcal{L}_a = \frac{1}{2}\partial_\mu a \partial^\mu a - \xi \frac{\alpha_s}{8\pi}\frac{a}{f_a} G^{a\mu\nu}\tilde{G}^a_{\mu\nu} - \xi_\gamma \frac{\alpha_a}{8\pi}\frac{a}{f_a} F^{\mu\nu}\tilde{F}_{\mu\nu} + \mathcal{L}_{\rm int}[a,\Psi] \; ; \tag{1.11}$$

where we have used the notation introduced in Sec. 1.2 and

$$\mathcal{L}_{\rm int}[a,\Psi] = \frac{\partial_\mu a}{2f_a}\sum_\Psi C_{a\Psi}(\bar{\Psi}\gamma^\mu\gamma^5\Psi); \tag{1.12}$$

is the axion-fermion interaction. The axion interaction terms with photons and gluons can be written as

$$\begin{aligned} \mathcal{L}_{a\gamma} = -\xi_\gamma \frac{\alpha_a}{8\pi}\frac{a}{f_a} F^{\mu\nu}\tilde{F}_{\mu\nu} = -\frac{1}{4} g_{a\gamma} a F^{\mu\nu}\tilde{F}_{\mu\nu} = g_{a\gamma} a \mathbf{E}\cdot\mathbf{B} \; ; \\ \mathcal{L}_{ag} = -\xi_\gamma \frac{\alpha_a}{8\pi}\frac{a}{f_a} F^{\mu\nu}\tilde{F}_{\mu\nu} = -\frac{1}{4} g_{ag} a G^{a\mu\nu}\tilde{G}^a_{\mu\nu} \; . \end{aligned} \tag{1.13}$$

From Eq. (1.11) it is clear that axions are introduced as massless. Nevertheless, they interact with gluons thus they pick-up an effective mass which is approximately given by [Raf96]

$$m_a f_a \approx m_\pi f_\pi \; ; \tag{1.14}$$

as can be seen from the expansion of the axion-gluon interaction potential around its minimum. By virtue of the mass acquired by axions they can mix with π_0 as shown in Fig. 1.2. The properties of these interactions are model dependent, i.e. they depend on the implementation of the PQ mechanism. The most common axions models are summarized below.

1.3.1 Peccei-Quinn-Weinberg-Wilczek model (PQWW)

In the PQWW model [Pec77a, Pec77b, Wei78, Wil78] the axion degree of freedom emerges by introducing an extra doublet of Higgs, H_u, in addition to that of the Standard Model, H_d. The former gives mass to the u-type quarks and the latter to the d-type quarks and leptons. This model has interactions related to the electroweak scale, i.e. $f_a \approx 250$ GeV, and was excluded by a number of experimental constraints [Kim86]. For example, the $a - \pi^0$ oscillations allow the decay $K^+ \to \pi^+ a$, which is not observed and thus gives a bound on the axion-up g_{au} and axion down g_{ad} coupling constants

$$\begin{aligned} &\mathrm{BR}(K^+ \to \pi^+ a) < 3.8 \times 10^{-8} \ ; \\ &g_{au}^2,\, g_{ad}^2 < 4 \times 10^{-10} \ . \end{aligned} \tag{1.15}$$

Nevertheless, these experiments fail when f_a grows, making impossible the detection of axions through high energy physics.

1.3.2 Invisible axions models

The only working axions models seem to be those that provide light, weakly interacting and long-lived axions, named *invisible axions models*. In this context, two invisible axions models are analyzed.

Kim-Shifman-Vainsthein-Zakharow model (KSVZ)

In this model [Shi80] one introduces a new complex scalar field Φ which is a $SU(2) \otimes U(1)$ singlet, described by a potential $V(|\Phi|)$, and a new heavy quark doublet Q. The Lagrangian can be written [Raf96]

$$\mathcal{L} = (\frac{i}{2}\bar{\mathrm{Q}}\partial_\mu\gamma^\mu\mathrm{Q} + \mathrm{h.c}) + \partial_\mu\Phi^\dagger\partial^\mu\Phi - \mathrm{V}(|\Phi|) - \mathrm{G_Q}(\bar{\mathrm{Q}}_\mathrm{L}\Phi\mathrm{Q}_\mathrm{L} + \mathrm{h.c}) \ ; \tag{1.16}$$

where the first two are kinetic terms, the potential $V(|\Phi|)$ is chosen to be a *mexican hat* and the last is the Yukawa interaction term.This Lagrangian is invariant under the transformations

$$\begin{aligned} &\Phi \to e^{i\alpha}\Phi \ ; \\ &\mathrm{Q_L} \to \mathrm{e}^{\mathrm{i}\gamma^5\frac{\alpha}{2}}\mathrm{Q_L} \ ; \\ &\mathrm{Q_R} \to \mathrm{e}^{-\mathrm{i}\gamma^5\frac{\alpha}{2}}\mathrm{Q_R} \ ; \end{aligned} \tag{1.17}$$

The potential $V(|\Phi|)$ exhibits spontaneous simmetry breaking, after which

$$\Phi \to \frac{f_a + \rho}{\sqrt{2}} e^{i\frac{a}{f_a}} \; ; \tag{1.18}$$

where ρ and a are respectivetly the radial and the angular excitations, and the heavy quark gets a mass term

$$\mathcal{L}_{m_Q} = -G_{\mathrm{Q}} \frac{f_a}{\sqrt{2}} e^{i\frac{a}{f_a}} \bar{\mathrm{Q}}_L \mathrm{Q}_{\mathrm{R}} \; . \tag{1.19}$$

Thus the axion field a appears as a phase of the complex scalar field.
Since the quark mass $m_{\mathrm{Q}} \sim G_{\mathrm{Q}} f_a$ is very large, at low energy the only important interaction is with two gluons and two photons. In this model axions do not interact with leptons and quarks at tree level, while an interaction with hadrons at the loop level is made possible by the two gluon vertex. Therefore these axions are called *hadronic axions*.

Dine-Fischler-Srednicki-Zhitnitsky model (DFSZ)

The DFSZ model [Din81] introduces an electroweak scalar singlet Φ and two Higgs doublets, H_u and H_d. The main difference with the KSVZ model is that in this case at low energy a coupling between fermions and axions is allowed. See [Dil20] for more details on specific axion models.

1.4 Axion-Like Particles

Axion-like particles (ALPs) are very light pseudo-scalar bosons with a two-photon coupling $g_{a\gamma}$ which are predicted by several extensions of the Standard Model like four-dimensional ordinary and supersymmetric models [Cor07, Bae09], Kaluza-Klein theories [Tur96] and expecially superstring theories [Svr06, Cic12].
In the minimal models ALPs only couple with photons via the two photons vertex represented by the Lagrangian

$$\mathcal{L} = -\frac{1}{4} g_{a\gamma} a F^{\mu\nu} \tilde{F}_{\mu\nu} = g_{a\gamma} a \mathbf{E} \cdot \mathbf{B} \; . \tag{1.20}$$

However, differently from the QCD axion the mass and the coupling $g_{a\gamma}$ are two unrelated quantities. Therefore one can express experimental bounds on

the possible values of m_a and $g_{a\gamma}$ in the plane $(m_a, g_{a\gamma})$.
The existence of ALPs could have many interesting consequences [Dol17]. For instance, light ALPs with $m_a \sim O(\mu\text{eV})$ could constitute cold dark matter [Ari13]. ALPs with $O(\text{eV}) < \text{m}_\text{a} < \text{O(MeV)}$ have important cosmological and astrophysical implications, affecting the Big Bang Nucleosynthesis (BBN), the Cosmic Microwave Background (CMB) and the evolution of stars [Mil15]. Furthermore, ALPs with masses in the MeV to GeV range may have implications in particle physics. For instance, they could explain the muon magnetic moment [Baul17, Mar16] and play an important role in the electroweak simmetry breaking [Ell16]. For these reasons detecting ALPs is a challenging and well-motivated experimental effort.

1.5 ALP bounds

The ALPs parameter space $(m_a, g_{a\gamma})$ can be constrained by laboratory experiments, cosmological and astrophysical arguments. It is useful to distinguish between light ALPs, which have masses $m_a \leq O(\text{eV})$, and heavy ALPs, with masses $m_a > O(\text{eV})$, since they could be detected through different ways and their could have different physical implications.

1.5.1 Light ALPs

In Fig. 1.3 all relevant constraints for the light ALPs-photon coupling are shown. Laboratory constraints on light ALPs are mainly imposed by "light shining through walls" (LSW) experiments and experiments dealing with photon polarization. The formers exploit photon-ALP conversions in external electric and magnetic fields. Currently the best experimental limit, $g_{a\gamma} < 3.5 \times 10^{-8}$ GeV^{-1} at 95% CL for $m_a \leq 0.3$ eV, has been estabilished by the OSQAR (Optical Search for QED Vacuum Birifrangence, Axions and Photon Regeneration) experiment at CERN [Bal14]. The experiment ALPS-II (Any Light Particle) at DESY is also based on the same concept of OSQAR and has the aim to reach a bound of $g_{a\gamma} < 10^{-11}$ GeV^{-1} [Ehre20]. PVLAS (Polarization of the vacuum with laser) experiment exploits instead magnetically induced vacuum polarization and it is sensitive to ALPs in the mass range $m_a = 1 - 1.5$ meV and it provides additional bounds [Del15].
Low-mass weakly-interacting particles might be produced in hot stellar plas-

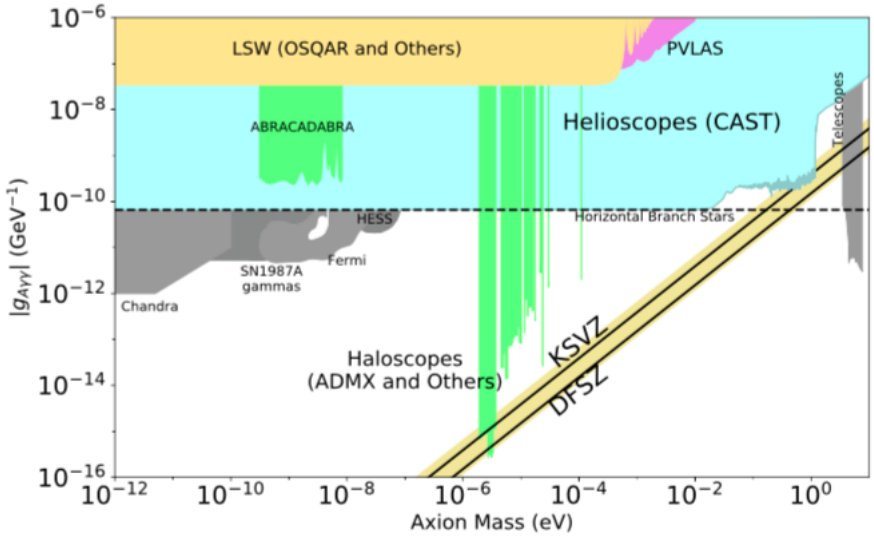

Figure 1.3: Parameter space for light ALPs. Single exclusion regions are explained in the text. (Figure taken from *Particle Data Group 2020, in press*).

mas and can transport energy out of stars. In particular, ALPs may be produced through Primakoff process in the Sun core and searched at helioscope experiments, that exploit reverse conversion of axions coming from the Sun in a magnet at Earth pointing towards the Sun. The most recent helioscope is CAST at CERN (CERN Axion Solar Telescope) and it has estabilished the best experimental limit of $g_{a\gamma}$ for $m_a < 0.02$ eV, namely [Pat16]

$$g_{a\gamma} < 6.6 \times 10^{-11}\ \text{GeV}^{-1} \quad (95\%\ \text{C.L.})\ ; \tag{1.21}$$

The next generation axion-helioscope currently under investigation is called IAXO (International Axion Observatory) and it could improve the CAST bound reaching a sensitivity down to $g_{a\gamma} \leq 10^{-12}$ GeV^{-1} [Ira11, Arm19].
Other constraints are provided by the argument that stellar lifetimes and their energy-loss rates must be not in conflict with experimental observations. For instance, globular-cluster (GC) stars, i.e. bound systems of stars with nearly the same age and different just for their mass, allow tests of stellar-evolution theory. Moreover, the reduction in lifetime arising from the accelerated consuption of helium in stars on the horizontal branch (HB) could give indication of energy-losses caused by axion-like particles emission. The bound set is $g_{a\gamma} < 6.6 \times 10^{-11}$ GeV^{-1} and $m_a \lesssim 1$ keV [Aya14], comparable

with the one placed by CAST.
Other bounds are set by the Supernova SN 1987A, which would have emitted a burst of ALPs due to Primakoff process in its core. These axions would have partially converted again into γ-rays in the galactic B-field. Therefore the lack of γ-rays provides an additional bound to the axion-photons coupling [Pay14]

$$g_{a\gamma} < 5.3 \times 10^{-12}\ \mathrm{GeV}^{-1}\ , \quad \text{for}\ \ \mathrm{m_a} \leq 4.4 \times 10^{-10}\mathrm{eV}\ . \tag{1.22}$$

The region of the parameter space $g_{a\gamma} \sim 10^{-12} - 10^{-11}$ GeV^{-1} for $m_a \leq 10^{-14}$ eV could be probed by the already mentioned experiments IAXO and ALPS-II.
This region of the parameter space can be also probed by searching for the gamma ray spectrum of distant active galactic nuclei (AGN). Axion-photon mixing in cosmic B-field would induce irregularities in the spectra because of photon-ALP mixing in a certain energy range. In this regard, the H.E.S.S. collaboration has set a bound $g_{a\gamma} \leq 2.1 \times 10^{-11}$ GeV^{-1}, for 1.5×10^{-8} eV $\leq \mathrm{m_a} \leq 6.0 \times 10^{-8}$ eV, from the non-irregular gamma ray spectrum of AGN PKS 2155-304 [Abra13]. The Fermi-LAT collaboration has put a more stringent bound on the ALP-photon coupling from the observations of the gamma ray spectrum of NGC 1275 [Aje16].
For masses $m_a \leq 10^{-12}$ eV galaxy clusters become very efficient at interconverting ALPs and photons at X-rays energies. In this case bounds are set on the ALP-photon coupling constant from the constraints on spectral irregularities in the spectra of luminous X-ray sources located in or behind the galaxy clusters. Observations of the AGN NGC 1275 provided by Chandra's observations lead to the stringent bound [Rey19]

$$g_{a\gamma} < 8 \times 10^{-14}\ \mathrm{GeV} \quad \text{for}\ \mathrm{m_a} \leq 10^{-12}\ \mathrm{eV}\ \ (99.7\%\ \mathrm{C.L.})\ . \tag{1.23}$$

Axions with mass $m_a \sim 1-100$ μeV would be in the *cold dark matter* (CDM) regime. Galactic halo axions in the CDM regime could be detected through microwave cavity experiments, which exploits their resonant conversion into a quasi-monochromatic microwave signal into a cavity permeated with a strong B-field. An example of microwave cavity experiment is ADMX [Asz03], that has excluded the green area on the right in Fig. 1.3. In the intermediate region neV $\leq \mathrm{m_a} \leq 0.1$ μeV one may search for the oscillating electric current

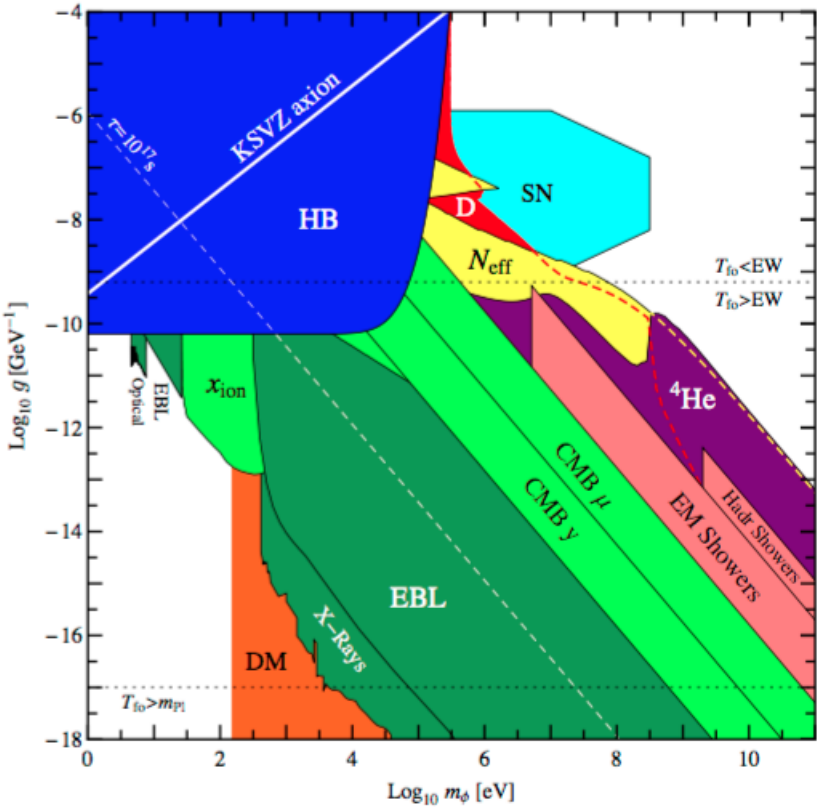

Figure 1.4: Parameter space for heavy axion-like particles. The blue region is excluded by energy-loss in Helium Burning (HB) stars in Globular Cluster systems, while the greenish zones are excluded exploiting cosmological arguments discussed in the text. Figure taken from [Cad11].

induced by DM axions in a strong magnetic field. For instance ABRACADABRA [Oue18] followed this approach and excluded the green region on the left in Fig. 1.3.

1.5.2 Heavy ALPs

Constraints on heavy ALPs can be set by astrophysical and cosmological arguments. These are shown in Fig. 1.4. In particular, in this Thesis work we are interested in ALPs with mass up to $m_a \sim 10^2$ eV, which can be constrained by the ionization of primordial hydrogen ($x_{\rm ion}$), the optical and the extragalactic background light (EBL) regions in Fig. 1.4. These regions

are excluded by exploiting cosmological arguments. ALPs with mass $m_a > 10$ eV decay through the channel $a \to \gamma\,\gamma$, with a lifetime less than the age of the Universe. Thus, the $x_{\rm ion}$ region is excluded by the constraint that the ionization of primordial hydrogen caused by the photons from decaying ALPs must not contribute significantly to the optical depth after recombination [Cad11]. The optical region is not allowed because if photons are produced in ALP decays inside galaxies, they would show up as a peak in galactic spectra that must not exceed the known backgrounds. Finally, photons produced from ALP decays when the Universe is transparent must not exceed the extragalactic background light (EBL).

Chapter 2

Axions from the Sun: Primakoff production

In this Chapter we discuss axions emission from the Sun through the Primakoff effect and their possible detection through helioscope experiments. In Section 2.1 we give an overview of the Standard Solar Model (SSM), used as reference to calculate the expected solar ALP flux. In Section 2.2 we discuss the Primakoff effect in the Sun and we calculate the ALP flux from such a process. In Section 2.3 we present the possible way of detecting axions from Primakoff process in the Sun at Earth and we discuss the direct detection of ALPs in helioscope experiments, presenting in particular the recent results of the CAST experiment at CERN.

2.1 Standard Solar Models

The *Standard Solar Model* (SSM) is an important reference in astrophysics, as it reproduces the thermodynamical profiles of the Sun and all the useful variables, i.e. temperature, electron density, chemical abundances and so on. The model has been developed in the eighties and its predictions have been compared with the different observations. The SSM is obtained by solving the stellar evolution equations in several time steps up to the solar age $t_\odot = 4.5 \times 10^9$ yr [Raf96, Tur16]. As a first solar evolution equation one uses the condition of hydrostatic equilibrium

$$\frac{\mathrm{d}p}{\mathrm{d}r} = -\frac{G_N M_r \rho}{r^2} \; ; \tag{2.1}$$

where p and ρ are the pressure and mass density at the radial position r, G_N is Newton's constant and M_r is the integrated mass up to the radius r. This equation expresses the balance between pressure and gravitational force of a spherical shell of the star, which prevents it from exploding or imploding. The second equation is given by the constraint of energy conservation

$$\frac{\mathrm{d}L(r)}{\mathrm{d}r} = 4\pi\epsilon\rho \; ; \tag{2.2}$$

where $L(r)$ is the net flux of energy through a shell of radius r and ϵ is the rate of energy production expressed in units of erg s^{-1}. These two first equations need an equation of state for the plasma $p(T, \rho, X_i)$ to be solved, where T is the temperature and X_i is the fraction of mass of each element in it. Finally, one needs the equation for the energy transfer from the center to the surface in the Sun. The transport of energy can be both radiative and convective, depending on which one is more favorable for the star. In the inner part of the Sun, i.e. the *radiative part*, the diffusion approximation is appropriate and the transfer of energy is controlled by the radial temperature gradient which is related to the energy flux through the equation

$$L(r) = -\frac{4\pi r^2}{3\kappa\rho}\frac{\mathrm{d}(aT)^4}{\mathrm{d}r} \; ; \tag{2.3}$$

where aT^4 is the energy stored in the radiation field, given by the Stephan law, and κ is the opacity in units of $\mathrm{cm}^2\ \mathrm{g}^{-1}$. The upper layers of the Sun are instead featured by a convective transport of energy. A schematic overview of the interior of the Sun is shown in Fig. 2.1. The inner part is the *core* and it is surrounded by the *radiative* zone, whose name is related to the radiative transport of energy in it. The intermediate region is a transition one and it is called *tachocline*. Finally, the outer layers constitute the so called *convective zone*. The equations Eqs. (2.1), (2.2), (2.3) must satisfy the constraint on the present-day luminosity of the Sun $L_\odot = 3.85 \times 10^{33}$ erg s^{-1} and on the present-day solar radius $R_\odot = 6.96 \times 10^{10}$ cm.

In order to compute a Standard Solar Model one needs, in addition to the luminosity, the age and the radius of the Sun, some input information [Raf96], such as the photon opacity, the equation of state, nuclear cross sections, diffusion coefficients, the abundances of metals. The gravitational settling of helium and metals is a standard physical effect which has been included only recently in the computation of the standard model. Because of this effect,

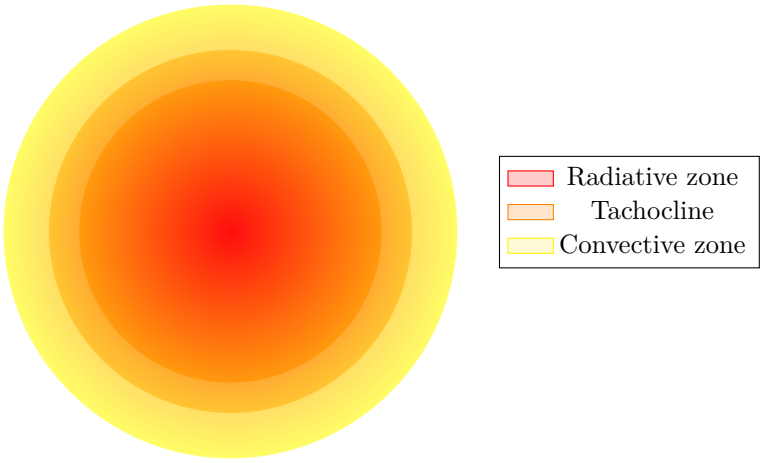

Figure 2.1: Schematic view of the solar interior. The red inner part is the *core*, surrounded by the *radiative zone*. The intermediate orange region is called *tachochline* and the outer yellow part is the *convective zone*.

the concentration of helium in the central region becomes higher that the one obtained considering nuclear burning alone and this leads to a slightly higher temperature. The settling of metal leads to a similiar effect and to an increase of the neutrino fluxes. These settlings were included for the first time by John Bachall and Pinsonneault [Bac92], who calculated the expected solar neutrino fluxes. The discrepancy between the observed neutrino fluxes and the predicted ones provides an evidence of *neutrino oscillation*. Actually, some nonstandard effects as strong magnetic fields, fast rotation in the deep interior and others are included in nonstandard solar models that we will discuss in the next chapter. Nevertheless, the discussion of such effects is not of interest in this context. The SSM is important to compute the expected solar neutrino and axion fluxes at Earth. In the present thesis we will be interested just in the axion flux.

2.2 Primakoff process in the Sun

2.2.1 Cross section and emission rate

The two-photon coupling of axions described by the Lagrangian

$$\mathcal{L} = -\frac{1}{4} g_{a\gamma} a F^{\mu\nu} \tilde{F}_{\mu\nu} = g_{a\gamma} a \mathbf{E} \cdot \mathbf{B} \; ; \tag{2.4}$$

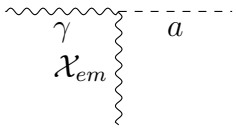

Figure 2.2: Primakoff conversion between axions and photon in an external electromagnetic field $\mathcal{X}_{em}$.

allows for the conversion $a \leftrightarrow \gamma$ in an external electric or magnetic field because of the amplitude shown in Fig. 2.2 [Raf96]. In stars, this process allows for the production of pseudoscalar particles in the electric fields of nuclei and electrons [Dic78]. Axions can be produced in a hot thermal plasma because of the fluctuating electric and magnetic fields, namely through the fluctuations of $\mathbf{E} \cdot \mathbf{B}$ caused both by the thermal electromagnetic radiation and the collective and random motion of charged particles. The dominant contribution to the emission rate is given by those fluctuations where the electric field $\mathbf{E}$ is generated by charged particles and the magnetic field $\mathbf{B}$ by the transverse electromagnetic radiations, i.e. by photons. Actually, also the so called "electro Primakoff effect" may be allowed, where the magnetic field is provided by moving particles in the plasma. Nevertheless, its contribution is extremely small compared to the one given by the classical Primakoff effect, as it can be shown by a direct computation [Raf86]. This can be intuitively explained because in the Sun electrons are non-relativistic, so that the magnetic field $\mathbf{B}$ associated with them is very weak.
Axions also interact with other particles, such as the electrons and nuclei, but since we are considering a minimal model in which ALPs only couple to photons we can focus on the Primakoff flux. Moreover, most of the experiments trying to detect axion fluxes exploit the axion-two photon vertex, thus we can neglect all the other axions couplings in the Sun [And07]. On the basis of the above considerations the Primakoff process is important when the non relativistic condition $T \ll m_e$ occurs, i.e. when both the electrons and nuclei in the plasma can be regarded as heavy relative to typical energies for the ambient photons. In this limit we can ignore recoil effects and recover the differential cross section for a target with charge Ze [Raf86, Raf96]

$$\frac{d\sigma_{\gamma\to a}}{d\Omega} = \frac{g_{a\gamma}^2 Z^2 \alpha}{8\pi} \frac{|\mathbf{k} \times \mathbf{k_a}|^2}{\mathbf{q^4}} \; ; \tag{2.5}$$

where $\mathbf{k}$ is the photon momentum, $\mathbf{k_a}$ is the axion momentum and $\mathbf{q} = \mathbf{k} - \mathbf{k_a}$ the momentum transfer. Due to the heaviness of the target the photon and axion energies are the same. Actually, one must include the screening effects that cut off the long-range Coulomb potential. In a nondegenerate medium the screening scale is given by the Debye-Hückel formula

$$k_s^2 = \frac{4\pi\alpha}{\mathrm{T}}(n_e + \sum_j Z_j^2 n_j) \; ; \tag{2.6}$$

where n_e is the electron number density, n_j is the number density of the j-th ion of charge Z_j, T is the temperature and α is the electromagnetic fine structure constant. With this prescription the differential cross section is modified

$$\frac{d\sigma_{\gamma\to a}}{d\Omega} = \frac{g_{a\gamma}^2 Z^2 \alpha}{8\pi} \frac{|\mathbf{k}\times\mathbf{k_a}|^2}{\mathbf{q^4}} \frac{\mathbf{q^2}}{\mathbf{q^2}+\mathbf{k_s^2}} \; . \tag{2.7}$$

Summing over all target species one can compute the transition rate of a photon of energy ω into an axion of the same energy

$$\Gamma_{\gamma\to a} = \frac{g_{a\gamma}\mathrm{T}k_s^2}{32\pi}\left[\left(1+\frac{k_s^2}{4\omega^2}\right)\ln\left(1+\frac{4\omega^2}{k_s^2}\right)-1\right] \; ; \tag{2.8}$$

where the axion mass and the plasma mass of the initial-state photon were neglected relative to the energy ω.

When propagation into a medium is considered, photons acquire an effective mass which coincides with the *plasma frequency* in the case of a plasma, i.e. in the Sun $m_\gamma = \omega_{\mathrm{pl}}$ which is defined as

$$\omega_{\mathrm{pl}}^2 = 4\pi\alpha\frac{n_e}{m_e} \; ; \tag{2.9}$$

where m_e is the electron mass and n_e is the electron number density. In this work we consider the Primakoff process for axions with negligible mass and photons with $\omega_{\mathrm{pl}} \sim 1 - 100$ eV and energies $\omega \sim$ keV. Thus we are allowed to use the expression Eq. (2.8) for the transition rate.

2.2.2 Solar axion spectrum

The expected ALP flux at Earth produced by Primakoff process in the Sun can be calculated as [And07]

$$\Phi_a = \frac{1}{4\pi \mathrm{D}_\odot^2}\int_0^{R_\odot} \mathrm{d}r 4\pi r^2 \int_{\omega_{\mathrm{pl}}}^\infty \mathrm{d}\omega \frac{4\pi k^2}{(2\pi)^3}\frac{\mathrm{d}k}{\mathrm{d}\omega} 2 f_\gamma \Gamma_{\gamma\to a} \; ; \tag{2.10}$$

where $f_\gamma = (e^{\omega/T} - 1)^{-1}$ is the Bose-Einstein distribution of the thermal photon bath, $D_\odot = 1.521 \times 10^{11}$ m is the solar distance from the Earth, $R_\odot = 6.96 \times 10^8$ m is the radius of the Sun and $\Gamma_{\gamma\to a}$ is the transition rate. However, this approximation fails at energies near and below a typical solar plasma frequency, i.e. at energies near and below ~ 0.3 keV, because we have neglected both recoil effects and collective motions, considering the charged particles as static. The differential flux of axions expected at Earth in units of $\mathrm{cm}^{-2}\ \mathrm{s}^{-1}\ \mathrm{keV}^{-1}$ is

$$\frac{d\Phi_a}{d\omega} = \frac{R_\odot^3}{4\pi \mathrm{D}_\odot^2} \int_0^1 \mathrm{d}r 4\pi r^2 \frac{4\pi\omega^2}{(2\pi)^3} 2 f_\gamma \Gamma_{\gamma\to a} \ ; \tag{2.11}$$

where we have used the dispersion relation of photons $\omega^2 = k^2 + \omega_{\mathrm{pl}}^2$ and the approximation $dk/d\omega = \omega/k \approx 1$, which is justified because the plasma frequencies are $\sim O(\mathrm{eV})$ while the energies $\omega \sim O(\mathrm{keV})$. Moreover we have introduced the dimensionless variable $r \to r/R_\odot$.
In general we do not need to treat the Sun as a point source, but we cas consider it as a two-dimensional disk featured by an apparent surface luminosity $\varphi(\omega, r)$, with $0 \le r \le 1$ [And07]. The total ALP number flux at the Earth is

$$\Phi_a = 2\pi \int_0^1 \mathrm{d}r \int_{\omega_{pl}}^\infty \mathrm{d}\omega \varphi(\omega, \mathrm{r}) \ ; \tag{2.12}$$

where $\varphi(\omega, r)$ is in units of $\mathrm{cm}^{-2}\ \mathrm{s}^{-1}\ \mathrm{keV}^{-1}$. Then we rewrite the integral over the solar volume as

$$\begin{gathered} 4\pi \int_0^1 \mathrm{d}r\ r^2 \longrightarrow 2\pi \int_0^1 \mathrm{d}r\ r \int_{\text{line of sight}} \mathrm{d}z \ ; \\ \int_{\text{line of sight}} \mathrm{d}z = 2 \int_r^1 \mathrm{d}\rho \frac{\rho}{\sqrt{\rho^2 - r^2}} \ ; \end{gathered} \tag{2.13}$$

where ρ is the dimensionless radial position in the Sun and we have assumed that the Sun is a two-dimensional disk, i.e. we are neglecting parallax effects. Finally we obtain

$$\varphi(\omega, r) = \frac{R_\odot^3}{2\pi^3 \mathrm{D}_\odot^3} \int_r^1 \mathrm{d}\rho \frac{\rho}{\sqrt{\rho^2 - r^2}} \omega k f_\gamma \Gamma_{\gamma\to a} \ ; \tag{2.14}$$

where all the quantities in the integral are functions of the dimensionless variable ρ and must be taken from a standard solar model.

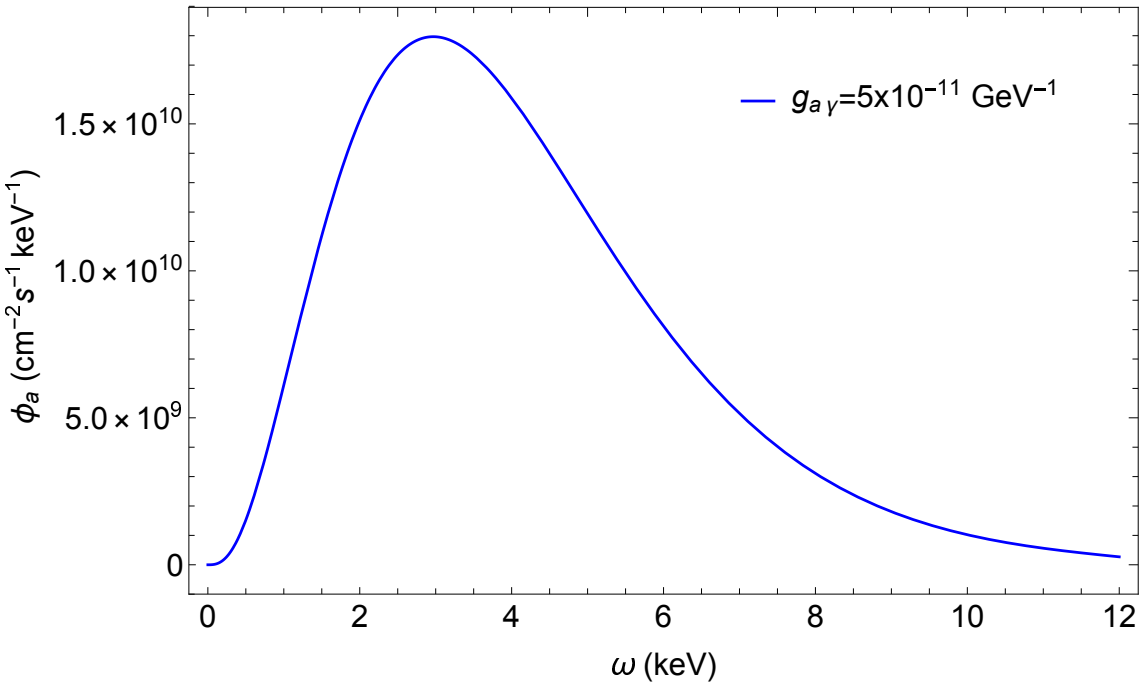

Figure 2.3: ALP flux expected at Earth in units of (cm^{-2} s^{-1} keV^{-1}). An axion-photon coupling $g_{a\gamma} = 5 \times 10^{-11}$ GeV^{-1} is assumed.

The differential ALP flux at Earth has been computed by the integration of Eq. 2.11 over the Standard Solar Model AGSS09 [Ser09, Aud03]. The expected ALP flux spectrum is shown in Fig. (2.3) where a coupling $g_{a\gamma} = 5 \times 10^{-11}\mathrm{GeV}^{-1}$ is assumed. In order to compute the total flux one has to integrate Eq. (2.11) over the axion energies. The ALP flux parameters are found to be

$$\Phi_a = 3.43 \times 10^{11}\ g_{10}^2\ \mathrm{cm}^{-2}\mathrm{s}^{-1}\ ; \tag{2.15}$$

$$L_a = 1.72 \times 10^{-3}\ g_{10}^2\ L_\odot\ ; \tag{2.16}$$

$$\langle\omega\rangle = 4.15\ \mathrm{keV}\ ; \tag{2.17}$$

$$\tag{2.18}$$

where $g_{10} = g_{a\gamma}/10^{-10}$ GeV^{-1}, $\langle\omega\rangle$ is the average energy and L_a the ALP luminosity expressed is terms of the Sun luminosity $L_\odot$. The peak of the distribution is found at $\omega = 3.00$ keV.
An analytic approximation to the solar ALP flux spectrum is provided by a

fit with the three-parameter function

$$\frac{\mathrm{d}\Phi_a}{\mathrm{d}\omega} = C\left(\frac{\omega}{\omega_0}\right)^{\alpha} e^{-(\alpha+1)\frac{\omega}{\omega_0}} \; ; \tag{2.19}$$

where C is a normalization constant and the fit parameter ω_0 is found to be equal to the average energy $\langle\omega\rangle$. If we match our numerical spectrum with this fit we find

$$\frac{\mathrm{d}\Phi_a}{\mathrm{d}\omega} = 5.74 \times 10^{10}\; g_{10}^2\; e^{-0.848\omega}\omega^{2.523} \; ; \tag{2.20}$$

where $g_{10} = g_{a\gamma}/10^{-10}$ GeV^{-1} and the energy is expressed in keV.

2.3 Detection of solar axions

2.3.1 Helioscope experiments

The most relevant technique to search for solar axions is the axion helioscope [Sik83, Van88]. Axion helioscopes exploit the conversion of solar ALPs into photons, in particular X-rays, in strong laboratory magnetic fields. Indeed, by virtue of the the two-photon vertex solar axions can be converted back into photons by passing through an electromagnetic field. If the background field is static, the energy of the photons produced in the laboratory magnet is equal to the one of the axions flux and a X-ray flux with energy of few keV is expected at the detector [Ira18]. The basic layout of an axion helioscope consists in a magnet with a strong field set in a cavity of length L. The magnet is put on a moving platform with two X-ray detectors, one at each end of the cavity, allowing it to track the Sun several hours per day. A schematic picture of an axion helioscope setup is shown in Fig. 2.4.
The idea of axion helioscope was proposed by P. Sikivie [Sik83], who pointed out that axions produced in conversions in the Sun and arriving at Earth can convert back to photons in a strong and inhomogeneous magnetic field in the laboratory. This idea was then refined by K. van Bibber, G. Raffelt *et al.* [Van88] who proposed an helioscope that involved the use of a buffer gas to restore the coherence between axion and photon over long distances traveled in the laboratory magnetic field. The *first generation* helioscope has been realised at Brookhaven National Laboratory (BNL) [Laz92], followed by the Tokyo Axion helioscope SUMICO [Ino08, Mor98, Zio05], that used a more powerful magnet than the BNL predecessor.

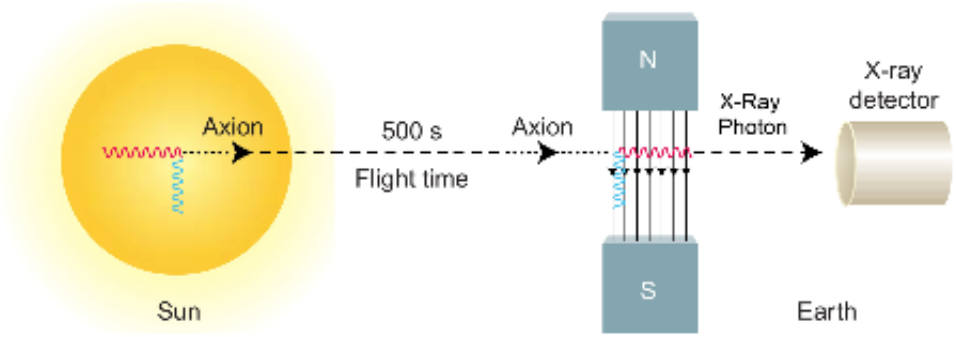

Figure 2.4: Conceptual design of an axion helioscope. Axions passing through the helioscope cavity filled with a transverse magnetic field (represented with the blue photon) are coverted to photons (X-rays). These photons are then detected at a X-ray detector at the end of the cavity and their spectrum is expected to be the one of axions produced in the Sun. Figure taken from [Bat18].

2.3.2 CAST experiment

The third generation helioscope is the CERN Axion Solar Telescope (CAST) at CERN. It is a solar axion search using a decommissioned LHC test magnet with a field up to $B = 9$ T and a length $L = 9.26$ m [Zio99]. The magnet tracks the Sun about 3 hours per day. A schematic layout of CAST is shown in Fig. 2.5. CAST collected data between 2003 and 2011 and its observational program was divided into three different phases. During the first phase (2003-2004) the helioscope operated with the magnet bores in vacuum to probe masses $m_a \lesssim 0.02$ eV. The probability of axion-photon conversion over a distance L traveled in a transverse magnetic field in vacuum is [Ana17]

$$P(a \to \gamma) = \left(\frac{g_{a\gamma}B}{q}\right)^2 \sin^2\left(\frac{qL}{2}\right) ; \tag{2.21}$$

where $q = k - k_a \sim m_a^2/2\omega$ is the photon-axion moment different in the relativistic limit. In order to detect photons a coherent axion-photon conversion is needed, i.e. the photon and the axion must stay coherent over a distance L, that is the condition $qL \lesssim 1$ must apply. This condition at CAST is satisfied for $m_a \lesssim 0.2$ eV, while for higher masses the sensitivity of the experiment decreases until it is completely lost. In the case of coherent conversion the

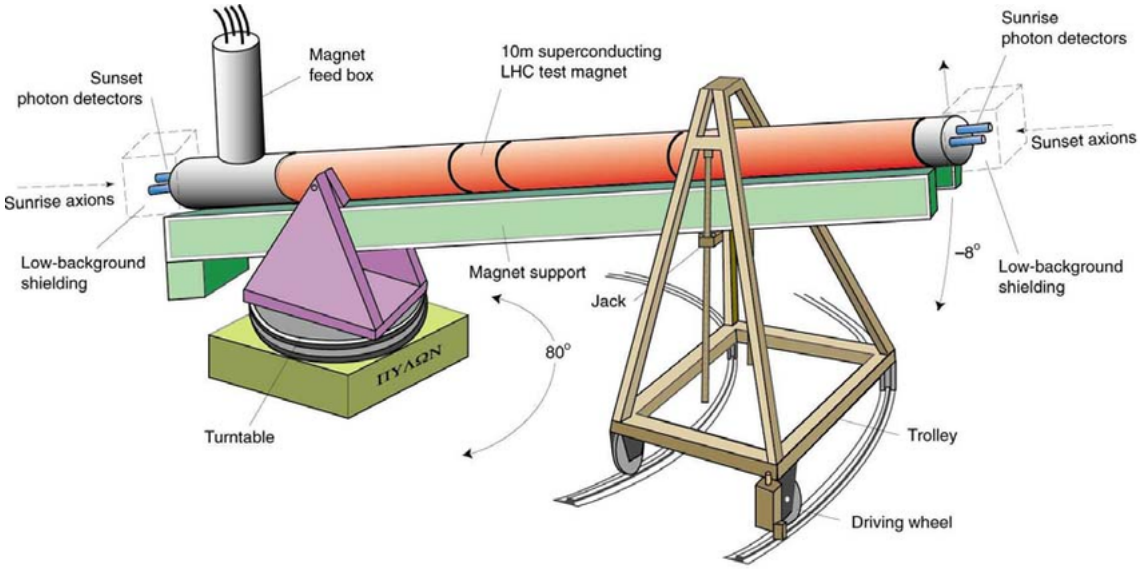

Figure 2.5: Schematic arrangement of CAST helioscope. Solar axions are converted into a beam of photons of cross sectional area $\mathcal{A}$ in the cavity filled with a magnetic field B. Subsequently, photons are detected at one of the two X-ray detectors set at each end of the cavity. Figure taken from [Bar04].

expected photon flux at the end of the magnet is

$$\frac{\mathrm{d}\Phi_\gamma}{\mathrm{d}\omega} = \frac{\mathrm{d}\Phi_a}{\mathrm{d}\omega} P(a \to \gamma) \; . \tag{2.22}$$

with $P(a \to \gamma)$ given by Eq. (2.21). If we use the expression of $\mathrm{d}\Phi_a/\mathrm{d}\omega$ found with our data in Eq. (2.20), from Eq. (2.22) we obtain the following expected photon flux

$$\frac{\mathrm{d}\Phi_\gamma}{\mathrm{d}\omega} = 0.086 \ \mathrm{cm}^{-2} \ \mathrm{day}^{-1} \ \mathrm{keV}^{-1} \ \mathrm{g}_{10}^4 \ \omega^{2.523} \mathrm{e}^{-0.848\omega} \left(\frac{\mathrm{L}}{9.26 \ \mathrm{m}} \right)^2 \left(\frac{\mathrm{B}}{9.0 \ \mathrm{T}} \right)^2 ; \tag{2.23}$$

where $g_{10} = g_{a\gamma}/10^{-10} \ \mathrm{GeV}^{-1}$. Since the axion-photon conversion probability depends on $g_{a\gamma}^2$, the detection rate would scale as $g_{a\gamma}^4$. The expected photon flux at the detector is shown in Fig. 2.6. In vacuum phase CAST provided the first bound for $m_a \lesssim 0.02$ eV [Zio04, And07]

$$g_{a\gamma} < 8.8 \times 10^{-11} \ \mathrm{GeV}^{-1}, \ (95\% \ \mathrm{C.L.}) \; . \tag{2.24}$$

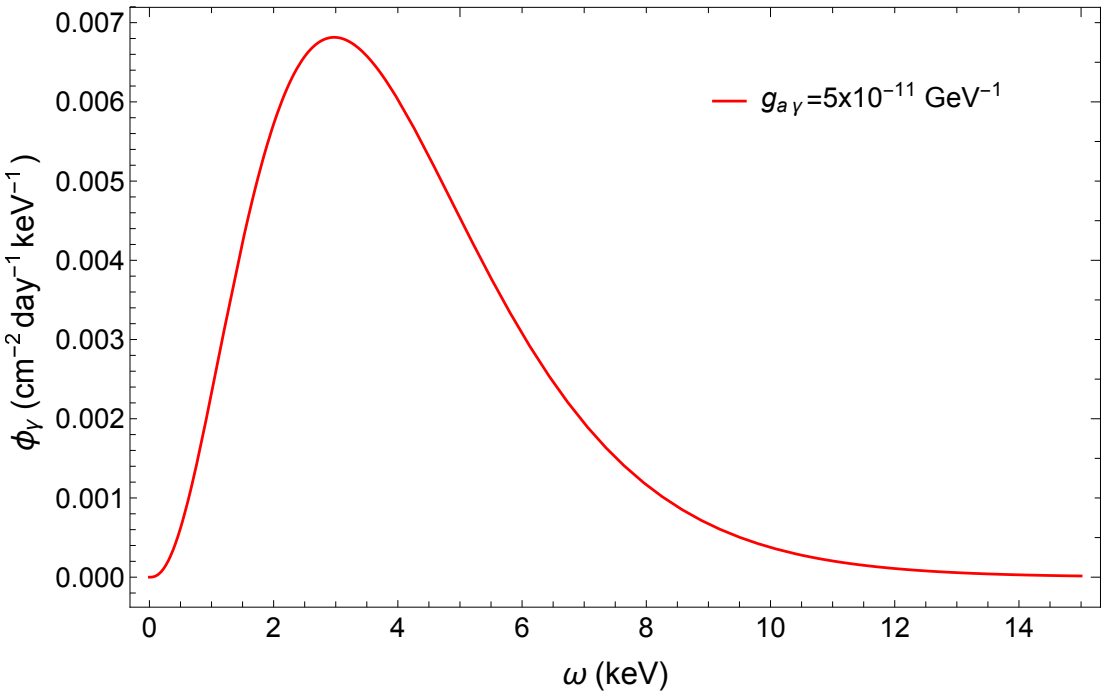

Figure 2.6: Expected photon flux at the detector on Earth in units of (cm^{-2} day^{-1} keV^{-1}). The flux show a peak at $\omega = 3$ keV. A coupling $g_{a\gamma} = 5 \times 10^{-11}$ GeV^{-1} is assumed.

CAST has recently (2017) revisited the vacuum phase improving the X-ray optics, reaching the bound for $m_a < 0.02$ eV [Ana17]

$$g_{a\gamma} < 0.66 \times 10^{-10} \text{ GeV}^{-1} \, . \tag{2.25}$$

It is worth stressing that this final limit is consistent with the assumption that the solar axion losses are a negligible perturbation of the standard solar models. Indeed, the luminosity in Eq. (2.25) implies that the solar axion flux is bounded $L_a \lesssim 1.3 \times 10^{-3} \; L_\odot$ [And07]. Helioseismological measurments of the sound-speed profile obtained in the context of standard solar models which include axion losses allow values of $g_{a\gamma} < 1 \times 10^{-9}$ GeV^{-1}, i.e. allow for $L_a \lesssim 0.2 L_\odot$ [Sch98]. Therefore the axion flux corresponding to the CAST limit does not lie in the range where it would affect helioseismology [Bac04]. A mismatch between the axion and photon momenta occurs if the coherence condition $qL \lesssim 1$ fails. In this case one has to fill the pipes with a low-Z gas whose pressure is adjusted in such a way that $m_a^2 = \omega_{\rm pl}^2$ to restore the coherence. For a general axion-photon momentum difference q and in presence of

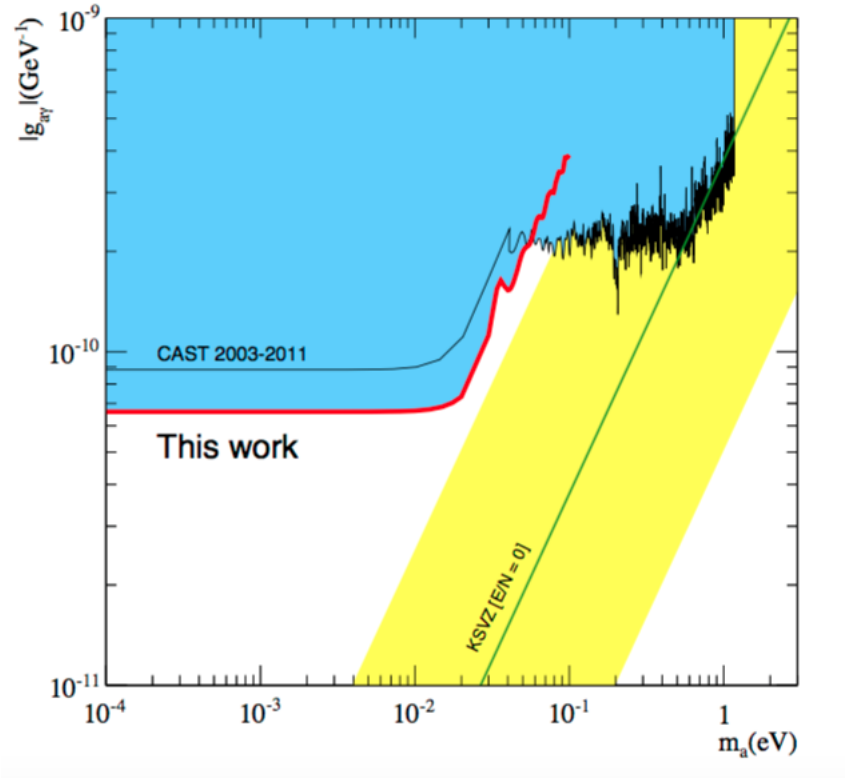

Figure 2.7: Exclusion region in the $(m_a, g_{a\gamma})$ plane achieved by CAST in the vacuum, ^{4}He and ^{3}He phase. "This work" refers to the bound set by the 2017 study [Ana17].Other exclusion regions explained in Sec. 1.5 are also shown. Figure taken from [Ana17].

a gas filling the cavity the axion-photon conversion probability is [Van88]

$$P(a \to \gamma) = \frac{(g_{a\gamma}B/2)^2}{q^2 + \frac{\Gamma^2}{4}}[1 + e^{-\Gamma L} - 2e^{-\Gamma L/2}\cos(qL)] \; ; \tag{2.26}$$

where Γ is the damping coefficient provided by the gas. After the vacuum phase the cavity was first filled with ^{4}He (2005-2006) and then with ^{3}He gas (2008-2011) to obtain a sensitivity up to $m_a = 1.17$ eV. Data from these phases provided the bounds [Ari08, Ari11, Au14]

$$\begin{aligned} g_{a\gamma} &\lesssim 2.3 \times 10^{-10}\ \text{GeV}^{-1}\ (95\%\ \text{C.L.})\ \text{for}\ 0.02\ \text{eV} \lesssim \text{m}_\text{a} \lesssim 0.64\ \text{eV}\ ; \\ g_{a\gamma} &\lesssim 3.3 \times 10^{-10}\ \text{GeV}^{-1}\ (95\%\ \text{C.L.})\ \text{for}\ 0.64\ \text{eV} \lesssim \text{m}_\text{a} \lesssim 1.17\ \text{eV}\ ; \end{aligned} \tag{2.27}$$

with the mass value m_a dependent on the pressure of the gas. The regions of parameter space excluded by CAST are shown in Fig. 2.7. CAST has

been the first axion helioscope to reach a sensitivity to $g_{a\gamma}$ values below 10^{-10} GeV^{-1}. In the region of axion masses $m_a \gtrsim 0.1$ eV the experiment has entered the region of QCD axion models and has excluded KSVZ axions for masses $m_a \sim 1$ eV.

2.3.3 Next generation helioscope

The International Axion Observatory (IAXO) is the next generation helioscope, currently at the design state, and it aims at improving the CAST signal-to-noise by more than a factor 10^4, that is to more than an order of magnitude in $g_{a\gamma}$ [Arm19]. IAXO will use a X-ray focusing optics and will have as a central component a superconducting magnet with a multibore configuration, to produce an intense magnetic field over a large volume. IAXO is expected to probe a large fraction of unexplored ALP parameter, as the one of QCD axion models in the mass range $m_a \sim 1$ meV $-$ 1 eV. As a first step towards IAXO, the collaboration aims at building its precursor, Baby-IAXO, which would allow to obtain results at an intermediate level between CAST current best limit and the future IAXO. The conceptual arrangement of IAXO is shown in Fig. 2.8.
Another axion helioscope at the design state is AMELIE, i.e. An Axion Modulation hELIoscope Experiment, which is expected to be sensitive to the higher axion masses provided by axion models [Gal15]. AMELIE would use a low background large volume Time Projection Chamber (TPC) immersed in an intense magnetic field. Therefore, contrary to the usual helioscopes it may directly detect the photons converted into the buffer gas. Its strong point is the flexibility of the TPC, which can be used with different gases and pressures, making AMELIE sensitive to axion masses from few meV to several eV. For a 5 T, m^3 scale TPC AMELIE may reach sensitivities $g_{a\gamma} \sim 2 \times 10^{-10}$ GeV^{-1} in the mass range 0.01 eV $\lesssim m_a \lesssim 0.1$ eV.

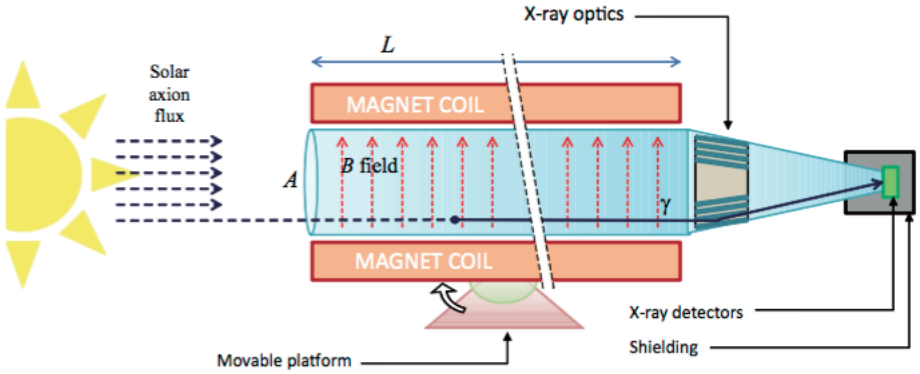

Figure 2.8: Conceptual arrangement of an enhanced axion helioscope with X-ray focalization. Axions are converted into photons by the transverse magnetic field in the bore and then focalized onto a small spot thorugh X-ray optics. Figure taken from [Arm19].

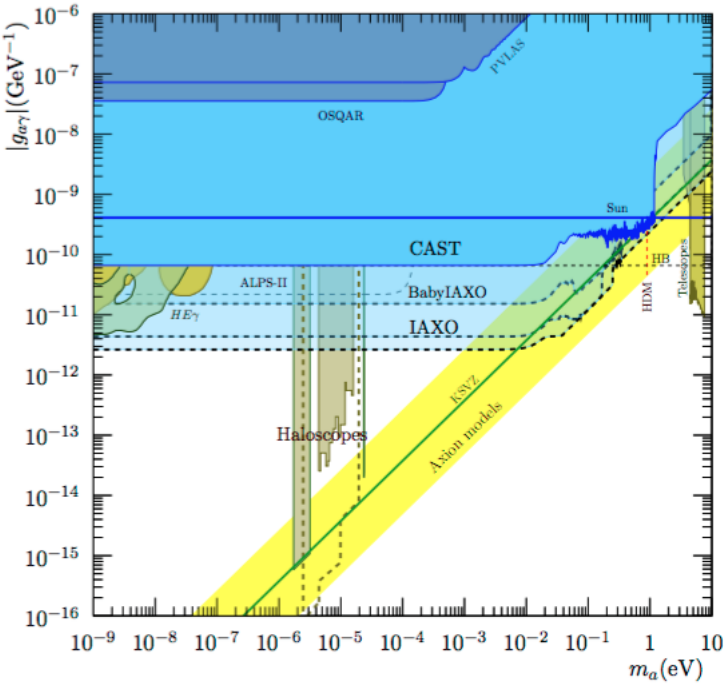

Figure 2.9: Sensitivity prospects of BabyIAXO and IAXO (semitransparent region) in the context of previous experiments and bounds. Figure taken from [Arm19].

Chapter 3

Electromagnetic waves in plasma and axion-photon mixing

In this Chapter we discuss the propagation of electromagnetic waves in a plasma and the phenomenon of axion-photon mixing. In Section 3.1 we obtain Maxwell's equations in a plasma and photon dispersion relations both for transverse and longitudinal photon modes. In Section 3.2 we present mixing equations of ALPs and photons in a plasma and we derive the photon-ALP conversion probability.

3.1 Photon dispersion in Plasma

The Sun interior is a hot plasma which mostly consists of electrons, protons and alpha particles at temperature that can reach $T \sim$ few keV. Moreover, large scale magnetic fields might exist in the Sun, as we will discuss in Chapter 4. Therefore, in order to characterize this plasma we have to deal with a combined system of electromagnetic fields and a conducting fluid. In the solar plasma only electrons partecipate to the motion and the ions provide just a uniform background of charge. We closely follow the treatment given in the classical textbook of Jackson [Jac75].

3.1.1 Maxwell's equations in a plasma

We start considering the behaviour of an electrically neutral, conducting fluid immersed in electromagnetic fields and we assume that the fluid is nonpermeable [Jac75]. Moreover, we describe it through a matter density $\rho(\mathbf{x}, t)$, a velocity $\mathbf{v}(\mathbf{x}, t)$, a pressure $p(\mathbf{x}, t)$ and a real conductivity σ. The two hydrodynamics equations are

$$\frac{\partial \rho}{\partial t} + \boldsymbol{\nabla} \cdot (\rho \mathbf{v}) = \mathbf{0} \; ; \tag{3.1}$$

$$\rho \frac{\mathrm{d}\mathbf{v}}{\mathrm{d}t} = -\nabla p + (\mathbf{J} \times \mathbf{B}) \; ; \tag{3.2}$$

where the first represents the continuity equation and the second the force equation, respectively. Moreover, ∇p is a pressure term, $\mathbf{J} \times \mathbf{B}$ is the magnetic-force term and $\mathbf{J}$ is the current. In Eq. (3.2) we are neglecting the viscous term $\mathbf{F}_v = \eta \nabla^2 \mathbf{v}$ and the gravitational force $\rho \mathbf{g}$. In general, we have radiation plus an external magnetic field thus the total magnetic field is

$$\mathbf{B} = \mathbf{B}_{\mathrm{rad}} + \mathbf{B}_{\mathrm{ext}} \; ; \tag{3.3}$$

where $\mathbf{B}_{\mathrm{rad}}$ is the field provided by the photon radiation itself and $\mathbf{B}_{\mathrm{ext}}$ is a possible external field. The derivative in Eq. (3.2) is the so called *convective derivative*

$$\frac{d}{dt} = \frac{\partial}{\partial t} + \mathbf{v} \cdot \nabla \; . \tag{3.4}$$

For the electromagnetic field we start from the usual Maxwell Lagrangian, assuming that this is not coupled to any other field

$$\mathcal{L}_{\mathrm{em}} = -\frac{1}{4} F_{\mu\nu} F^{\mu\nu} - A_\mu J^\mu_{\mathrm{ext}} \; ; \tag{3.5}$$

where A^μ is the potential vector and J^μ_{ext} is the source term. From Eq. (3.5) we obtain the classical Maxwell equations in the explicitly covariant form as

$$\partial_\mu F^{\mu\nu} = J^\nu \; ; \tag{3.6}$$

$$\partial_\gamma F_{\alpha\beta} + \partial_\alpha F_{\beta\gamma} + \partial_\beta F_{\gamma\alpha} = 0 \; . \tag{3.7}$$

The Equations (3.6)–(3.7) can be written in a not explicitly covariant form

$$\nabla \times \mathbf{E} + \frac{\partial \mathbf{B}}{\partial t} = 0 \; ; \tag{3.8}$$

$$\boldsymbol{\nabla} \cdot \mathbf{E} = \rho_{\mathbf{e}} \; ; \tag{3.9}$$

$$\boldsymbol{\nabla} \cdot \mathbf{B} = 0 \; ; \tag{3.10}$$

$$\nabla \times \mathbf{B} = \mathbf{J} \; ; \tag{3.11}$$

where $\mathbf{J}$ is the current density, ρ_e is the electrical charge density and in the last equation, i.e. in Ampère's law, we have neglected the displacement current. We can just consider Eqs. (3.8) and (3.11) since the others give negligible corrections and set the initial conditions. Finally, we need to take into account Ohm's law to make the current density $\mathbf{J}$ explicit. In a simple conducting medium this law is

$$\mathbf{J}_{\rm re} = \sigma \mathbf{E}_{\rm re} \; ; \tag{3.12}$$

where $\mathbf{J}_{\rm re}$ and $\mathbf{E}_{\rm re}$ are the current density and the electric field measured in the rest frame of the medium. If this is moving in the laboratory with a velocity $\mathbf{v}$ the current density in the laboratory frame becomes

$$\mathbf{J} = \mathbf{J}_{\rm re} + \rho_e \mathbf{v} \; . \tag{3.13}$$

For a one-component conducting fluid $\rho_e = 0$ and Ohm's law reads

$$\mathbf{J} = \sigma(\mathbf{E} + \mathbf{v} \times \mathbf{B}) \; . \tag{3.14}$$

Eqs. (3.1), (3.2), (3.8), (3.11), (3.14) are the equations of magnetohydrodynamics.

3.1.2 High-frequency plasma oscillations

We now assume that the electrons are described by the density $n_e(\mathbf{x}, t)$ and they have an average velocity $\mathbf{v}(\mathbf{x}, t)$. In the high-frequency limit the equations for the electron fluid are

$$\frac{\partial n_e}{\partial t} + \boldsymbol{\nabla} \cdot (n_e \mathbf{v}) = 0 \; ; \tag{3.15}$$

$$\frac{\partial \mathbf{v}}{\partial t} + (\mathbf{v} \cdot \nabla)\mathbf{v} = \frac{e}{m}\Big(\mathbf{E} + \mathbf{v} \times \mathbf{B}\Big) - \frac{1}{m n_e}\nabla p \tag{3.16}$$

$$\rho_e = e(n_e - n_e^0) \; ; \tag{3.17}$$

$$\mathbf{J} = e n \mathbf{v} \; ; \tag{3.18}$$

where ∇p describes the effects of the thermal kinetic energy of the electrons, ρ_e is the electron charge density, $\mathbf{J}$ is the electron current and $-en_e^0$ is the equilibrium charge density of electrons. With this prescription Maxwell's equations can be written as

$$\boldsymbol{\nabla} \cdot \mathbf{E} = e(n_e - n_e^0) \; ; \tag{3.19}$$

$$\boldsymbol{\nabla} \cdot \mathbf{B} = 0 \; ; \tag{3.20}$$

$$\nabla \times \mathbf{E} + \frac{\partial \mathbf{B}}{\partial t} = 0 \; ; \tag{3.21}$$

$$\nabla \times \mathbf{B} - \frac{\partial \mathbf{E}}{\partial t} = e n_e \mathbf{v} \; . \tag{3.22}$$

We now use a perturbative approach to linearize the equation of motions, considering small deviations from the equilibrium values

$$n_e = n_e^0 + \delta n(\mathbf{x}, t) \; ; \tag{3.23}$$

$$\mathbf{v} = \mathbf{v}(\mathbf{x}, t) \; . \tag{3.24}$$

The linearized equations of motion at the first order, assuming that there is no external magnetic field but just the radiation field, i.e. $\mathbf{B} \equiv \mathbf{B}_{\text{rad}}$, become

$$\frac{\partial \delta n}{\partial t} + n_e^0 \boldsymbol{\nabla} \cdot \mathbf{v} = \mathbf{0} \; ; \tag{3.25}$$

$$\frac{\partial \mathbf{v}}{\partial t} - \frac{e}{m}\mathbf{E} + \frac{1}{m n_e^0}\left(\frac{\partial p}{\partial n_e}\right)_0 \nabla \delta n = 0 \; ; \tag{3.26}$$

$$\boldsymbol{\nabla} \cdot \mathbf{E} = e \delta n \; ; \tag{3.27}$$

$$\nabla \times \mathbf{B}_{\text{rad}} - \frac{\partial \mathbf{E}}{\partial t} = e n_e^0 \mathbf{v} \; ; \tag{3.28}$$

to which we should add the two homogeneous Maxwell's equations. We have neglected the term $\mathbf{v} \times \mathbf{B}_{\text{rad}}$ because both the fluctuation field and the velocity are of first order, thus their product is of second order. The equations Eqs. (3.25)–(3.26) can be combined, leading to a wave equation plus a non homogeneous term, i.e. the pressure one, for the density fluctuations $\delta n(\mathbf{x}, t)$

$$\frac{\partial^2 \delta n}{\partial t^2} + \left(\frac{e^2 n_e^0}{m}\right)\delta n - \frac{1}{m}\left(\frac{\partial p}{\partial n_e}\right)_0 \nabla^2 \delta n = 0 \; . \tag{3.29}$$

Moreover, we can obtain an equation for the electric field through the combination of the time derivative of Eq. (3.28) and Eq. (3.26)

$$\frac{\partial^2 \mathbf{E}}{\partial t} + \left(\frac{e^2 n_e^0}{m}\right)\mathbf{E} - \frac{1}{m}\left(\frac{\partial p}{\partial \rho}\right)_0 \nabla(\boldsymbol{\nabla} \cdot \mathbf{E}) = \nabla \times \frac{\partial \mathbf{B}_{\text{rad}}}{\partial t} \; . \tag{3.30}$$

The structures of the left-hand sides of Eq. (3.29) and Eq. (3.30) are identical, thus nothing prevents us from setting $\partial \mathbf{B}_{\rm rad}/\partial t = 0$, from which Faraday's law implies that $\nabla \times \mathbf{E} = 0$. Thus the electric field $\mathbf{E}$ is a longitudinal field which can be derived as the gradient of a scalar potential. It implies that every component of the field $\mathbf{E}$ satisfies an equation of the form Eq. (3.29). If we neglect the pressure term we obtain that the density, velocity and electric field all oscillate with the plasma frequency $\omega = \omega_{\rm p}$, where

$$\omega_{\rm p}^2 = \frac{4\pi\alpha n_e^0}{m_e} \, . \tag{3.31}$$

In the case in which the pressure term is not negligible we obtain instead the following dispersion relation

$$\omega^2 = \omega_{\rm p}^2 + \frac{1}{m}\left(\frac{\partial p}{\partial n_e}\right)_0 k^2 \, . \tag{3.32}$$

We assume the adiabatic law

$$p = p_0 \left(\frac{n_e}{n_e^0}\right)^\gamma \, ; \tag{3.33}$$

where $\gamma = 3$ because there is just one transitional degree of freedom. Thus

$$\frac{1}{m}\left(\frac{\partial p}{\partial n}\right)_0 = 3\frac{p_0}{m n_e^0} \, . \tag{3.34}$$

If we use the relation $p_0 = n_e^0 KT$ and the equipartition theorem $m\langle u^2\rangle = KT$ to define the *root-mean-square* (rms) velocity, we can rewrite the dispersion relation Eq. (3.32) as

$$\omega^2 = \omega_p^2 + 3\langle u^2\rangle k^2 \, . \tag{3.35}$$

This dispersion relation is valid only in the limit of long wavelengths and corresponds to a quantum called *plasmon*. In order to study the different plasma oscillations we consider the plane wave approximation, i.e. we assume that all the quantities vary as $e^{i(\mathbf{k}\cdot\mathbf{x}-\omega t)}$. Eqs. (3.25)–(3.28) and the two

homogeneous Maxwell's equations [Eqs. (3.19)–(3.20)] can be written as

$$\delta n = \frac{\mathbf{k}\cdot\mathbf{v}}{\omega} n_e^0 \; ; \tag{3.36}$$

$$\mathbf{v} = \frac{ie\mathbf{E}}{m\omega} + \frac{3\langle u^2\rangle}{\omega}\frac{\delta n}{n_0}\mathbf{k} \; ; \tag{3.37}$$

$$\mathbf{k}\cdot\mathbf{E} = -ie\delta n \; ; \tag{3.38}$$

$$\mathbf{k}\cdot\mathbf{B} = 0 \; ; \tag{3.39}$$

$$\mathbf{k}\times\mathbf{B} = -\omega\mathbf{E} - ien_e^0\mathbf{v} \; ; \tag{3.40}$$

$$\mathbf{k}\times\mathbf{E} = \omega\mathbf{B} \; . \tag{3.41}$$

Maxwell's equations can be solved for $\mathbf{v}$. In particular, we can combine Eqs. (3.40)–(3.41) to obtain

$$\mathbf{v} = \left(\frac{ie}{m\omega}\right)\frac{1}{\omega_p^2}[(\omega^2 - c^2k^2)\mathbf{E} + (\mathbf{k}\cdot\mathbf{E})\cdot\mathbf{k}] \; . \tag{3.42}$$

Inserting Eq. (3.42) in Eq. (3.37) we obtain an equation for the electric field $\mathbf{E}$

$$(\omega^2 - \omega_{\rm p}^2 - k^2)\mathbf{E} + (1 - 3\langle u^2\rangle)(\mathbf{k}\cdot\mathbf{E})\mathbf{k} = 0 \; . \tag{3.43}$$

The two different types of plasma oscillations can be made explicit if we write the field $\mathbf{E}$ in terms of its parallel and perpendicular components relative to $\mathbf{k}$

$$\mathbf{E} = \mathbf{E}_\parallel + \mathbf{E}_\perp \; ; \tag{3.44}$$

$$\mathbf{E}_\parallel = \left(\frac{\mathbf{k}\cdot\mathbf{E}}{k^2}\right)\mathbf{k} \; . \tag{3.45}$$

Therefore, from Eq. (3.43) we obtain the two equations

$$(\omega^2 - \omega_{\rm p}^2 - 3\langle u^2\rangle k^2)\mathbf{E}_\parallel = 0 \; ; \tag{3.46}$$

$$(\omega - \omega_{\rm p}^2 - k^2)\mathbf{E}_\perp = 0 \; . \tag{3.47}$$

The equation for $\mathbf{E}_\parallel$ Eq. (3.46) corresponds to longitudinal waves with the dispersion relation expressed in Eq. (3.35), that is to the *longitudinal plasmons* (LP). The equation for $\mathbf{E}_\perp$ corresponds instead to two transverse waves, i.e. to two photon states of polarization, propagating with the dispersion relation

$$\omega^2 = \omega_{\rm p}^2 + k^2 \; . \tag{3.48}$$

We will denote these as transverse photons (TP). In particular, Eq. (3.48) corresponds to the classical dispersion relation for photons modified by the addition of a "mass" term $\omega_{\rm p}^2$. We can conclude that photons acquire an effective mass $m_\gamma^2 = \omega_{\rm p}^2$ while propagating in a plasma and being massive acquires also a third polarization state, i.e. the longitudinal plasmon. Let us focus on the solar plasma. If we use values from the Standard Solar Model AGS09 [Ser09] we can estimate the pressure term in Eq. (3.34) at every position in the Sun interior. This term ranges in the interval $\sim [10^{-7}, 10^{-3}]$, thus if we rewrite the dispersion relation in Eq. (3.46) as

$$\left(\frac{\omega}{\omega_{\rm p}}\right)^2 = 1 + \frac{3p_0}{mn_e^0}\left(\frac{k}{\omega_{\rm p}}\right)^2 ; \tag{3.49}$$

we obtain that the second term on the right hand side is negligible with respect to the unity. Therefore in the Sun the dispersion relation for longitudinal modes simply reduces to $\omega^2 = \omega_{\rm p}^2$. The dispersion relation for longitudinal and transverse modes in a plasma is shown in Fig. 3.1.
The results obtained in this section are valid only if there is not any external magnetic field. In this case we must modify Maxwell's equations, as we will discuss in the Section 3.1.3.

3.1.3 Plasma oscillations in presence of an external magnetic field

Let we assume now that an external magnetic field $\mathbf{B}_{\rm ext}$ is present in the plasma [Jac75]. This is the most interesting case for our discussion, since in the Sun large scale and very strong B-field are present, as we will discuss in Chapter 4. We neglect the pressure term and the collisions. The equations

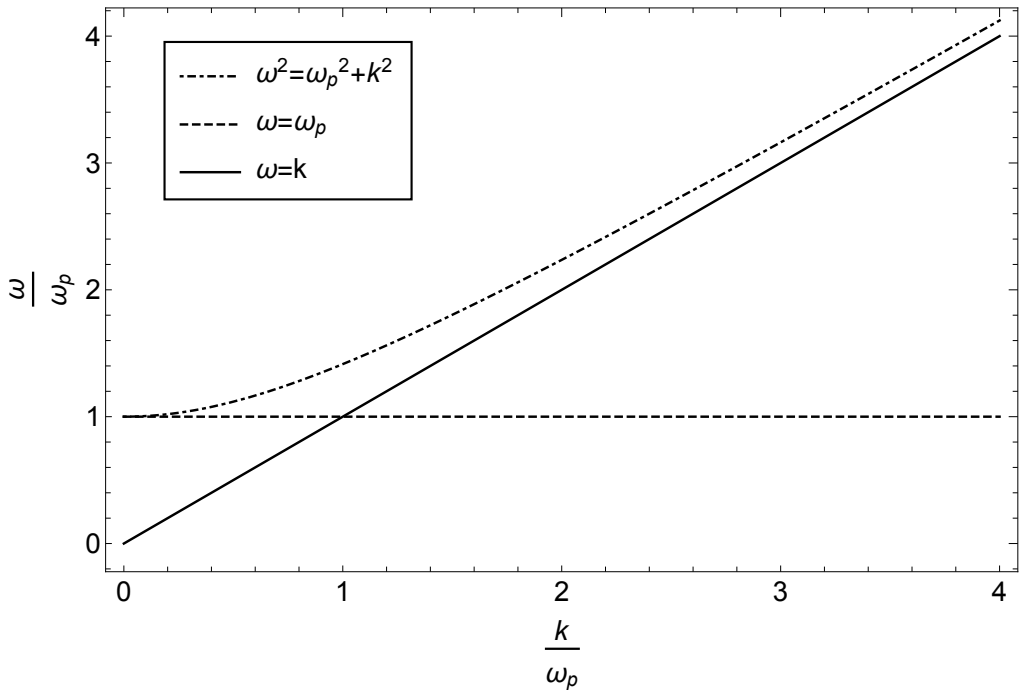

Figure 3.1: Dispersion relation in a plasma for longitudinal photon modes, i.e. $\omega = \omega_{\rm p}$, and transverse modes, i.e. $\omega^2 = k^2 + \omega_{\rm p}^2$. As k increases, the dispersion relation for transverse modes asymptotically tends to $\omega^2 = k^2$.

of motion and Maxwell's equations are

$$\frac{\partial n_e}{\partial t} + \boldsymbol{\nabla} \cdot (n_e \mathbf{v}) = 0 \; ; \tag{3.50}$$

$$\frac{\partial \mathbf{v}}{\partial t} + (\mathbf{v} \cdot \nabla)\mathbf{v} = \frac{e}{m}\Big(\mathbf{E} + \mathbf{v} \times \mathbf{B}\Big) - \frac{1}{m n_e}\nabla p \tag{3.51}$$

$$\boldsymbol{\nabla} \cdot \mathbf{E} = e(n_e - n_e^0) \; ; \tag{3.52}$$

$$\boldsymbol{\nabla} \cdot \mathbf{B} = \mathbf{0} \; ; \tag{3.53}$$

$$\nabla \times \mathbf{E} + \frac{\partial \mathbf{B}}{\partial t} = 0 \; ; \tag{3.54}$$

$$\nabla \times \mathbf{B} - \frac{\partial \mathbf{E}}{\partial t} = e n_e \mathbf{v} \; . \tag{3.55}$$

where we are considering the total magnetic field expressed in Eq. (3.3). We can write down the linearized equations of motion and Maxwell's equations if we assume that all variables vary as $e^{i(\mathbf{k}\cdot\mathbf{x} - \omega t)}$ and if we consider small

deviations from the equilibrium values

$$n_e = n_e^0 + \delta n(\mathbf{x}, t) \; ; \tag{3.56}$$

$$\mathbf{v} = \mathbf{v}(\mathbf{x}, t) \; . \tag{3.57}$$

We obtain at the first order in perturbations and neglecting the pressure term

$$\delta n = \frac{\mathbf{k} \cdot \mathbf{v}}{\omega} n_e^0 \; ; \tag{3.58}$$

$$\mathbf{v} = \frac{ie}{m\omega}(\mathbf{E} + \mathbf{v} \times \mathbf{B}_{\rm ext}) \; ; \tag{3.59}$$

$$\mathbf{k} \cdot \mathbf{E} = -ie\delta n \; ; \tag{3.60}$$

$$\mathbf{k} \cdot \mathbf{B} = 0 \; ; \tag{3.61}$$

$$\mathbf{k} \times \mathbf{B} = -\omega \mathbf{E} - ien_e^0 \mathbf{v} \; ; \tag{3.62}$$

$$\mathbf{k} \times \mathbf{E} = \omega \mathbf{B} \; . \tag{3.63}$$

where in Eq. (3.59) we are considering only the external field because $\mathbf{v} \times \mathbf{B}_{\rm rad}$ is of second order in the perturbation, while $\mathbf{v} \times \mathbf{B}_{\rm ext}$ is of first order. We assume that the external field has an amplitude B_0 and direction identified by the versor $\hat{\mathbf{b}}$, i.e. $\mathbf{B}_{\rm ext} = B_0 \hat{\mathbf{b}}$. Solving this system and proceeding as in the previous case without an external field ones recover the dispersion relation

$$\omega^2(\omega^2 - \omega_{\rm p}^2)(\omega^2 - \omega_{\rm p}^2 - k^2)^2 = \omega_B^2(\omega^2 - k^2)[\omega^2(\omega^2 - \omega_{\rm p}^2 - k^2) + \omega_{\rm p}^2(\mathbf{k} \cdot \hat{\mathbf{b}})^2] \; ; \tag{3.64}$$

where we have introduced the cyclotron frequency

$$\omega_B = \frac{eB}{m} \; . \tag{3.65}$$

From Eq. (3.64) it is evident that the longitudinal and transverse modes are coupled because of the external magnetic field. These become uncoupled if the condition $\omega_B \ll \omega_{\rm p}$ stands. If we use the Standard Solar Model AGS09 [Ser09] we obtain that this situation is satisfied everywhere in the Sun. The behaviour of ω_B and $\omega_{\rm p}$ as a function of $r/R_\odot$ is shown in Fig. 3.2. If $\omega_B \ll \omega_{\rm p}$ we can obtain two seperate dispersion relations for $\mathbf{k} \parallel \mathbf{b}$ and $\mathbf{k} \perp \mathbf{b}$. In the former case, $(\mathbf{k} \cdot \mathbf{b})^2 = k^2$ and neglecting in Eq. (3.64) the terms proportional to $\omega_B/\omega_{\rm p}$ we obtain

$$\omega^2 \approx k^2 + \omega_{\rm p}^2 \; . \tag{3.66}$$

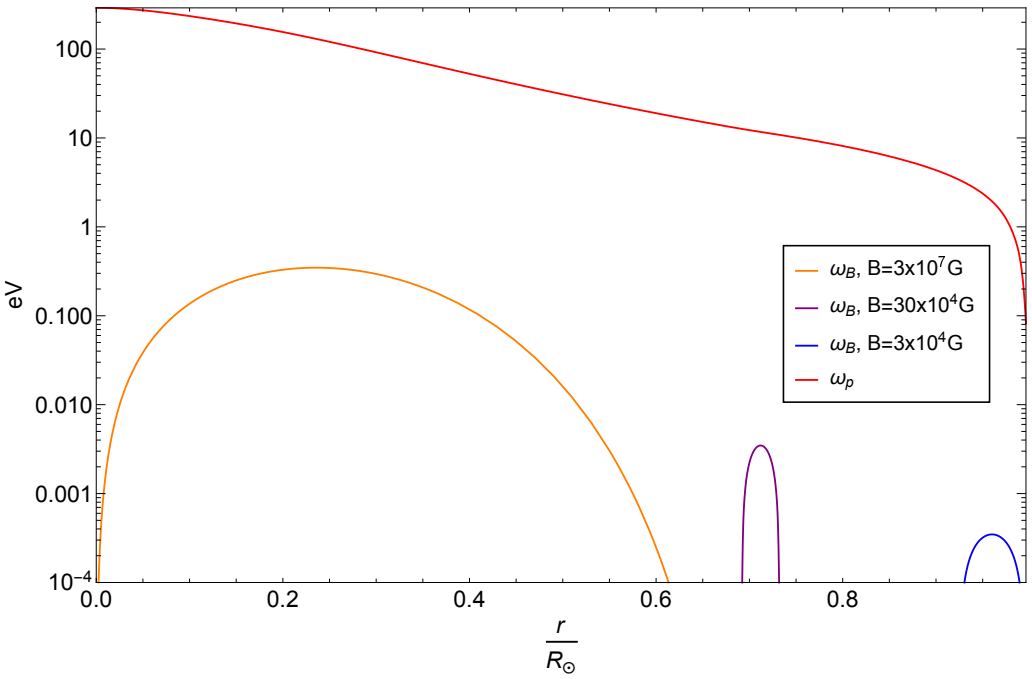

Figure 3.2: Behaviour of the plasma frequency $\omega_{\rm p}$ and cyclotron frequency ω_B in different zones of the Sun interior. The condition $\omega_B \ll \omega_{\rm p}$ always occurs. In the simulation only the maximum amplitudes of the B-field in different regions have been used.

In the latter case $(\mathbf{k}\cdot\mathbf{b})^2 = 0$ and from Eq. (3.64) in this limit we obtain

$$\omega^2 \approx \omega_{\rm p}^2 \,. \tag{3.67}$$

3.2 Photon-ALP mixing in a plasma

Let us now consider an ALP-photon system in a plasma [Raf96]. We start from the Lagrangian of a photon coupled with the pseudoscalar field a, i.e. the ALP field

$$\mathcal{L} = -\frac{1}{4}F_{\mu\nu}F^{\mu\nu} + \frac{1}{2}(\partial_\mu a \partial^\mu a - m_a^2 a^2) - \frac{1}{4}g_{a\gamma}aF_{\mu\nu}\tilde{F}^{\mu\nu} + J_\mu A^\mu \,; \tag{3.68}$$

where $g_{a\gamma}$ is the axion-photon coupling, J_μ is the electromagnetic current, A^μ is the vector potential, $F_{\mu\nu}$ is the electromagnetic field tensor and $\tilde{F}_{\mu\nu} =$

$1/2\epsilon_{\mu\nu\rho\sigma}F^{\rho\sigma}$ its dual. From Eq. (3.68) one recovers Maxwell's equations

$$\partial_\mu F^{\mu\nu} = J^\nu + g_{a\gamma}\tilde{F}^{\mu\nu}\partial_\mu a \ ; \tag{3.69}$$

$$(\Box + m_a^2)a = -\frac{1}{4}g_{a\gamma}F_{\mu\nu}\tilde{F}^{\mu\nu} \ ; \tag{3.70}$$

$$\partial_\mu \tilde{F}^{\mu\nu} = 0 \ . \tag{3.71}$$

In this context we consider a strong external magnetic field $\mathbf{B}_{\rm ext}$ such that the total field in Eq. (3.3) is $\mathbf{B} \approx \mathbf{B}_{\rm ext}$. The plasma equations Eqs. (3.15), (3.17) stay unaffected by the presence of the ALP. We can make a distinction between transverse and longitudinal modes, since we are in the limit of high plasma oscillation as we discussed in Section 3.1.3.

3.2.1 Transverse modes

Transverse modes are characterized by an electric field $\mathbf{E}$ transverse to the photon momentum and a magnetic field $\mathbf{B}$ transverse to both. According to the discussion of Section 3.1 the photon dispersion relation for TP is

$$\omega^2 = k^2 + \omega_{\rm p}^2 \ ; \tag{3.72}$$

where $\omega_{\rm p}^2 = m_\gamma^2$. Actually, in vacuum transverse modes are the only ones allowed, but in this case their dispersion relation is the common $\omega^2 = k^2$. For the purpose of our discussion we rewrite just three Maxwell's equations in a non-explictly covariant form

$$\boldsymbol{\nabla} \cdot \mathbf{E} = \rho_e - g_{a\gamma}\mathbf{B}_{\rm ext} \cdot \nabla a \ ; \tag{3.73}$$

$$\nabla \times \mathbf{B}_{\rm ext} - \partial_t \mathbf{E} = -g_{a\gamma}\mathbf{B}_{\rm ext}\partial_t a + \mathbf{J} \ ; \tag{3.74}$$

$$(\Box + m_a^2)a = -g_{a\gamma}\mathbf{B}_{\rm ext} \cdot \partial_t \mathbf{A} \ ; \tag{3.75}$$

where $\rho = -en_e$ is the electron charge density, $\mathbf{A}$ is the time-varying part of the vector potential for the external magnetic field and $\Box = \partial_t^2 - \nabla^2$. Note that we are considering only the electrons in plasma equations, because as we discussed in Sections 3.1.2 we are assuming that ions provide a uniform background which does not partecipate in plasma motion. For the transverse mode $\mathbf{k} \cdot \mathbf{B}_{\rm ext} = 0$. Thus for clarity of notation we identify the magnetic field $\mathbf{B}_{\rm ext} \equiv \mathbf{B}_{\rm T}$, to denote that it is a *transverse* field. Moreover, we make the

assumption that $\mathbf{E} \ll \mathbf{B}_{\rm T}$. Therefore Eqs. (3.74)–(3.75) become

$$\Box \mathbf{A} = g_{a\gamma} \mathbf{B}_T \partial_t a \; ; \tag{3.76}$$

$$(\Box + m_a^2) a = -g_{a\gamma} \mathbf{B}_T \cdot \partial_t \mathbf{A} \; . \tag{3.77}$$

Finally, the equations of motions for the plasma and Maxwell's equations for the transverse modes are

$$\Box \mathbf{A} = g_{a\gamma} \mathbf{B}_T \partial_t a \; ; \tag{3.78}$$

$$(\Box + m_a^2) a = -g_{a\gamma} \mathbf{B}_T \cdot \partial_t \mathbf{A} \tag{3.79}$$

$$\frac{\partial n}{\partial t} + \boldsymbol{\nabla} \cdot (n \mathbf{v}) = 0 \; ; \tag{3.80}$$

$$\frac{\partial \mathbf{v}}{\partial t} + (\mathbf{v} \cdot \nabla) \mathbf{v} = \frac{e}{m} \Big(\mathbf{E} + \mathbf{v} \times \mathbf{B}_{\rm T} \Big) - \frac{1}{m n_e} \nabla p \; . \tag{3.81}$$

The goal is computing the TP-ALP conversion probability, for which plasma equations are not necessary, assuming that no photons absorption exists in the plasma. We specialize to a wave of frequency ω propagating in the z-direction and we denote with $A_\perp$ and $A_\parallel$ the components of the vector potential $\mathbf{A}$ perpendicular and parallel to $\mathbf{B}_T$ respectively. Thus the equation of motion for the TP-ALP system becomes [Raf88, Ans88]

$$\left[\omega^2 + \partial_z^2 + 2\omega^2 \begin{pmatrix} \Delta_\perp/\omega & n_R & 0 \\ n_R & \Delta_\parallel/\omega & g_{a\gamma} B_T/2\omega \\ 0 & g_{a\gamma} B_T/2\omega & -m_a^2/2\omega^2 \end{pmatrix} \right] \begin{pmatrix} A_\perp \\ A_\parallel \\ a \end{pmatrix} = 0 \; ; \tag{3.82}$$

where n_R corresponds to the so called *Faraday effect*, which denotes the possibility of rotation of the plane of polarization in optically active media with a consequent mixing of $A_\perp$ and $A_\parallel$. Moreover

$$\Delta_\perp = \Delta_{\rm p} + \Delta_\perp^{\rm CM} \; ; \tag{3.83}$$

$$\Delta_\parallel = \Delta_{\rm p} + \Delta_\parallel^{\rm CM} \; ; \tag{3.84}$$

$$\Delta_{\rm p} = -\frac{2\pi\alpha n_e}{m_e} \omega^{-1} \; . \tag{3.85}$$

The terms $\Delta_{\perp,\parallel}^{\rm CM}$ describe the Cotton-Mouton effect, i.e. the birifrangence of fluids in the presence of a transverse magnetic field. The vacuum Cotton-Mouton effect arises from QED one-loop corrections to the photon polarization when an external magnetic field is present. In this case we define

$\Delta_{\rm QED} = |\Delta_\perp^{\rm CM} - \Delta_\parallel^{\rm CM}|$ and it is defined as

$$\Delta_{\rm QED} = \frac{24\alpha^2}{135}\frac{\rho_B}{m_e^4}\omega \ . \tag{3.86}$$

This QED correction is found to be negligible with respect to $\Delta_{\rm p}$ in the case of solar plasma. For transverse modes only the component $A_\parallel$ of the vector potential couples to the ALP. Moreover, if we neglect the Faraday effect ($n_R = 0$) and we assume that the magnetic field is uniform, we can reduce the general 3×3 problem of Eq. (3.82) to the 2×2 system consisting of $A_\parallel$ and a. In the ultrarelativistic limit, i.e. for energies $\omega \gg m_a$ and $\omega \gg \omega_{\rm p}$, we can linearize Eq. (3.82). As a result of linearization we obtain a linear Schrödinger like equation [Raf88, Ans88]

$$i\partial_z \begin{pmatrix} A_\parallel \\ a \end{pmatrix} = -\omega \mathbb{1} + \begin{pmatrix} \frac{\omega_p^2}{2\omega} & g_{a\gamma}B_T/2 \\ g_{a\gamma}B_T/2 & \frac{m_a^2}{2\omega} \end{pmatrix} \begin{pmatrix} A_\parallel \\ a \end{pmatrix} \ ; \tag{3.87}$$

Thus the Hamiltonian for the transverse modes reads (up to an overall phase diagonal term)

$$H_T = \begin{pmatrix} \frac{\omega_p^2}{2\omega} & g_{a\gamma}B_T/2 \\ g_{a\gamma}B_T/2 & \frac{m_a^2}{2\omega} \end{pmatrix} \ . \tag{3.88}$$

Finally, we obtain the TP-ALP conversion probability after traveling a distance z in a uniform magnetic field B_T [Raf96]

$$P(\gamma_T \to a) = (\Delta_{a\gamma}^T z)^2 \frac{\sin^2(\Delta_{\rm osc}^T z/2)}{(\Delta_{\rm osc}^T z/2)^2} \ ; \tag{3.89}$$

where we have introduced

$$\Delta_{a\gamma}^T = g_{a\gamma}B_T/2 \ ; \tag{3.90}$$

$$\Delta_{\rm osc}^T = \sqrt{4{\Delta_{a\gamma}^T}^2 + \left(\frac{\omega_{\rm p}^2 - m_a^2}{2\omega}\right)^2} \ . \tag{3.91}$$

It is important to stress that the TP-ALP conversion exhibits a *resonant* behaviour, i.e. the TP-ALP conversion probability becomes maximal for a particular condition. Indeed, from Eq. (3.89) we obtain that the probability is maximal when $m_a^2 = \omega_{\rm p}^2$, i.e. when $\Delta_{\rm osc}^T$ has its minimum, that is the only case in which the axion dispersion relation crosses the transverse photon one, as shown in Fig. 3.3.

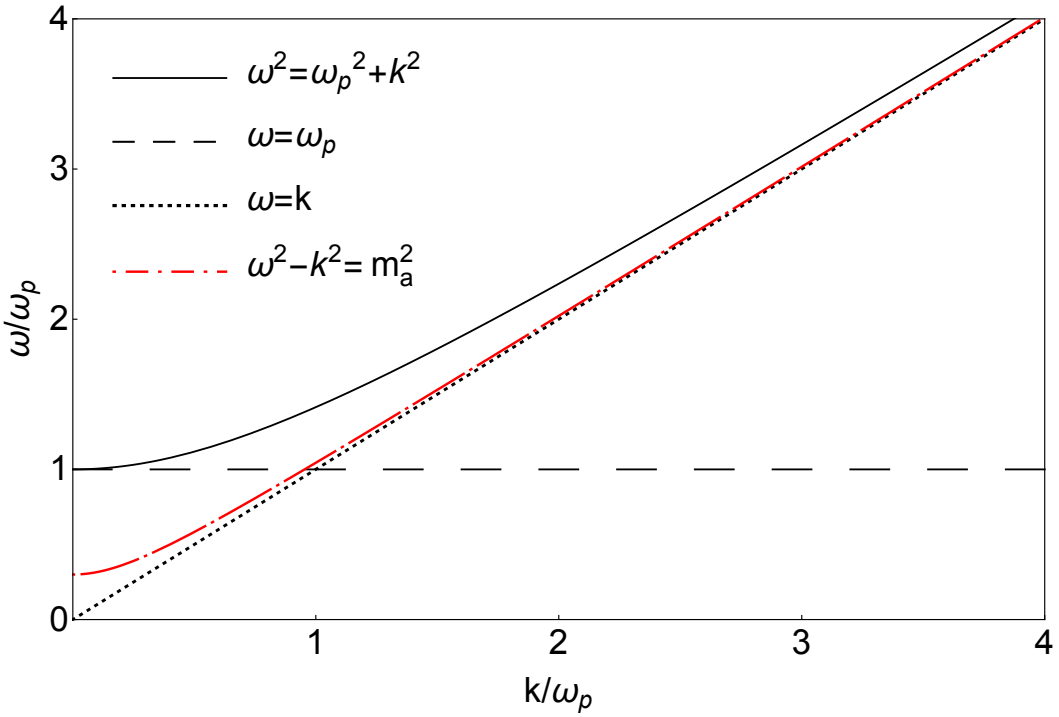

Figure 3.3: Dispersion relation for an ALP with mass m_a, which was made large enough to be distinguished from that of an ordinary photon (black continuos line). The ALP dispersion crosses the one of the LP for $\omega = \omega_{\rm p}$, where the resonance occurs. For the transverse modes, the only possibility of crossing between the axion dispersion relation and the transverse photon one is $m_a^2 = \omega_{\rm p}^2$.

3.2.2 Longitudinal modes

Longitudinal modes are allowed only in presence of a medium, that is in our discussion is the solar plasma. The photon dispersion relation for LP is

$$\omega^2 = \omega_{\rm p}^2 \, . \tag{3.92}$$

In this case $\boldsymbol{\nabla}\cdot\mathbf{B}\neq 0$, thus the plasma equations of motion and the relevant Maxwell's equations are [Ter18, Men19, Das04]

$$\frac{\partial n_e}{\partial t}+\boldsymbol{\nabla}\cdot(n_e\mathbf{v})=0\ ; \tag{3.93}$$

$$\frac{\partial \mathbf{v}}{\partial t}+(\mathbf{v}\cdot\nabla)\mathbf{v}=\frac{e}{m}\Big(\mathbf{E}+\mathbf{v}\times\mathbf{B}\Big)-\frac{1}{mn_e}\nabla p\ ; \tag{3.94}$$

$$\boldsymbol{\nabla}\cdot(\mathbf{E}+g_{a\gamma}\mathbf{B}a)=e(n_e-n_e^0)\ ; \tag{3.95}$$

$$(\Box+m_a^2)a=g_{a\gamma}a\mathbf{E}\cdot\mathbf{B}\ . \tag{3.96}$$

The goal is now compute the LP-ALP conversion probability, assuming that no LP absorption exists in the plasma. In the case of longitudinal modes we have to combine Eqs. (3.93) and (3.94) with Maxwell's equations. We consider a uniform external magnetic field along the z-direction $\mathbf{B}=B_L\mathbf{u}_z$ and we consider the plane wave approximation, i.e. we assume that all the fields vary as $e^{i(\mathbf{k}\cdot\mathbf{x}-\omega t)}$. Moreover, we take into account a small perturbation to the electron number density

$$n_e=n_e^0+\delta n\ ; \tag{3.97}$$

where n_e^0 is the equilibrium value and $\delta n\ll n_0$. If we finally take $\omega=\omega_{\rm p}=\omega_a$, i.e. the photon energy coincident with the plasma frequency and with the ALP energy, we can linearize Maxwell's equations Eqs. (3.95)-(3.96) for longitudinal modes. Thus we obtain [Ter18]

$$i\partial_t\begin{pmatrix}A_L\\ a_k\end{pmatrix}=\begin{pmatrix}\omega_p & \frac{g_{a\gamma}B_L}{2}\\ \frac{g_{a\gamma}B_L}{2} & \omega_a\end{pmatrix}\begin{pmatrix}A_L\\ a_k\end{pmatrix}\ ; \tag{3.98}$$

where we have introduced the fields $\delta n=in_eA_L$ and $a=\omega_{\rm p}m_ea_k/ek$. Thus the Hamiltonian of the system is

$$H_L=\begin{pmatrix}\omega_p & \Delta_{a\gamma}^L\\ \Delta_{a\gamma}^L & \omega_a\end{pmatrix}\ . \tag{3.99}$$

The LP-ALP conversion probability is again

$$P(\gamma_{\rm LP}\to a)=(\Delta_{a\gamma}^L t)^2\frac{\sin^2(\Delta_{\rm osc}^L t/2)}{(\Delta_{\rm osc}^L t/2)^2}\ ; \tag{3.100}$$

where

$$\Delta_{a\gamma}^{L} = \frac{g_{a\gamma} B_L}{2} \; ; \tag{3.101}$$

$$\Delta_{\rm osc}^{L} = \sqrt{4{\Delta_{a\gamma}^{L}}^{2} + (\omega_a - \omega_{\rm p})^2} \; . \tag{3.102}$$

The LP-ALP conversion is a resonant process and the resonance occurs for $\omega = \omega_{\rm p}$, when the ALP dispersion relation crosses the LP one, as shown in Fig. 3.3.

Chapter 4

Axions from the Sun: Photon conversions in magnetic field

In this Chapter we discuss the ALPs production in the Sun from photon conversions in the solar magnetic fields. In Section 4.1 we describe the models for large-scale magnetic field in the Sun and we present simulations of the magnetic field profiles. In Section 4.2 we calculate the photon-ALP conversion probability in the solar magnetic fields for both transvserse and longitudinal photon modes. Moreover, we introduce a kinetic approach to compute the ALP production rate, taking into account photon absorption in the solar plasma. In Section 4.3 we compute the ALP flux expected at Earth from different conversion processes in the Sun and we present the expected spectra of these fluxes. In Section 4.4 we derive a new bound on the coupling constant $g_{a\gamma}$ based on ALP emissivity from production in solar B-fields and we discuss the perspective of detection for ALPs produced through conversions in the solar magnetic field.

4.1 Large scale magnetic field in the Sun

In this thesis work we are interested in the magnetic activity of the Sun, whose dynamic magnetic field is responsible for all solar magnetic phenomena, such as sunspots and the solar wind. The former are dark patches on the solar surface which can be seen with the nacked eye and that many theories have tried to explain without success. In 1908 Hale first introduced the solar magnetic field to explain that the sunspots were the site of such a field

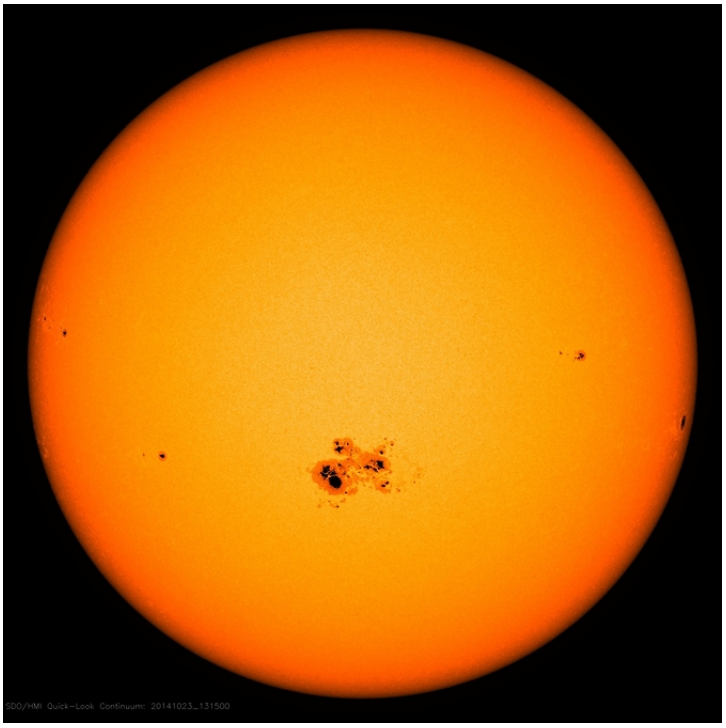

Figure 4.1: Sunspots can be seen on the lower part of the Sun. The image is from NASA's Solar Dynamic Observatory and was captured on October 23th, 2004. Image credit: NASA/SDO.

which caused the splitting of spectral lines through the Zeeman effect [Hal08]. A picture of sunspots is shown in Fig. (4.1). Actually, the observation of sunspots is not the only evidence of the precence of a magnetic field in the Sun. Nevertheless, we just mention this one for its hystorical importance, since solar magnetic field was first introduced on the basis of its observation. Current theories that describe the Solar magnetic field involve the existence of an hydromagnetic dynamo operating within the Sun (for more details about the dynamo theory see [Mof78, Par79]). A dynamo process was first proposed by Larmor in 1919 [Lar19] to explain how the magnetic field was mantained in the Sun. He suggested that this was possible because of the motion of an electrically conducting fluid, i.e. the ionized plasma in the Sun. The motion of such a fluid induces electric currents that are needed to sustain the field. However, the dynamo problem is much more complicated, but its mathematical discussion goes beyond the purposes of this thesis.
Progress in this context was done by dividing the magnetic field in a *toroidal*

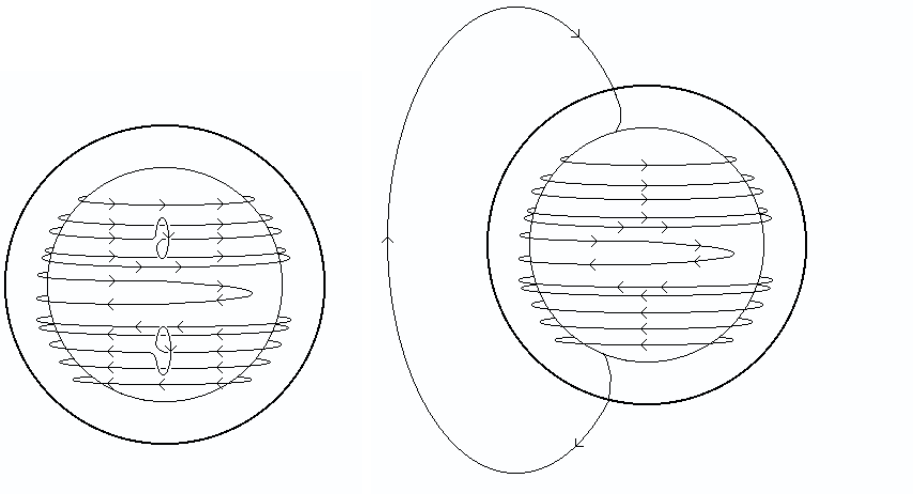

(a) α-effect. **(b)** ω-effect.

Figure 4.2: In Fig. 4.2a α-effect is shown: toroidal lines of the magnetic field are lifted and twisted by the turbolent motions. It results in the conversion of toroidal field into poloidal one. In Fig. 4.2b ω-effect is shown. Poloidal field is stretched into toroidal one by the differential rotation around the Sun axis. Figures taken from [Hat14].

and *poloidal* component. These terms refer to the directions relative to a torus reference: the former encircle the central part of the torus, the latter follows a ring around the surface. It was in 1955 that Parker presented his work about the hydromagnetic dynamo theory for the Sun [Par79] in terms of the so called $\alpha - \omega$ kynematic dynamo. This theory explains how the two components of the magnetic field are sustained by the fluid flow. Indeed, there are both a differential latitudinal rotation, corresponding to the parameter ω, and turbolent movements, described by the parameter α. The differential rotation causes for a stretching of the poloidal field into a toroidal one (ω effect), while the turbolent motions are able to slow down the lift and twist of the toroidal field, giving it enough time to be amplified (α effect). These two effects allow to convert a toroidal field into a poloidal one, thus the initial field is restored and the dynamo cycle is completed. The α and ω effects are schematically shown in Fig. 4.2. Since the toroidal field is believed to cause the sunspots on the surface of the Sun, the toroidal component could be larger than the poloidal one in the convective zone. In this thesis work we will consider only the toroidal part of the field. The

magnetic field of the Sun is most important in three different regions, namely the *radiative* zone ($r \lesssim 0.7\ R_\odot$), the exterior zone called the *convective* zone ($r \gtrsim 0.9\ R_\odot$) and the intermediate region between these two ones called the *tachocline* ($r \sim 0.7\ R_\odot$).
We describe toroidal magnetic field in the Sun as [Dzi95]

$$\mathbf{B}_\phi = a(r)\frac{\mathrm{d}}{\mathrm{d}\theta}P_k(\cos\theta)\mathbf{e}_\phi\ ; \tag{4.1}$$

where $P_k(\cos\theta)$ is the Legendre polynomial of degree k, $\mathbf{e}_\phi$ is the azimuthal direction of the field and $a(r)$ is its profile. We assume that $k = 2$, i.e. that the field is quadrupolar, which is consistent with the surface-magnetism manifestation [Cou03]. For $a(r)$ two different profiles are considered [Gou90]. The radiative zone is simulated considering the following profile

$$a(r) = \begin{cases} K_\lambda\left(\frac{r}{r_0}\right)^2\left(1-\left(\frac{r}{r_0}\right)^2\right)^\lambda & \text{if } r \leq\ r_0 \\ 0 & \text{otherwhise} \end{cases}\ ; \tag{4.2}$$

where $K_\lambda = (1+\lambda)(1+1/\lambda)^\lambda B_{\mathrm{rad}}$, $r_0 = 0.712 R_\odot$, being $\lambda = 10\ r_0 + 1$ and B_{rad} the amplitude of the field, i.e. its highest value. In the radiative zone $1\times10^7\ \mathrm{G} \lesssim \mathrm{B_{rad}} \lesssim 3\times10^7\ \mathrm{G}$. This range was determined by Couvidat *et al.* [Cou03]. They used the precision on solar sound speed and density to rule out field with intensity $B_0 \sim 10^8$ G and arguments on the solar oblateness to set the upper value. The field profile in the tachocline is instead simulated as

$$a(r) = \begin{cases} B_{\mathrm{tach}}\left(1-\left(\frac{r-r_0}{d}\right)^2\right) & \text{if } |r-r_0| \leq d \\ 0 & \text{otherwhise} \end{cases}\ ; \tag{4.3}$$

where r_0 is the center of the zone and d is its half-width. As benchmark parameters in the tachocline we set $d = 0.02\ R_\odot$ and $r_0 = 0.712\ R_\odot$, while $3\times10^5\ \mathrm{G} \lesssim \mathrm{B_{tach}} \lesssim 5\times10^5\ \mathrm{G}$. These bounds were set by Antia *et al.* by the observation of the splittings of solar oscillation frequencies [Ant00]. Similiarly, the field profile in the upper layers is simulated as in Eq. (4.3)

$$a(r) = \begin{cases} B_{\mathrm{conv}}\left(1-\left(\frac{r-r_0}{d}\right)^2\right) & \text{if } |r-r_0| \leq d \\ 0 & \text{otherwhise} \end{cases}\ ; \tag{4.4}$$

with $r_0 = 0.96\ R_\odot$, $d = 0.035\ R_\odot$ and $2\times10^4\ \mathrm{G} \lesssim \mathrm{B_{conv}} \lesssim 3\times10^4\ \mathrm{G}$. These bounds were set by Antia *et al.* from an analysis of the Global Oscillation

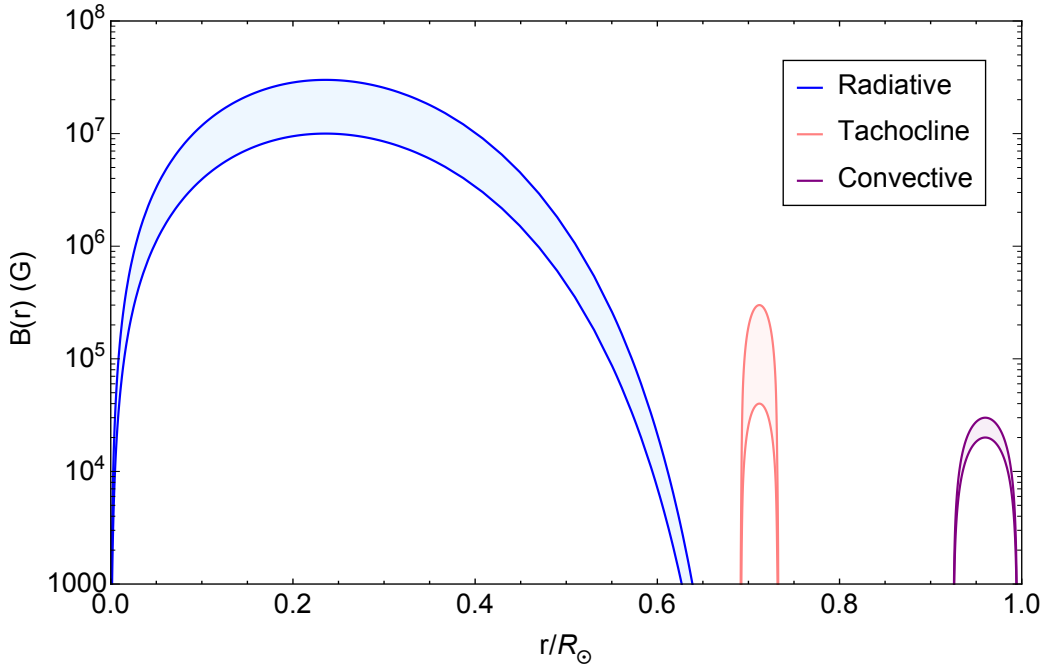

Figure 4.3: Profile of solar magnetic field $B(r)$ as a function of radius $r/R_\odot$. In each region we take the following ranges: $B_{\rm rad} \in [1,3] \times 10^7$ G [Cou03], $B_{\rm tach} \in [3,5] \times 10^5$ G [Ant00] and $B_{\rm tach} \in [2,3] \times 10^4$ G [Ant00].

Network Group (GONG). To summarize, we simulate magnetic fields with the following ranges [Ant00]

$$B_{\rm rad} \in [1;3] \times 10^7 \text{ G} ; \tag{4.5}$$

$$B_{\rm tach} \in [3;5] \times 10^5 \text{ G} ; \tag{4.6}$$

$$B_{\rm conv} \in [2;3] \times 10^4 \text{ G} . \tag{4.7}$$

The simulated magnetic fields with the amplitudes in the range of the previous three equations are shown in Fig. 4.3.

4.2 Photons conversions in solar magnetic fields

Conversions of solar thermal photons into ALPs in solar magnetic fields is allowed because of the Lagrangian [Raf88]

$$\mathcal{L} = -\frac{1}{4} g_{a\gamma} a F_{\mu\nu} \tilde{F}^{\mu\nu} = g_{a\gamma} a \mathbf{E} \cdot \mathbf{B} . \tag{4.8}$$

Let us consider a photon beam with energy ω propagating in the solar plasma along the z direction. We assume that the magnetic $\mathbf{B}$ field is homogeneous. As we discussed in Chapter 3 the cyclotron frequency $\omega_{\rm B}$ is always much less than the plasma frequency $\omega_{\rm p}$, i.e. the condition $\omega_{\rm B} \ll \omega_{\rm p}$ always applies in the Sun. Thus, in order to study conversions into ALPs, according to Sec. 3.1.3 we can decouple the photon transverse modes from the longitudinal ones.

Photon transverse modes

For photon transverse modes, the TP-ALP conversion probability after the beam has traveled a distance z in the B-field is Eq. (3.89) [Raf96]

$$P(\gamma_T \to a) = (\Delta^T_{a\gamma} z)^2 \frac{\sin^2(\Delta^T_{\rm osc} z/2)}{(\Delta^T_{\rm osc} z/2)^2} \; ; \tag{4.9}$$

where in solar units

$$\Delta^T_{a\gamma} = \frac{g_{a\gamma} B_T}{2} \simeq 1.2 \times 10^{-1} \left(\frac{g_{a\gamma}}{10^{-11}\ \text{GeV}^{-1}} \right) \left(\frac{B_T}{3 \times 10^5\ \text{G}} \right) R_\odot^{-1} \; ; \tag{4.10}$$

$$\Delta_{\rm p} = -\frac{\omega_{\rm p}^2}{2\omega} \simeq -2.46 \times 10^{17} \left(\frac{\omega}{\text{keV}} \right)^{-1} \left(\frac{n_e}{10^{26} \text{cm}^{-3}} \right) R_\odot^{-1} \; ; \tag{4.11}$$

$$\omega_{\rm p} \simeq 1.31 \times 10^{18} \sqrt{\frac{n_e}{10^{26}\ \text{cm}^{-3}}} R_\odot^{-1} \; ; \; ; \tag{4.12}$$

$$\Delta_a = -\frac{m_a^2}{2\omega} \simeq -1.76 \times 10^{14} \left(\frac{m_a}{10\ \text{eV}} \right)^2 \left(\frac{\omega}{\text{keV}} \right)^{-1} R_\odot^{-1} \; ; \tag{4.13}$$

$$\Delta^T_{\rm osc} = \sqrt{4 {\Delta^T_{a\gamma}}^2 + (\Delta_{\rm p} - \Delta_a)^2} \; ; \tag{4.14}$$

B_T is the component of the magnetic field transverse to the propagation direction of the photon and $\omega_{\rm p}$ the plasma frequency. The plasma frequency has been computed using the Solar Model AGSS09 [Ser09]. For the solar B-field we used the model of the previous Section. The results are shown in Fig. (4.4). The conversion probability in Eq. (4.9) is maximum at *resonance*, when $\Delta_{\rm p} = \Delta_a$, i.e. $m_a^2 = \omega_{\rm p}^2$. From Fig. (4.4) we see that the resonance occurs in the radiative zone at $r \sim 0.3 R_\odot$ for $m_a \sim 100$ eV. Instead, the resonance in the tachocline occurs at $r \sim 0.7 R_\odot$ for $m_a \sim 10$ eV. Indeed, for these values of m_a the curve Δ_a crosses $\Delta_{\rm p}$.
Finally, we need to take into account the photon absorption coefficient rate

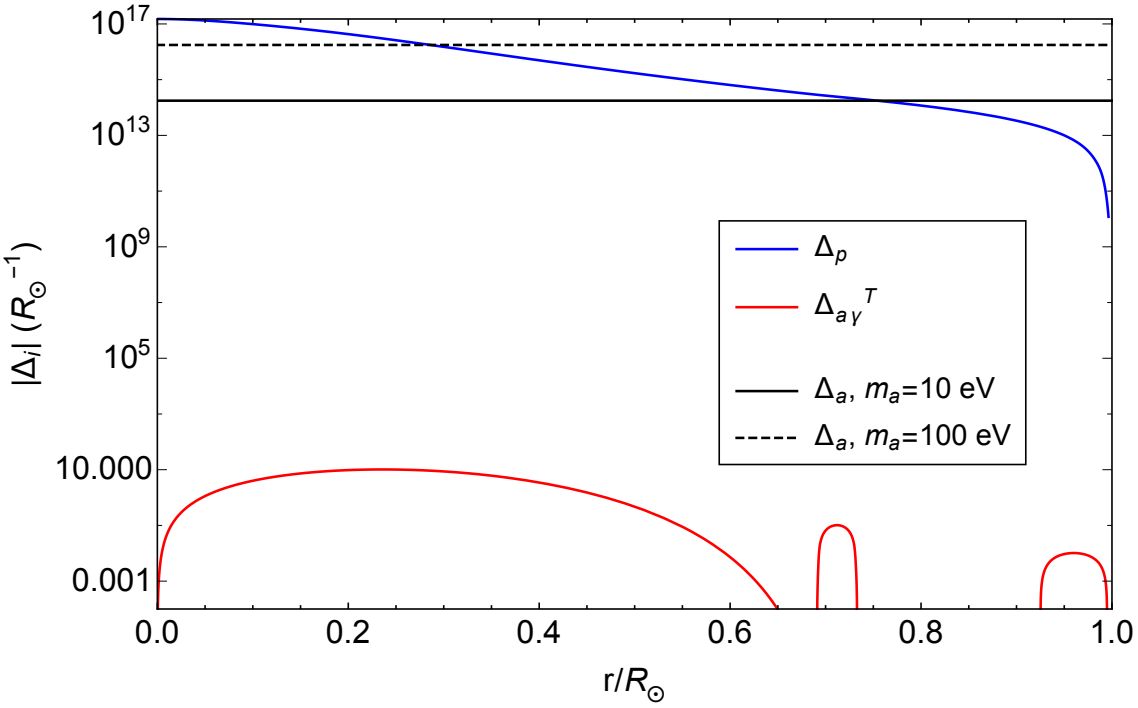

Figure 4.4: Oscillation parameters of Eqs. (4.10)–(4.14)–(4.11)–(4.13) as a function of $r/R_\odot$.

$\Gamma_{\rm abs}$ in the Sun interior. This is defined as the inverse of the photon mean free path which is approximately linear with $r/R_\odot$ [Kri16]. The behaviour of $\Gamma_{\rm abs}$ compared to the oscillation parameters of the photon transverse modes is shown in Fig. (4.5). We see that the photon absorption coefficient $\Gamma_{\rm abs}$ in the solar plasma is not negligible with respect to the other oscillation parameters, but rather is always larger than the parameter $\Delta_{a\gamma}$. This means we need to include the photon absorption in our discussion and to use a kinetic approach, as we will do in the next section.

We conclude this Section giving an estimation of the conversion probability. First, we consider the resonant case and we assume that the distance traveled by the photon in the B-field is equal to its mean free path $\Gamma_{\rm abs}^{-1}$. For the photon transverse modes the resonance occurs when $m_a^2 = \omega_{\rm p}^2$, thus $\Delta_{\rm osc}^T \equiv \Delta_{a\gamma}^T \ll \Gamma_{\rm abs}$ as we see from Fig. (4.5). Therefore in Eq. (4.9) we have that $\sin^2(\Delta_{\rm osc}^T \Gamma_{\rm abs}^{-1})/(\Delta_{\rm osc}^T \Gamma_{\rm abs}^{-1})^2 \approx 1$, since $\Delta_{\rm osc}^T (\Gamma_{\rm abs}^{-1}) \ll 1$. The TP-ALP

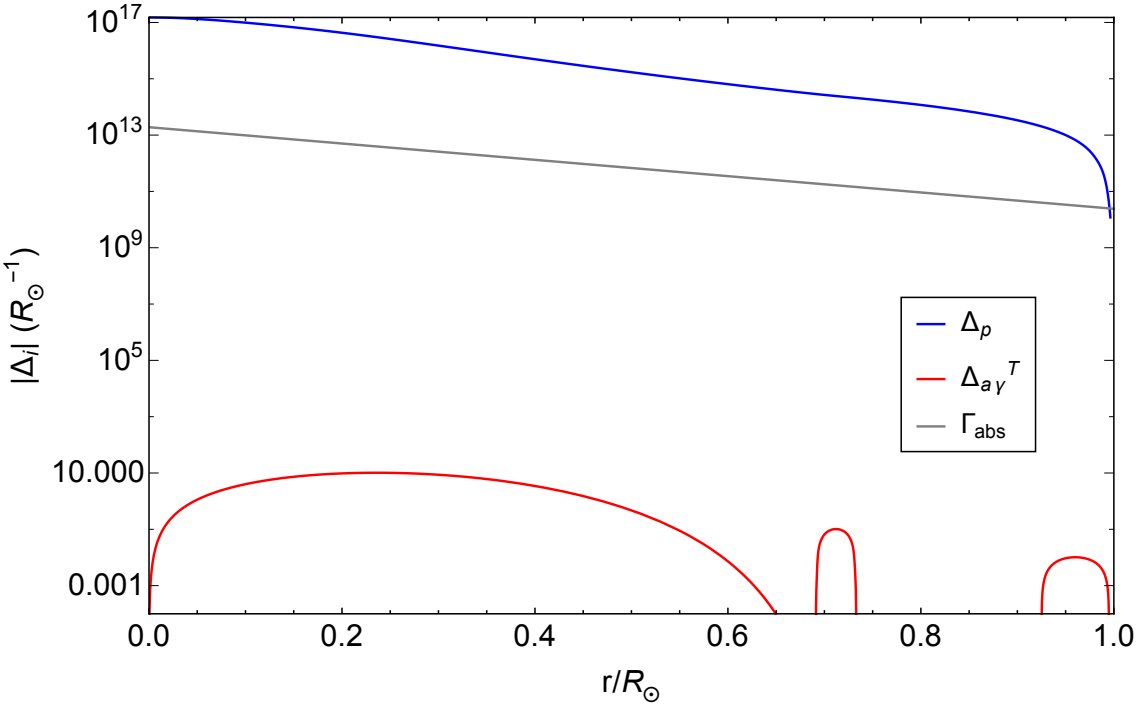

Figure 4.5: Behaviour of photon absorption rate compared to the oscillation parameters of the photon transverse modes.

conversion probability is

$$P(\gamma_T \to a) \approx \left(\frac{g_{a\gamma} B_T \Gamma_{\rm abs}^{-1}}{2}\right)^2 \approx 1.33 \times 10^{-22} \left(\frac{g_{a\gamma}}{5 \times 10^{-11}\ \text{GeV}^{-1}}\right)^2 \left(\frac{B_T}{3 \times 10^5\ \text{G}}\right)^2 \left(\frac{0.4\ \text{cm}}{\Gamma_{\rm abs}}\right)^2 ; \tag{4.15}$$

where we have normalized the expression considering the resonance at $r \sim 0.7\ R_\odot$. [Kri16].

Finally, we consider the off-resonance conversion probability. For the photon transverse modes when the resonance condition does not apply we can take $m_a \sim 0$, that is $\Delta_{\rm osc}^T \approx \Delta_p$. From Fig. 4.5 we see that $\Delta_{\rm p} \gg \Gamma_{\rm abs}$, thus in Eq. (4.9) we can approximate $\sin^2(\Delta_{\rm osc}^T \Gamma_{\rm abs}^{-1}) \approx 1/2$, since there are many photon oscillations within a mean free path $\Gamma_{\rm abs}^{-1}$ and we can just consider the average of the oscillatory term. In this case the TP-ALP conversion

probability is

$$P(\gamma_T \to a) \approx \frac{1}{2}\left(\frac{g_{a\gamma}B_T/2}{\Delta_{\rm p}}\right)^2 \approx 2.14\times10^{-36}\left(\frac{g_{a\gamma}}{5\times10^{-11}\ {\rm GeV}^{-1}}\right)^2\left(\frac{B_T}{3\times10^5\ {\rm G}}\right)^2\left(\frac{10^{26}\ {\rm cm}^{-3}}{n_e}\right)^2\left(\frac{\omega}{\rm keV}\right)^2 ; \tag{4.16}$$

where we have normalized the quantities relatively to their values at $r \sim 0.7\ R_\odot$. Thus, at the same position in the Sun, where $n_e \approx 10^{-23}\ {\rm cm}^{-3}$ and $\omega \sim$ keV, the off-resonance TP-ALP conversion probability is $\sim 10^{-30}$, i.e. it is about 8 order of magnitude smaller than the resonant one.

Photon longitudinal modes

For the longitudinal modes the LP-ALP conversion probability after the beam has traveled a distance z in the homogeneous B-field is Eq. (3.100) [Ter18]

$$P(\gamma_L \to a) = (\Delta^L_{a\gamma} z)^2 \frac{\sin^2(\Delta^L_{\rm osc} z/2)}{(\Delta^L_{\rm osc} z/2)^2} ; \tag{4.17}$$

where in units of solar radius

$$\Delta^L_{a\gamma} = \frac{g_{a\gamma}B_L}{2} \simeq 1.2\times10^{-1}\left(\frac{g_{a\gamma}}{10^{-11}\ {\rm GeV}^{-1}}\right)\left(\frac{B_L}{3\times10^5\ {\rm G}}\right)R_\odot^{-1} ; \tag{4.18}$$

$$\Delta^L_{\rm osc} = \sqrt{4{\Delta^L_{a\gamma}}^2 + (\omega_a - \omega_{\rm p})^2} . \tag{4.19}$$

and $\omega_{\rm p}$ is defined in Eq. (4.12). B_L is the component of the magnetic field longitudinal to the propagation direction of the LP and ω_a is the ALP energy. The oscillation parameters for the longitudinal modes computed using the Solar Model AGSS09 [Ser09] are shown in Fig. (4.6). Also for photon longitudinal modes we need to take into account the photon absorption coefficient $\Gamma_{\rm abs}$ in the Sun interior. The behaviour of $\Gamma_{\rm abs}$ compared to the oscillation parameters of the photon longitudinal modes is shown in Fig. (4.7). Also in this case the photon absorption coefficient $\Gamma_{\rm abs}$ in the solar plasma is not negligible with respect to the other oscillation parameters, but is always larger than the parameter $\Delta_{a\gamma}$.
We can give an estimation of the LP-ALP conversion probability at the distance $z = \Gamma^{-1}_{\rm abs}$. In this case the resonance occurs for $\omega = \omega_{\rm p} = \omega_{\rm a}$, i.e.

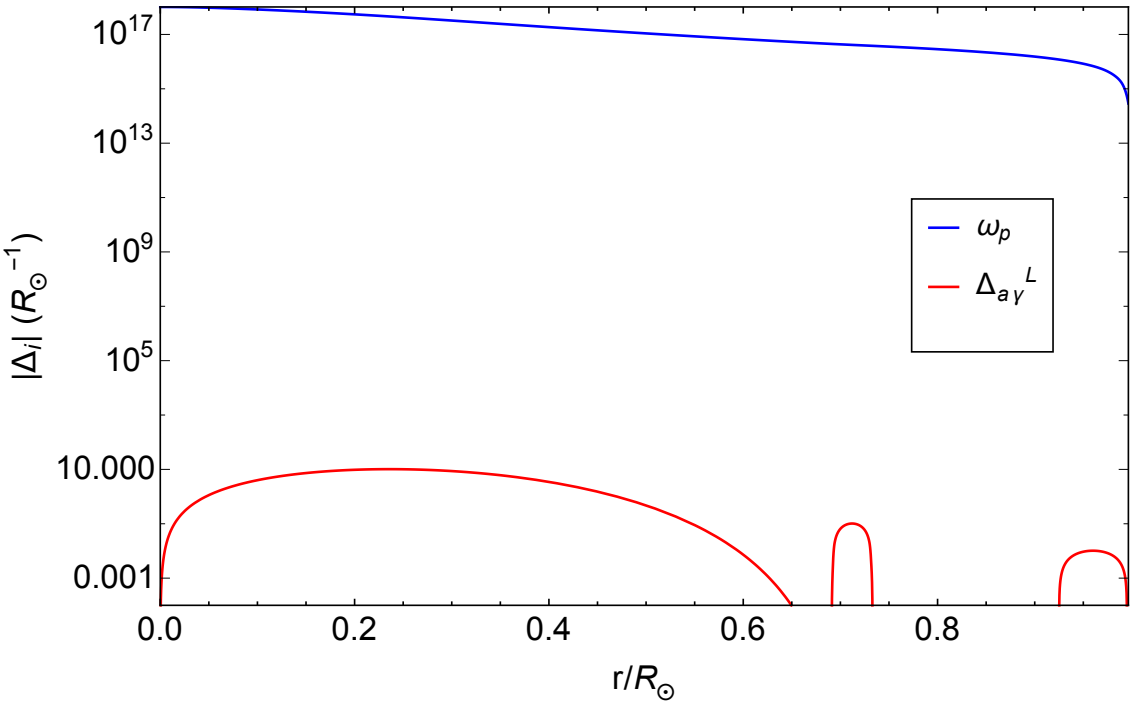

Figure 4.6: Ocillation parameters for LP-ALP conversion in units of $R_\odot^{-1}$.

for the LP energy equal to the plasma frequency and to the axion energy and the condition $\Delta_{\rm osc}(\Gamma_{\rm abs}^{-1}) \ll 1$ stands Eq. (4.17). Thus, if we consider the resonance at $z = \Gamma_{\rm abs}^{-1} \sim 0.4$ cm we find the same result of photon-ALP conversion probability expressed in Eq. (4.15)

$$\begin{aligned} P(\gamma_L \to a) &\approx \left(\frac{g_{a\gamma} B_L \Gamma_{\rm abs}^{-1}}{2}\right)^2 \\ &\approx 1.33 \times 10^{-22} \left(\frac{g_{a\gamma}}{5 \times 10^{-11}\ {\rm GeV}^{-1}}\right)^2 \left(\frac{B_L}{3 \times 10^5\ {\rm G}}\right)^2 \left(\frac{0.4\ {\rm cm}}{\Gamma_{\rm abs}}\right)^2 . \end{aligned} \tag{4.20}$$

For the photon longitudinal modes we can not work off-resonance starting from the equation of motion, since if ω is much different from $\omega_{\rm p}$ the linearization is not valid anymore.

4.2.1 Kinetic approach

The photon absorption rate $\Gamma_{\rm abs}$ in the Sun is not negligible with respect to the others oscillation parameters. Thus, TP-ALP and LP-ALP oscillations are interrupted by collisions and we have to consider an ensemble of photons rather than a single particle description. This *kinetic approach* is similiar to

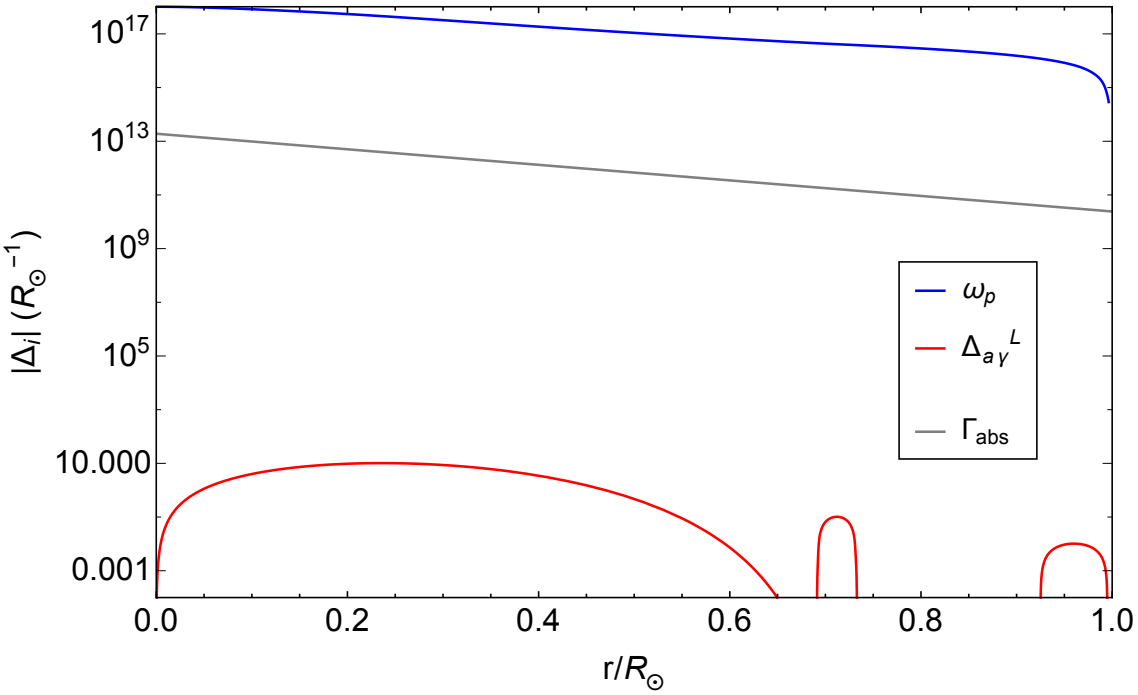

Figure 4.7: Behaviour of photon absorption rate compared to the oscillation parameters of the photon longitudinal modes.

the one used by G. Raffelt and G. Sigl for the relativistic mixed neutrinos in presence of collisions [Sig92]. It has been applied to deal with different mixing problems, such as the mixing of photons with hidden photons (HP) in the Sun [Red13] which we closely follow in our derivation.
We present a completely general formalism, starting from two bosonic fields A and S, which evolve according to the linearized equation of motion

$$i\partial_t \begin{pmatrix} A \\ S \end{pmatrix} = \begin{pmatrix} \omega_A & \mu \\ \mu & \omega_S \end{pmatrix} \begin{pmatrix} A \\ S \end{pmatrix} \ ; \tag{4.21}$$

where ω_A is the energy associated with the field A, ω_S the one associated with the field S and μ is a mixing term which we assume to be small relative to the diagonal terms. Moreover, we consider the case in which collisions occur for the A quanta (i.e. the photons in our case). In this case an adequate description of the problem is given in terms of density matrices [Sig92]. For a fixed momentum $\mathbf{k}$, the free evolution is governed by the Hamiltonian of two coupled harmonic oscillators

$$H = \sum_{i,j=A,S} a_i^\dagger \Omega_{ij} a_j \ ; \tag{4.22}$$

where $a_i^\dagger$ is the creation operator for a quanta i, a_i the annihilation one and

$$\Omega = \begin{pmatrix} \omega_A & \mu \\ \mu & \omega_S \end{pmatrix} = \frac{\omega_A + \omega_S}{2}\mathbb{1} + \begin{pmatrix} \frac{1}{2}\Delta\omega & \mu \\ \mu & -\frac{1}{2}\Delta\omega \end{pmatrix} ; \tag{4.23}$$

where $\Delta\omega = \omega_A - \omega_S$. The term $(\omega_A + \omega_S)/2$ can be reabsorbed as an overall diagonal phase. For such a system, we can define the oscillation frequency

$$\Delta_{\text{osc}} = \sqrt{4\mu^2 + \Delta\omega^2} \, . \tag{4.24}$$

We assume that the field A interacts with the medium, namely with the solar plasma, which can absorb a quantum with rate Γ_{abs} and produce one with rate Γ_{prod}. Consequently, assuming that the interaction does not couple different moment $\mathbf{k}$, the equation of motion for a single momentum mode, described by the density matrix ρ, is the Liouville equation [Sig92]

$$\dot{\rho} = -i[\Omega, \rho] + \frac{1}{2}\{G_{\text{prod}}, \mathbb{1} + \rho\} - \frac{1}{2}\{G_{\text{abs}}, \rho\} ; \tag{4.25}$$

where

$$\begin{aligned} G_{\text{prod}} &= \begin{pmatrix} \Gamma_{\text{prod}} & 0 \\ 0 & 0 \end{pmatrix} ; \\ G_{\text{abs}} &= \begin{pmatrix} \Gamma_{\text{abs}} & 0 \\ 0 & 0 \end{pmatrix} \, . \end{aligned} \tag{4.26}$$

The density matrix $\rho(\mathbf{k})$ for a single momentum state $\mathbf{k}$ can be written in terms of the creation and annhilation operators of quanta i, j as

$$\rho(\mathbf{k}) = \langle a_j^\dagger(\mathbf{k}) a_i(\mathbf{k}') \rangle = (2\pi)^3 \delta^{(3)}(\mathbf{k} - \mathbf{k}') \rho_{ij}(\mathbf{k}) ; \tag{4.27}$$

where $(2\pi)^3\delta^{(3)}(0)$ is expected to diverge, since it is related to the infinite quantization volume necessary for continuous momentum variables. Neverthless, this factor can be set equal to unity because it drops out of final results in all pratical cases [Raf96]. Note that in Eq. (4.25) the coummutator describes the dynamic evolution of the system while the anticommutators correspond to the collisions. In thermal equilibrium $\Gamma_{\text{prod}} = e^{-\omega/T}\Gamma_{\text{abs}}$ and the S type particles are not excited, while we assume that the A type particles obey the Bose-Einstein statistics $f_{\text{BE}} = (e^{\omega/T} - 1)^{-1}$. A non equilibrium

situation is described with a small deviation $\delta\rho$ from the thermal equilibrium state $\rho_{\rm eq}$, thus

$$\rho = \rho_{\rm eq} + \delta\rho = \begin{pmatrix} f_{\rm BE} & 0 \\ 0 & 0 \end{pmatrix} + \delta\rho \ . \tag{4.28}$$

In Eq. (4.25) the collision terms, i.e. the anticommutators, vanish for $\rho_{\rm eq}$, thus the Liouville equation reduces to

$$\dot{\rho} = -i[\Omega, \rho] - \frac{1}{2}\{G, \delta\rho\} \ ; \tag{4.29}$$

where we have introduced $G = {\rm diag}(\Gamma, 0)$, with $\Gamma = (1 - e^{-\omega/T})\Gamma_{\rm abs}$ [1], i.e. the total collisional rate. We can write $\delta\rho$ as

$$\delta\rho = \begin{pmatrix} n_A & g \\ g & n_S \end{pmatrix} \ ; \tag{4.30}$$

where n_A is the occupation numbers of A quanta, n_S the occupation numbers of S quanta and g represents the mixing between the two levels. If we insert Eqs. (4.28)–(4.30) into Eq. (4.29) we obtain the equations of motion

$$\dot{n}_A = -\Gamma n_A - 2\mu{\rm Im}(g) \ ; \tag{4.31}$$

$$\dot{n}_S = 2\mu{\rm Im}(g) \ ; \tag{4.32}$$

$$\dot{g} = -\big(\frac{1}{2}\Gamma + i\Delta\omega\big)g + i\mu(f_{\rm BE} + n_A - n_S) \ . \tag{4.33}$$

The mixing μ is always small so basically we are never far from the thermal equilibrium, i.e. $f_{\rm BE} \gg n_A$ and $f_{\rm BE} \gg n_S$. In this limit Eq. (4.33) reads

$$\dot{g} = -\big(\frac{1}{2}\Gamma + i\Delta\omega\big)g + i\mu f_{\rm BE} \ . \tag{4.34}$$

Assuming the initial condition $g(0) = 0$ the solution of Eq. (4.34) is then

$$g(t) = \frac{1 - e^{-(i\Delta\omega + \Gamma/2)t}}{\Delta\omega - i\frac{\Gamma}{2}}\mu f_{\rm BE} \ . \tag{4.35}$$

After an initial transient, Eq. (4.35) approaches the steady-state solution

$$g_\infty = \frac{\Delta\omega + i\Gamma/2}{\Delta\omega^2 + \Gamma^2/4}\mu f_{\rm BE} \ . \tag{4.36}$$

[1] The total collisional rate Γ is different for transverse and longitudinal photons because it depends on different processes. Thus, in principle we should define the two collisional rates Γ_T and Γ_L for TP and LP, respectively.

If we insert this latter in Eq. (4.32) we finally obtain the S quanta production rate

$$\Gamma_S^{\rm prod} \equiv \dot{n}_S = \frac{\Gamma\mu^2}{(\omega_A-\omega_S)^2+\Gamma^2/4}\frac{1}{e^{\omega/T}-1}\ . \tag{4.37}$$

From Eq. (4.37) we obtain that the $A-S$ mixing process is *resonant*, i.e. it is maximal for $\omega_A=\omega_S$. The result in Eq. (4.37) is completely general and it is valid both at the resonance and off-resonance, since it has been obtained on the only assumption that the mixing term μ is small relative to the diagonal terms $\sim\Delta\omega$. This condition always applies in the solar plasma, both for photon transverse modes and longitudinal ones. Thus we can specialize Eq. (4.37) to the cases of TP-ALP and LP-ALP conversion rates.

Photon transverse modes

The linearized equations of motion for photon transverse modes read [2]

$$i\partial_t\begin{pmatrix}A_\parallel\\ a\end{pmatrix} = H_T\begin{pmatrix}A_\parallel\\ a\end{pmatrix}\ ; \tag{4.38}$$

where $A_\parallel$ is the photon polarization state parallel to the transverse solar B-field, a is the axion field and

$$H_T=\begin{pmatrix}\frac{\omega_{\rm p}^2}{2\omega} & \frac{g_{a\gamma}B_T}{2}\\ \frac{g_{a\gamma}B_T}{2} & \frac{m_a^2}{2\omega}\end{pmatrix} = \frac{\omega_{\rm p}^2-m_a^2}{2\omega}\mathbb{1}+\begin{pmatrix}\frac{1}{2}q & \Delta_{a\gamma}^T\\ \Delta_{a\gamma}^T & -\frac{1}{2}q\end{pmatrix}\ ; \tag{4.39}$$

where here $q=(\omega_{\rm p}^2-m_a^2)/2\omega$. Thus, with the substitutions $\mu\to\Delta_{a\gamma}$ and $\Delta\omega\to q$, we obtain from Eq. (4.37) the TP-ALP conversion rate

$$\Gamma_a^{\rm prod} = \left[\frac{\Gamma{\Delta_{a\gamma}^T}^2}{\left(\frac{\omega_{\rm p}^2-m_a^2}{2\omega}\right)^2+\Gamma^2/4}\right]\frac{1}{e^{\omega/T}-1}\ . \tag{4.40}$$

The expression in Eq. (4.40) is valid both on resonance and off-resonance and we will use it to estimate the ALP flux expected at Earth arising from these conversion processes.

[2] If we assume relativistic states, i.e. states such that $\omega\approx k$, we can consider the replacement $i\partial_z\to i\partial_t$ in the equation of motion.

Photon longitudinal modes

The linearized equation of motion for the photon longitudinal modes is

$$i\partial_t \begin{pmatrix} A_L \\ a_k \end{pmatrix} = H_L \begin{pmatrix} A_L \\ a_k \end{pmatrix} \ ; \tag{4.41}$$

where A_L is the LP state, a_k is the axion field redifined according to the definitions given in Chapter 3 and

$$H_L = \begin{pmatrix} \omega_p & \frac{g_{a\gamma}B_L}{2} \\ \frac{g_{a\gamma}B_L}{2} & \omega_a \end{pmatrix} = \frac{\omega_{\rm p}+\omega_a}{2}\mathbb{1} + \begin{pmatrix} \frac{1}{2}\Delta\omega & \Delta^L_{a\gamma} \\ \Delta^L_{a\gamma} & -\frac{1}{2}\Delta\omega \end{pmatrix} \ ; \tag{4.42}$$

where in this case $\Delta\omega = \omega_{\rm p} - \omega_a$. If we insert this expression of $\Delta\omega$ and we replace $\mu \to \Delta_{a\gamma}$ in Eq. (4.37) we obtain the LP-ALP conversion rate

$$\Gamma_a^{\rm prod} = \left[\frac{\Gamma {\Delta^L_{a\gamma}}^2}{(\omega_{\rm p}-\omega_a)^2+\Gamma^2/4}\right]\frac{1}{e^{\omega/T}-1} \ . \tag{4.43}$$

This expression has been recently obtained in [OH20] from a thermal field theory calculation. Contrarily to the photon transverse modes, the expression Eq. (4.43) is valid only on resonance, since it is based on the flavor evolution of on-shell LPs, i.e. it is obtained assuming that $\omega \sim \omega_{\rm p} \sim \omega_a$ and it is not applicable for ω very different from $\omega_{\rm p}$.

4.3 Solar ALP flux at Earth

The number of ALPs at Earth per unit of time in units of $\rm cm^{-2}\ s^{-1}$ is

$$\frac{dN_a}{dt} = \frac{g}{4\pi D_\odot^2}\int d^3\mathbf{r}\frac{d^3\mathbf{k}}{(2\pi)^3}\Gamma_a^{\rm prod} \ ; \tag{4.44}$$

where $D_\odot \sim 1.49\times10^{11}$ m is the Earth-Sun distance, $\Gamma_a^{\rm prod}$ is the ALP production rate expressed by Eq.(4.37), the factor g is the number of the polarization states of photons ($g=1$ for LPs and $g=2$ for photon transverse modes) and the integration is performed over all the photons energies $\mathbf{k}$ and over the solar volume. From Eq. (4.44) we recover the differential ALP flux expected at Earth in units of $\rm cm^{-2}\ s^{-1}\ keV^{-1}$

$$\frac{d\Phi_a}{d\omega} = \frac{g}{(2\pi)^3 D_\odot^2}\int_0^{R_\odot} dr r^2 \int d\Omega_{\mathbf{k}}\frac{dk}{d\omega}k^2\Gamma_a^{\rm prod} \ ; \tag{4.45}$$

where $R_\odot \approx 6.96 \times 10^8$ m is the solar radius and $\Omega_{\mathbf{k}}$ is the solid angle around the direction of photon momentum $\mathbf{k}$. If we assume relativistic states $\omega \approx k$ and $dk/d\omega \approx 1$. With these assumptions Eq. (4.45) becomes

$$\frac{d\Phi_a}{d\omega} \approx \frac{g}{(2\pi)^3 D_\odot^2} \int_0^{R_\odot} dr r^2 \int d\Omega_{\mathbf{k}} \omega^2 \Gamma_a^{\rm prod} \ . \tag{4.46}$$

We now focus on the estimation of the ALP flux at Earth from different conversion processes in the solar magnetic fields.

4.3.1 Flux from TP-ALP conversions in the Sun

For TP-ALP conversions in the Sun the ALP production rate is expressed by Eq. (4.40)

$$\Gamma_a^{\rm prod} = \left[\frac{\Gamma {\Delta_{a\gamma}^T}^2}{\left(\frac{\omega_{\rm p}^2 - m_a^2}{2\omega}\right)^2 + \Gamma^2/4} \right] \frac{1}{e^{\omega/T} - 1} \ . \tag{4.47}$$

This expression is valid both on resonance, i.e. when the condition $\omega_{\rm p}^2 = m_a^2$ applies, and off-resonance, when $m_a \neq \omega_{\rm p}$. Therefore we can specialize our discussion in these two different cases.

Resonant production

The TP-ALP conversion process is dominated by resonance, where the TP-ALP conversion probability [Eq. (4.9)] is maximum. All over the solar interior $\Gamma \ll m_a^2/2\omega$, as we see from Fig. 4.5, since for every fixed m_a we have that $m_a^2/2\omega = \Delta_{\rm p}$. Thus, the ALPs production process is narrowly concentrated around $\omega_p^2 = m_a^2$ and we may approximate it [Eq. (4.47)] with a delta function

$$\Gamma_a^{\rm prod} \approx \pi 2 {\Delta_{a\gamma}^T}^2 \delta\left(\frac{\omega_{\rm p}^2 - m_a^2}{2\omega}\right) \frac{1}{e^{\omega/T} - 1} \approx \frac{\pi}{2} (g_{a\gamma} B_T)^2 \delta\left(\frac{\omega_{\rm p}^2 - m_a^2}{2\omega}\right) \frac{1}{e^{\omega/T} - 1} \ . \tag{4.48}$$

If we insert the last expression in Eq. (4.46), we note that the integration over the volume gives

$$\int dr \delta(q) \approx \left| \frac{dq}{dr} \right|_{\rm res}^{-1} = 2\omega \left| \frac{d\omega_{\rm p}^2}{dr} \right|_{\rm res}^{-1} ; \tag{4.49}$$

where we have denoted with $q = (\omega_{\rm p}^2 - m_a^2)/2\omega$. Finally

$$\left| \frac{d\omega_{pl}^2}{dr} \right|_{res}^{-1} = \frac{1}{m_a^2} \left| \frac{d \ln n_e}{dr} \right|_{res}^{-1} = \frac{1}{m_a^2} R_e \ ; \tag{4.50}$$

where R_e is a parameter introduced assuming an exponential model for the electron density

$$n_e = n_e^0 e^{-r/R_e} \tag{4.51}$$

in the region $r \lesssim 0.8\ R_\odot$, with

$$R_e = R_\odot/9.89 \tag{4.52}$$

$$n_e^0 = 1.11 \times 10^{26}\ \text{cm}^{-3}\ . \tag{4.53}$$

If we consider the relation between the plasma frequency and the electron number density

$$\omega_{\rm p}^2 = 4\pi\alpha \frac{n_e}{m_e}\ ; \tag{4.54}$$

we obtain that $\ln \omega_{\rm p}^2 \sim \ln n_e \sim r/R_e$.
Furthermore, we notice that in the case of resonance $\Delta_{\rm osc}^T \ll \Gamma_{\rm abs}$ (see Fig. 4.5). Therefore, during the resonance the photons are continuously re-scattered such that information about their polarization is lost. The photon trajectories can form any angle with the magnetic field $\mathbf{B}$. Since the photon trajectories are not straight, this angle is not correlated with the magnetic field direction and the photon polarization. Therefore, we have to perform a local angular average in the resonance shell before performing the integral in $d\Omega_{\mathbf{k}}$ of Eq. (4.46). For a generic photon polarization, the B_T strength entering the conversion probability is

$$B_T = |\mathbf{B}(\mathbf{x}) \cdot \hat{\epsilon}| = |\mathbf{B}(\mathbf{x}) \sin\vartheta(\mathbf{x}) \cos\varphi|\ , \tag{4.55}$$

where $\mathbf{x}$ is the position vector of the resonance region in a particular direction $\hat{x}$, $\hat{\epsilon}$ is the photon polarization vector ($|\hat{\epsilon}| = 1$, $\hat{\epsilon} \times \hat{x} = 0$), ϑ is the angle between the magnetic field $\mathbf{B}(\mathbf{x})$ and the photon propagation direction $\hat{x}$ and φ the angle between $\mathbf{B}_T$ (the component of the magnetic field perpendicular to $\mathbf{x}$) and $\hat{\epsilon}$. We define

$$\langle B_T^2 \rangle = |\mathbf{B}|^2 \int \frac{d\varphi}{2\pi} \frac{d\Omega_\vartheta}{4\pi} \sin^2\vartheta \cos^2\varphi = \frac{1}{3}|\mathbf{B}|^2\ . \tag{4.56}$$

Therefore, in Eq. (4.48) we should substitute $B_T^2 \to \langle B_T^2 \rangle = |\mathbf{B}|^2/3$.
Finally, we obtain the ALP flux spectrum from resonant conversions in the solar magnetic field expected at Earth inserting Eqs. (4.48)–(4.50)–(4.56) in Eq. (4.46)

$$\frac{d\Phi_a}{d\omega} = \frac{1}{3\pi D_\odot^2} \left(\frac{g_{a\gamma} |\mathbf{B}(R_{\rm res})|}{m_a} \right)^2 R_{\rm res}^2 R_e \frac{\omega^3}{e^{\frac{\omega}{T_{\rm res}}} - 1}\ ; \tag{4.57}$$

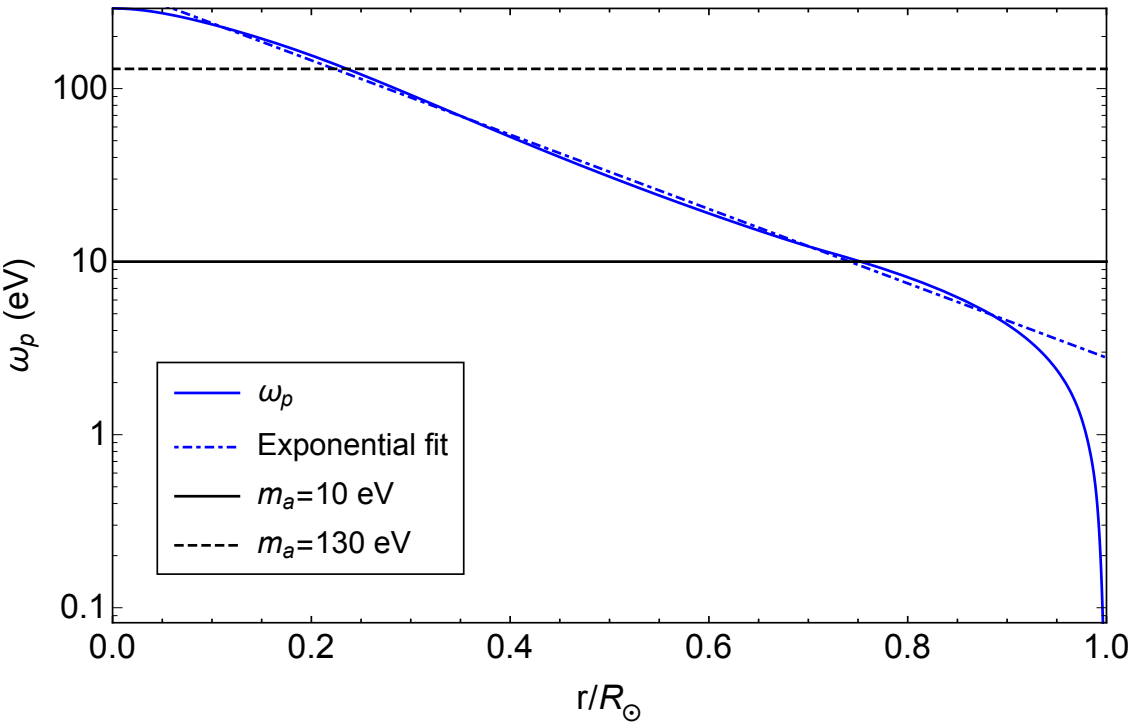

Figure 4.8: The plasma frequency $\omega_{\rm p}$ as a function of $r/R_\odot$ (blue line) and the exponential fit (orange line) are shown. Resonance occurs at $r \sim 0.25\ R_\odot$ and at $r \sim 0.75\ R_\odot$ for $m_a = 130$ eV and $m_a = 10$ eV, respectively.

where $R_{\rm res}$ is the position in the Sun where the resonance condition occurs for the fixed value of m_a and $T_{\rm res}$ is the temperature at the same position. From Fig. 4.8 we obtain that a resonance occurs for $m_a = 10$ eV and for $m_a = 130$ eV at $r \sim 0.7\ R_\odot$ and $r \sim 0.25\ R_\odot$, respectively in the tachocline and in the radiative zone, where the condition $m_a = \omega_{\rm p}$ is satisfied. First, let us consider the ALP spectrum for the resonance in the tachocline at $r \sim 0.7\ R_\odot$, where $m_a \sim 10$ eV and $B \sim 3 \times 10^5$ G. This one occurs at a position where the homogeneous B-field in the tachocline has its peaks, as shown in Fig. 4.3. We can obtain the total ALP flux Φ_a from resonant conversion in the solar magnetic fields expected at Earth by the integration of Eq. (4.57) over the energies ω. The flux parameter for $m_a = 10$ eV are

Table 4.1: Parameters of the solar ALP spectrum for different values of m_a.

m_a(eV)	C	ω_0 (keV)	α
10	9.4×10^{11}	0.61	2.46
130	1.36×10^{15}	2.80	2.47
0	8.3×10^{10}	3.15	3.16

found to be

$$\Phi_a = 2.48 \times 10^{10}\, g_{10}^2 \text{ cm}^{-2} \text{ s}^{-1} ; \tag{4.58}$$

$$\langle\omega\rangle = 0.6 \text{ keV} ; \tag{4.59}$$

$$L_a = 1.51 \times 10^{-5}\, g_{10}^2\, L_\odot ; \tag{4.60}$$

where L_a is the ALP luminosity, $L_\odot$ is the Sun luminosity, $\langle\omega\rangle$ is the average energy of the ALP flux spectrum and $g_{10} = g_{a\gamma}/10^{-10}$ GeV^{-1}. An analytic approximation to the solar ALP flux spectrum is provided by a fit with the three-parameter function [And07]

$$\frac{\mathrm{d}\Phi_a}{\mathrm{d}\omega} = g_{10}^2 C \left(\frac{\omega}{\omega_0}\right)^{\alpha} e^{-(\alpha+1)\frac{\omega}{\omega_0}} ; \tag{4.61}$$

where C is a normalization constant and the energy ω is expressed in keV. If we match this fit with our numerical data we obtain the parameters C, α and ω_0 shown in Table 4.1. In Fig. 4.9 we show a comparison between our numerical data and the fit function in Eq. (4.61) and their respective ratio. We find that the fit function reproduces well our numerical data in the central part of the spectrum, but in the tails at $\omega < 0.2$ keV and $\omega > 1$ keV there are larger discrepancies.

Let us focus now on the resonance at $r \sim 0.25\ R_\odot$, i.e. the one with $m_a = 130$ eV. This occurs in the radiative zone, at a position where the B-field assumes its peak value, as shown in Fig. 4.3. Here we present results obtained assuming $B = 3 \times 10^7$ G. For the resonant flux with mass $m_a = 130$ eV we find the following flux parameters

$$\Phi_a = 1.63 \times 10^{14}\, g_{10}^2 \text{ cm}^{-2} \text{ s}^{-1} \text{ keV}^{-1} ; \tag{4.62}$$

$$\langle\omega\rangle = 2.76 \text{ keV} ; \tag{4.63}$$

$$L_a = 0.2\, g_{10}^2\, L_\odot . \tag{4.64}$$

We resport in Table 4.1 the fitting parameters of the energy spectrum of Eq. (4.61). In Fig. 4.10 we show a comparison between our numerical data and the fit function in Eq. (4.61) and their respective ratio. Also in this case we find that the fit is accurate around the peak of the spectrum, while there are larger discrepancies for $\omega < 1$ keV and $\omega > 5$ keV.

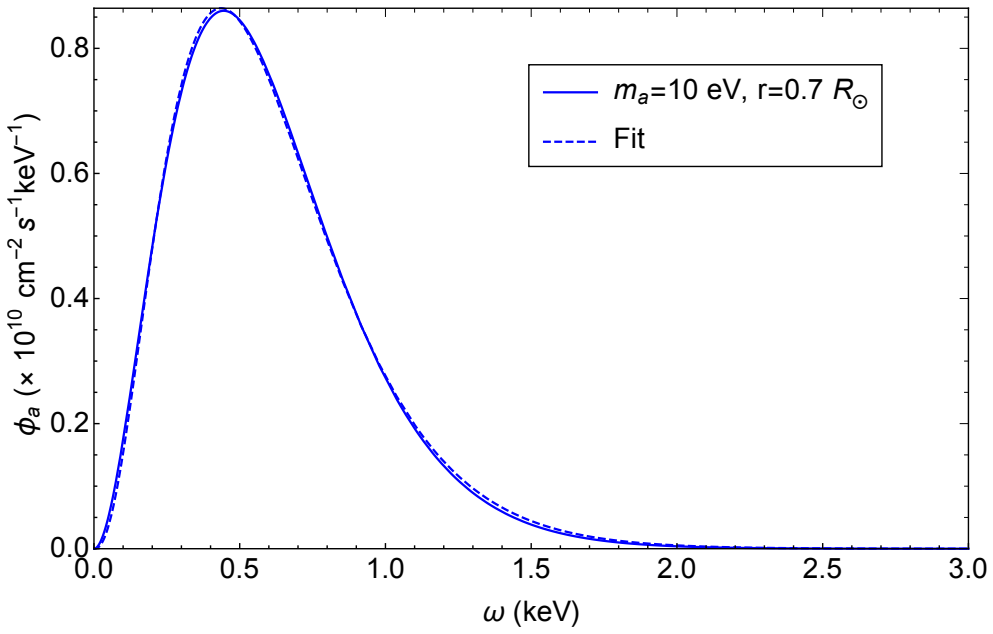

(a)

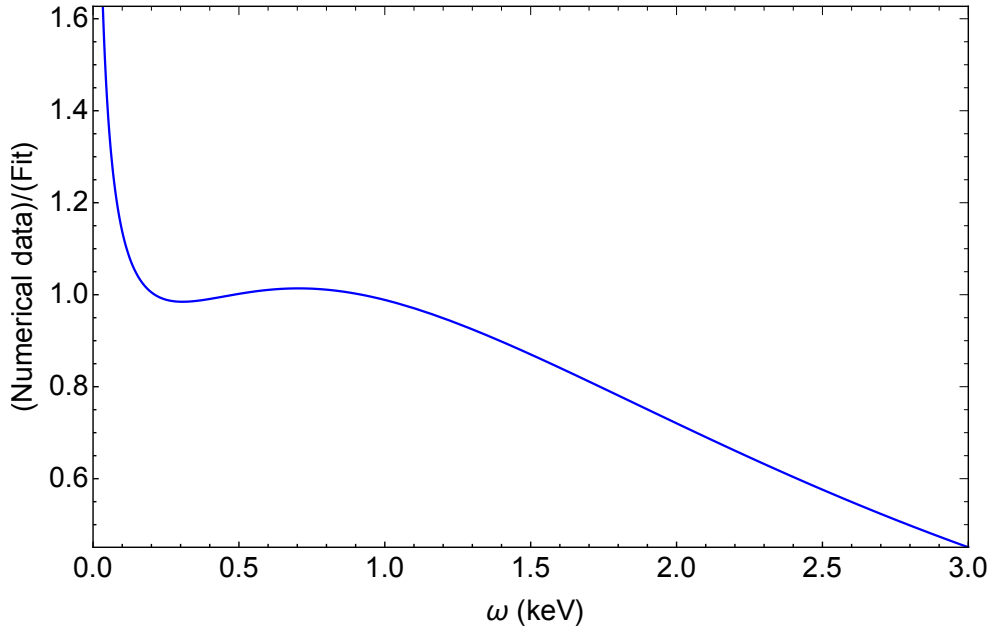

(b)

Figure 4.9: In Fig. 4.9a the numerical data for the resonant flux from resonant conversions in the tachocline is compared to the fit function of Eq. (4.61). The flux was computed assuming $B = 30 \times 10^4$ G and $g_{a\gamma} = 5 \times 10^{-11}$ GeV^{-1}. Fig. 4.9b shows the ratio between the numerical data and our fit.

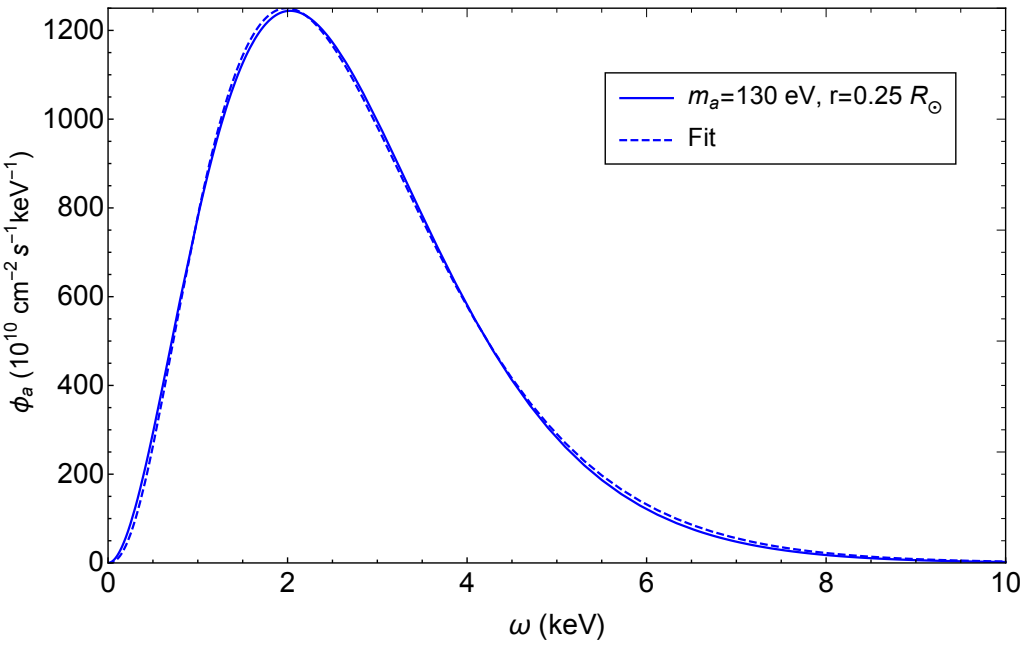

(a)

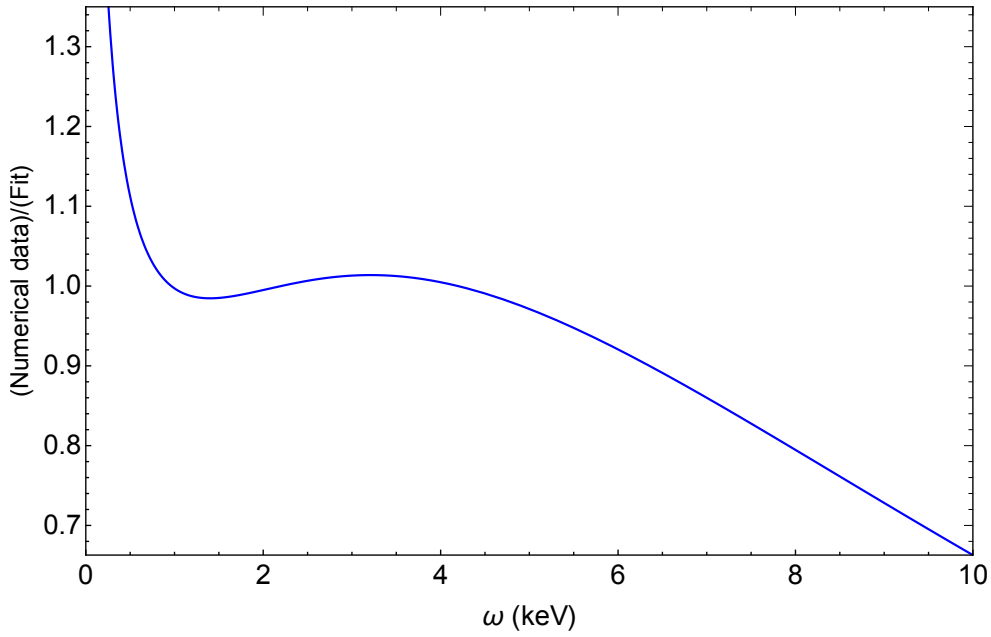

(b)

Figure 4.10: In Fig. 4.10a the numerical data for the resonant flux from resonant conversion in the radiative zone is compared to the fit function of Eq. (4.61). The flux was computed assuming $B = 3 \times 10^7$ G and $g_{a\gamma} = 5 \times 10^{-11}$ GeV^{-1}. Fig. 4.10b shows the ratio between the numerical data and our fit.

Non-resonant production

If we are far from resonance we can assume $m_a \approx 0$. In this case $\Delta_{\rm osc}^T \approx \Delta_{\rm p} \gg \Gamma_{\rm abs}$, as shown in Fig. 4.5. Thus, the rate in Eq. (4.40) reduces to

$$\Gamma_a^{\rm prod} \approx \Gamma \frac{{\Delta_{a\gamma}^T}^2}{(\omega_{pl}^2/2\omega)^2} \frac{1}{e^{\omega/T}-1} = \Gamma_{\rm abs}(1-e^{-\omega/T}) \frac{{\Delta_{a\gamma}^T}^2}{(\omega_{pl}^2/2\omega)^2} \frac{1}{e^{\omega/T}-1} \ . \quad (4.65)$$

If we insert Eq. (4.65) in Eq. (4.45) and we integrate over the Standard Solar Model AGSS09 [Ser09] we obtain the ALP flux spectrum at Earth from off-resonance production in the solar magnetic fields. In this case the direction ϑ between the field $\mathbf{B}$ and the photon direction of propagation does not change during the conversions, since many oscillations occur into a single photon mean free path. However, the azimuthal angle φ between the transverse field B_T and the photon polarization $\hat{\epsilon}$ would change. Thus, we perform an average over φ before the integral over $d\Omega_{\mathbf{k}}$ in Eq. (4.45) is performed, i.e.

$$\int d\Omega_{\mathbf{k}} \int_0^{2\pi} \frac{d\varphi}{2\pi} |\mathbf{B}|^2 \sin^2\vartheta(\mathbf{x}) \cos^2\varphi = \pi \frac{4}{3} |\mathbf{B}|^2 \ . \quad (4.66)$$

The dominant contribution comes from the radiative zone, since here the B-field amplitude reaches the highest value. The off-resonance contributions from the tachocline and the convective zone are negligible. Thus, for the radiative zone we use the B-field profile in Eq. (4.2) and we fix the peak value $B = 3 \times 10^7$ G. For the non-resonant ALP spectrum flux we find the following flux parameters

$$\Phi_a = 5.2 \times 10^9 g_{10}^2 \ {\rm cm}^{-2} \ {\rm s}^{-1} \ ; \quad (4.67)$$

$$\langle\omega\rangle = 3.24 \ {\rm keV} \ ; \quad (4.68)$$

$$L_a = 1.92 \times 10^{-8} \ g_{10}^2 \ L_\odot \ . \quad (4.69)$$

In Table 4.1 we present the fitting parameters of the energy spectrum of Eq. (4.61). The errors are shown in Fig. 4.11 where we compare the numerical data with our fit and we show their ratio.

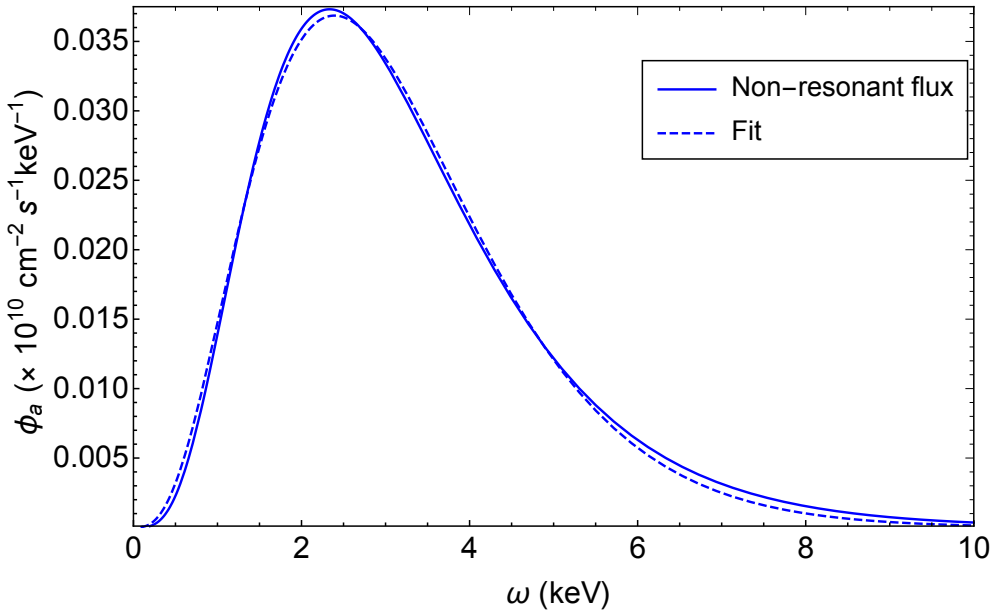

(a)

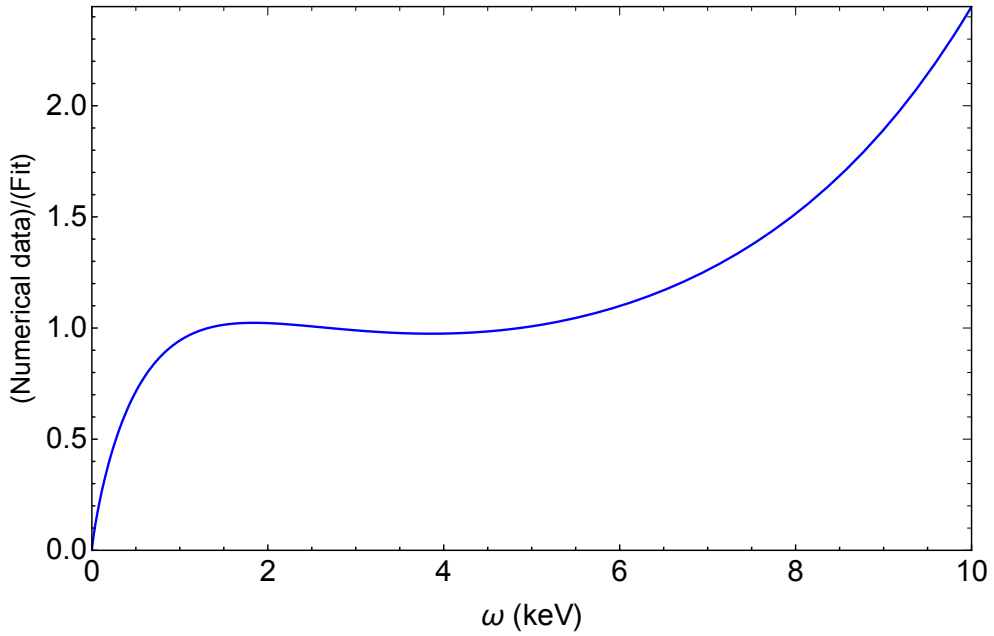

(b)

Figure 4.11: In Fig. 4.11a the numerical data for the non-resonant flux from conversions in the radiative zone is compared to the fit function of Eq. (4.61). The flux was computed assuming $B = 3 \times 10^7$ G and $g_{a\gamma} = 5 \times 10^{-11}$ GeV^{-1}. Fig. 4.10b shows the ratio between the numerical data and our fit.

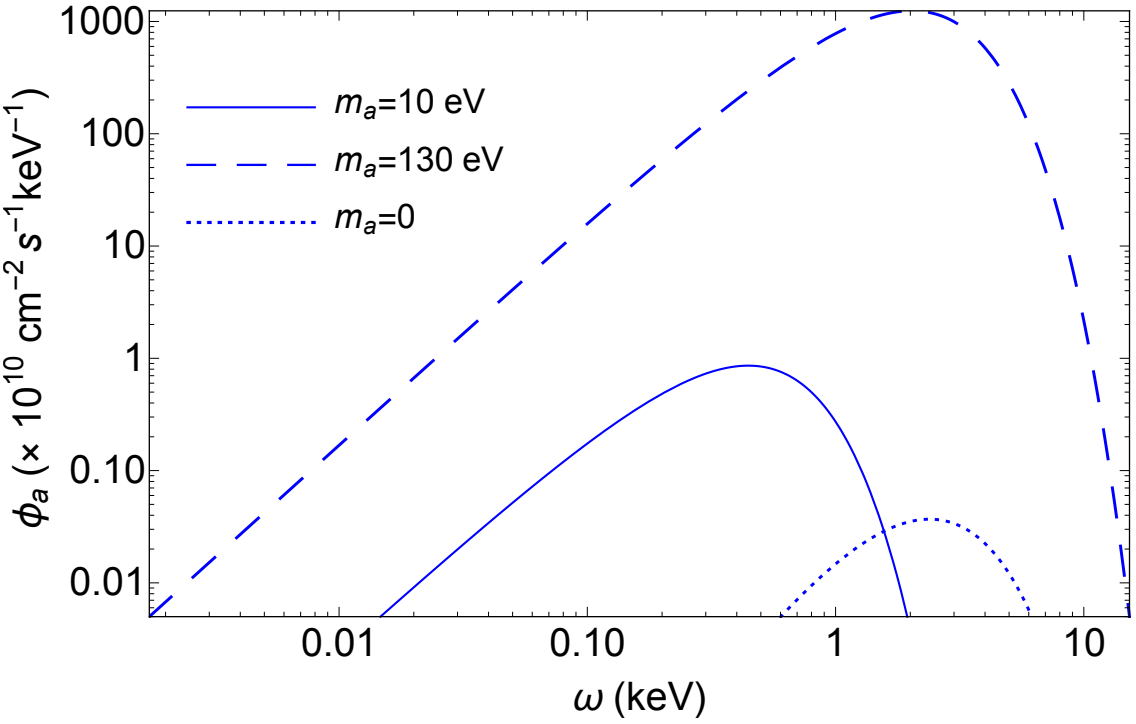

Figure 4.12: Comparison between the fluxes from TP-ALP conversions in solar magnetic field. The largest contribution is given by the resonant production.

In Fig. (4.12) we compare the fluxes from TP-ALP conversions in solar magnetic fields. We see that the non-resonant contribution is always smaller than the resonant one. Thus, we can neglect it in our discussion, since the major correction to the Primakoff flux will be given just by the fluxes from resonant conversions.

4.3.2 Flux from LP-ALP conversions in the Sun

The ALP production rate for LP-ALP conversions in the solar magnetic fields is Eq. (4.43)

$$\Gamma_a^{\rm prod} = \left[\frac{\Gamma {\Delta_{a\gamma}^L}^2}{(\omega_{\rm p}-\omega_a)^2+\Gamma^2/4}\right]\frac{1}{e^{\omega/T}-1}\,. \tag{4.70}$$

This expression is valid only on resonance, i.e. when $\omega_{\rm p} = \omega_{\rm a}$, since we are working on-shell and the result is not true for energies much different from $\omega_{\rm p}$. This result has been recently obtained in [OH20]. Neverthless, in

their work they obtained a more general result using a thermal field theory approach. On resonance our rate [Eq. (4.70)] perfectly reproduces their one. Since the largest contribution arises from conversions in the radiative zone, we will present results just for the largest value of the B-field in this region, i.e. $B = 3 \times 10^7$ G. Also in the case of LP-ALP conversions the process is extremely peaked around the resonance, thus we can approximate $\Gamma_a^{\rm prod}$ with a delta function

$$\Gamma_a^{\rm prod} \approx 2\pi {\Delta_{a\gamma}^L}^2 \delta(\omega_{\rm p} - \omega_a) \; . \tag{4.71}$$

In the case of LP there is just one projection of the magnetic field which is longitudinal to the photon propagation direction, i.e. $B_L = |\mathbf{B}\cos\vartheta|$. Then, in the resonant shell we should consider the average

$$\langle B_L^2 \rangle = \int \frac{d\varphi}{2\pi} \int \frac{d\Omega_\vartheta}{4\pi} |\mathbf{B}|^2 \cos^2\vartheta = \frac{1}{3}|\mathbf{B}|^2 \; . \tag{4.72}$$

If we insert this expression in Eq. (4.71) and then in Eq. (4.45) we obtain the ALP flux from LP-ALP conversion in the Sun

$$\begin{aligned} \frac{d\Phi_{LP}}{d\omega} &= \frac{1}{4\pi D_\odot^2} \int_\odot d^3\mathbf{r} \frac{\omega^2}{(2\pi)^3} \frac{g_{a\gamma}^2 |\mathbf{B}(r)|^2}{e^{\omega/T} - 1} \frac{2\pi^2}{3} \delta(\omega - \omega_p(r)) \\ &= \frac{1}{12\pi D_\odot^2} \int_0^{R_\odot} dr r^2 \frac{\omega^2 g_{a\gamma}^2 |\mathbf{B}(r)|^2}{e^{\omega/T} - 1} \delta(\omega - \omega_p(r)) \\ &= \frac{1}{12\pi D_\odot^2} r_0^2 \frac{\omega^2 g_{a\gamma}^2 |\mathbf{B}(r_0)|^2}{e^{\omega/T} - 1} \frac{1}{|\omega'(r_0)|} \; ; \end{aligned} \tag{4.73}$$

where r_0 is the position in the Sun where the resonance $\omega = \omega_{\rm p}$ occurs, $|\omega'(r_0)| = |d\omega_p/dr|$ computed at $r = r_0$ and we have denoted with $\omega \approx \omega_a \approx \omega_p$ the ALP and photon energies. The result in Eq. (4.73) has been recently obtained in [OH20]. The derivative in Eq. (4.73) can be expressed as

$$\left| \frac{d\omega_p}{dr} \right|_{r=r_0}^{-1} = \left| \frac{d\omega_p}{d\omega_p^2} \frac{d\omega_p^2}{dr} \right|_{r=r_0}^{-1} = \frac{2R_e}{\omega_p} \; ; \tag{4.74}$$

where the result in Eq. (4.50) was used. If we use the Standard Solar Model AGSS09 [Ser09] to compute the plasma frequencies we obtain the ALP flux spectrum shown in Fig. 4.13.

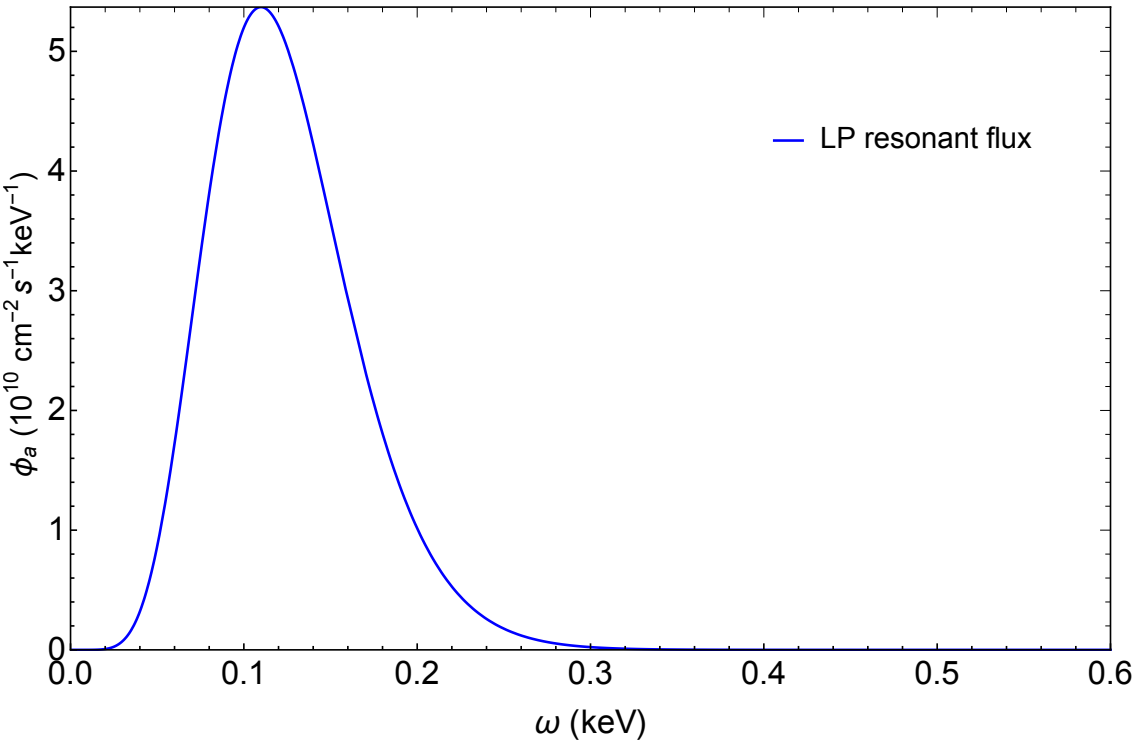

Figure 4.13: ALP flux expected at Earth from LP-ALP conversions in the Solar magnetic field. The flux was computed assuming $g_{a\gamma} = 5 \times 10^{-11}$ GeV^{-1} and $B = 3 \times 10^7$ G.

The flux shows a peak at $\omega \sim 0.12$ keV. The flux parameters are found to be

$$\Phi_a = 2.18 \times 10^{10}\, g_{10}^2 \text{ cm}^{-2} \text{ s}^{-1} ; \tag{4.75}$$

$$\langle \omega \rangle = 0.13 \text{ keV} ; \tag{4.76}$$

$$L_a = 3.34 \times 10^{-6}\, g_{10}^2\, L_\odot ; . \tag{4.77}$$

4.4 Bounds and detection perspectives

Let us focus on the contribute to the flux arising from all the conversion processes in the Sun shown in Fig. (4.14).

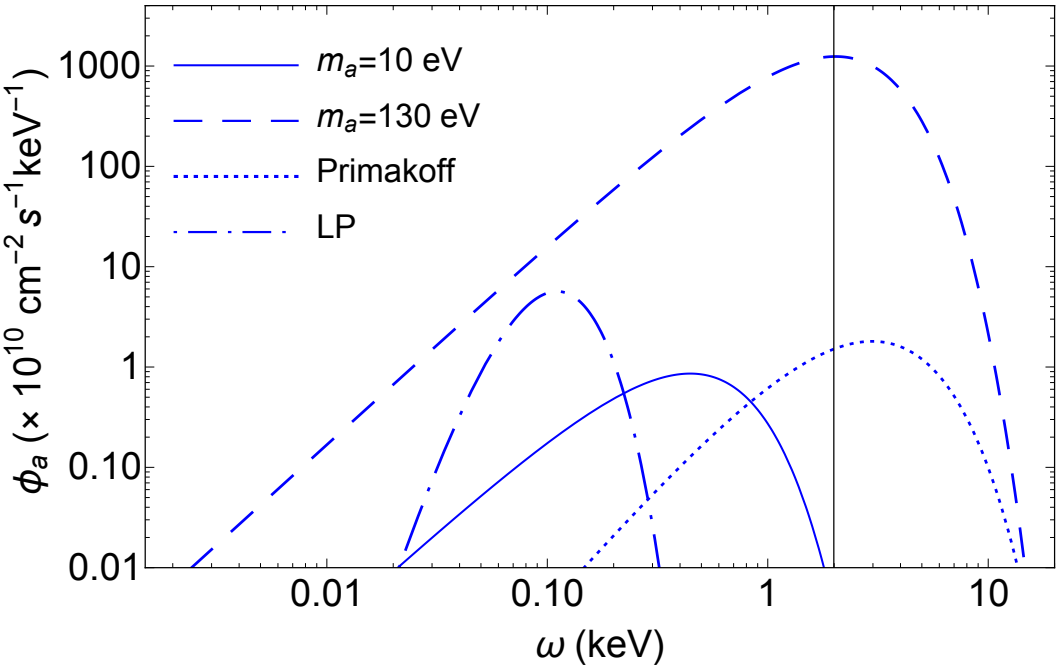

Figure 4.14: Contributions from all ALP fluxes from the Sun. The dotted line is the Primakoff flux. The continuous and the dashed blue lines are the flux from the resonant conversion in the solar magnetic field for an axion mass $m_a = 10$ eV and $m_a = 130$ eV, respectively. The dot-dashed blue line is the flux from the LP-ALP conversions. The vertical black line is the CAST energy threshold.

Both the flux from LP-ALP conversions and the one from TP-ALP resonant conversions for $m_a \sim 10$ eV are dominant at energies $\omega <$ keV, below the CAST threshold [And07] ($\omega < 2$ keV). Unfortunately, the flux at Earth from TP-ALP conversions in large scale solar magnetic fields for ALPs with mass $m_a \sim 10$ eV is not detectable with CAST, since the helioscope looses its sensitivities as the mass becomes larger than fews eV, as discussed in Chapter 2 (Sec. 2.3). In principle, as shown in Sec. 2.3, the proposed helioscope –AMELIE (An Axion Modulation hELIoscope Experiment)– could be sensitive to ALPs with masses from fews meV to several eV thanks to the use of a Time Projection Chamber [Gal15]. However, a dedicated investigation is necessary to assess the potential of such a detector to reach the $m_a \sim 10$ eV range in a range of energy lower than CAST.

The flux from LP-ALP conversions has been recently discussed by O'Hare *et al.* [OH20]. In their work they suggest the possibility of detecting ALPs

from LP conversions in the energy range 10^{-2} keV $\lesssim \omega \lesssim 10^{-1}$ keV through an upgraded version of IAXO. They forecast to have a sensitivity down to $m_a \simeq 10^{-2}$ eV.
Concerning the flux coming from resonant transverse photons-ALP conversions in the radiative zone of the Sun, corresponding to an axion mass $m_a \sim 130$ eV, the flux would be much larger than the Primakoff one above the CAST threshold. However, CAST cannot detect it due to the loss of coherence of ALP-photon conversions in the detector. In principle, axions with mass $m_a \sim 100$ eV could be detected with a dark matter detector like the Cryogenic Underground Observatory for Rare Events (CUORE), which exploits the inverse Bragg-Primakoff effect to detect solar axions [Li15]. CUORE is expected to cover a mass range $m_a \lesssim 100$ eV. Neverthless, as discussed in Sec. 1.5, for $m_a \geq 10$ eV there are some cosmological constraints to be taken into account in our discussion. Indeed, the ionization of primordial hydrogen ($x_{\rm ion}$), discussed in Section 1.5, sets the bound $g_{a\gamma} \lesssim 5 \times 10^{-13}$ GeV^{-1} for $m_a \sim 10^2$ eV. However, in cosmological models with low-reheating temperature these bounds can be easily evaded (see, e.g. [Jae17], for a discussion). On the contrary, our ALP signal from the Sun is not affected by the cosmological model. Therefore, its possible detection would also point towards a nonstandard cosmological scenario. Thus, this constraint seems to prevent the possibility of detecting axions with mass $m_a \sim 100$ eV coming from conversions in the solar radiative zone.
We conclude our discussion setting a new bound on $g_{a\gamma}$ considering the solar ALP flux from magnetic conversions. From the flux for $m_a \sim 130$ eV we obtain an ALP luminosity

$$L_a = 0.2\ g_{10}^2\ L_\odot\ . \tag{4.78}$$

Starting from this luminosity we can set an upper limit on $g_{a\gamma}$ requiring that the ALPs luminosity from the Sun cannot exceeds the solar photon luminosity $L_\odot$. If this happened we would see the Sun lose too much energy thorugh ALPs emission, which would have shortened the lifetime of the Sun. On the basis of this loss energy argument one can set a bound on the coupling $g_{a\gamma}$ imposing the condition [Vin15]

$$L_a \lesssim 0.03\ L_\odot\ ; \tag{4.79}$$

which is obtained from helioseismology.

Matching Eq. (4.79) with our data we find

$$g_{a\gamma} \lesssim 3.8 \times 10^{-11}\ \text{GeV}^{-1}\ \text{for}\ 100\ \text{eV} \lesssim m_a \lesssim 140\ \text{eV}\ ; \tag{4.80}$$

where we have considered the largest range of masses where the condition Eq. (4.79) occurs in the radiative region as we see from Fig. 4.15. The result Eq. (4.80) is obtained assuming the highest value for the amplitude of the B-field, i.e. $B = 3 \times 10^7$ G, and it is the best bound we can set on the coupling from energy loss arguments in the Sun. It is comparable or even better than the bound from Helium burning stars in GCs ($g_{a\gamma} < 6.6 \times 10^{-11}\ \text{GeV}^{-1}$) [Aya14]. If we take for the B-field the smallest amplitude in the radiative region, i.e. we assume $B = 1 \times 10^7$ G, we obtain the following bound in the same range of masses

$$g_{a\gamma} \lesssim 1.15 \times 10^{-10}\ \text{GeV}^{-1}\ \text{for}\ 100\ \text{eV} \lesssim m_a \lesssim 140\ \text{eV}\ . \tag{4.81}$$

If we consider smaller values of m_a, corresponding to resonant conversions at positions in the radiative zone $r \gtrsim 0.236\ R_\odot$, we obtain smaller ALP luminosities, then less stringent constraints. For instance, for $m_a \sim 30$ eV we obtain

$$g_{a\gamma} \lesssim 2.32 \times 10^{-10}\ \text{GeV}^{-1}\ \text{for}\ m_a = 30\ \text{eV}\ . \tag{4.82}$$

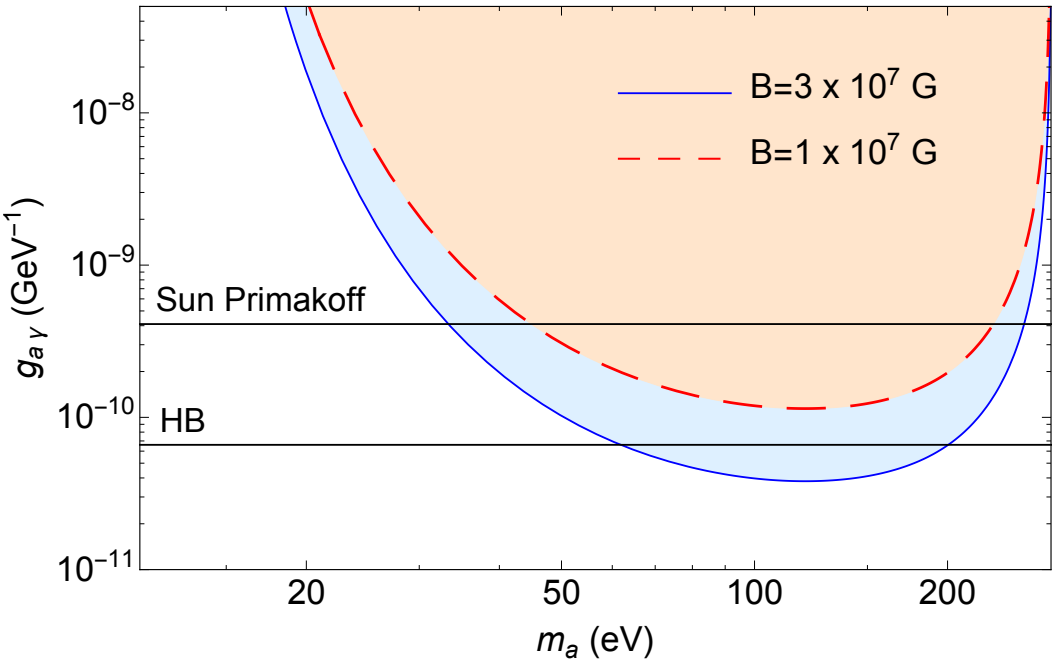

Figure 4.15: The blue region is the excluded one in the parameter space $(m_a, g_{a\gamma})$ by resonant processes in the Sun assuming a field with amplitude $B = 3 \times 10^7$ G. The orange region is the excluded one by the same process, assuming a field with amplitude $B = 1 \times 10^7$ G. The lower horizontal black line represents the bound set by the Helium Burning stars (HB) in the ALPs parameter space. The upper horizontal black line represents the bound set by energy-loss arguments from the Primakoff process in the Sun.

Conclusions

In this thesis Thesis we have characterized the ALP production in the large-scale solar magnetic fields and characterized the perspectives for their detection in helioscope experiments and dark matter detectors. In particular, we have considered both the resonant and non-resonant conversion of transverse photons, which had not been taken into account so far. At this regard, we considered realistic models for the solar B-field in the radiative zone, in the tachcoline and in the convective zone of the Sun. Thus, we first studied the problem from a theoretical point of view using a kinetic approach based on the evolution of the density matrix for the photon-ALP ensemble. With this approach, we estimated the production rate of ALPs in the Sun and we used it to estimate the ALP flux expected at Earth. The expression of the axion production rate obtained in this way is completely general and has been specialized to study both the resonant and non-resonant ALPs production. We found that the flux from longitudinal plasmon-ALP conversions is dominant at very low energies and it may be detected with an upgraded version of IAXO, as suggested by O'Hare *et al.* in their recent paper [OH20]. The non-resonant flux from transverse photon-ALPs conversion results to be always smaller than the Primakoff contribution. The resonant flux from transverse photon-ALP conversions for ALPs with mass $m_a \sim 10$ eV, associated to resonant conversions in the tachochline, is found to be dominant below the CAST threshold. A dedicate investigation is necessary to assess the experimental possibility to dectect such a low-energy flux. Conversely, the ALP flux arising from transverse photon-ALP conversions for ALPs with mass $m_a \sim 100$ eV in the radiative zone, is dominant above the CAST threshold and it is larger that the Primakoff one. In principle, this flux might be detected using the dark matter detector CUORE, however in a region where other astrophysical and cosmological constraints from decaying ALPs seem

to exlude this possibility.
Finally, we set a bound on the coupling $g_{a\gamma}$ arising from energy-loss argument in the Sun

$$g_{a\gamma} \lesssim 3.81 \times 10^{-11}\ \text{GeV}^{-1} \text{ for } 100\ \text{eV} \lesssim m_a \lesssim 140\ \text{eV}\ ; \tag{4.83}$$

which exceeds the one placed with the Helium-burning stars in Globular Clusters ($g_{a\gamma} < 6.6 \times 10^{-11}\ \text{GeV}^{-1}$) [Aya14].
Our work completes the recent one of O'Hare *et al.* [OH20] about the production of ALPs in the solar magnetic fields via longitudinal plasmons, since it includes also the photon transverse mode. Despite the challenges in measuring this flux, it is intriguing to realize that the Sun can be the source of an additional ALP flux on top of the well-studied one from Primakoff conversions. Of course, in the case a positive detection of this flux, one would shed new light not only on ALPs, but also on the magnetism in the Sun.

Bibliography

[Abe20] C. Abel *et al.* [nEDM], "Measurement of the permanent electric dipole moment of the neutron," Phys. Rev. Lett. **124**, no.8, 081803 (2020) doi:10.1103/PhysRevLett.124.081803 [arXiv:2001.11966 [hep-ex]].

[Abra13] A. Abramowski *et al.* [H.E.S.S.], "Constraints on axionlike particles with H.E.S.S. from the irregularity of the PKS 2155-304 energy spectrum," Phys. Rev. D **88** (2013) no.10, 102003 doi:10.1103/PhysRevD.88.102003 [arXiv:1311.3148 [astro-ph.HE]].

[Aje16] M. Ajello *et al.* [Fermi-LAT], "Search for Spectral Irregularities due to PhotonAxionlike-Particle Oscillations with the Fermi Large Area Telescope," Phys. Rev. Lett. **116** (2016) no.16, 161101 doi:10.1103/PhysRevLett.116.161101 [arXiv:1603.06978 [astro-ph.HE]].

[Ana17] V. Anastassopoulos *et al.* [CAST], "New CAST Limit on the Axion-Photon Interaction," Nature Phys. **13** (2017), 584-590 [arXiv:1705.02290 [hep-ex]].

[And07] S. Andriamonje *et al.* [CAST], "An Improved limit on the axion-photon coupling from the CAST experiment," JCAP **04** (2007), 010 doi:10.1088/1475-7516/2007/04/010 [arXiv:hep-ex/0702006 [hep-ex]].

[Ans88] A. A. Anselm (1988), *Phys. Rev. D,* 37, 2001.

[Ant00] H. M. Antia, S. M. Chitre and M. J. Thompson, "The sun's acoustic asphericity and magnetic fields in the solar convection

zone," Astron. Astrophys. **360** (2000), 335-344 [arXiv:astro-ph/0005587 [astro-ph]].

[Ari08] E. Arik *et al.* [CAST], "Probing eV-scale axions with CAST," JCAP **02** (2009), 008 [arXiv:0810.4482 [hep-ex]].

[Ari11] **CAST** Collaboration, E. Arik *et al.*, "Search for sub-ev mass solar axions by the CERN axion solar telescope with ^{3}He buffer gas,", *Phys. Rev. Lett.* **107** (Dec,2011) 261302.

[Ari13] P. Arias, D. Cadamuro, M. Goodsell, J. Jaeckel, J. Redondo and A. Ringwald, "WISPy Cold Dark Matter," JCAP **06** (2012), 013 doi:10.1088/1475-7516/2012/06/013 [arXiv:1201.5902 [hep-ph]].

[Arm19] E. Armengaud *et al.* [IAXO], "Physics potential of the International Axion Observatory (IAXO)," JCAP **06** (2019), 047 [arXiv:1904.09155 [hep-ph]].

[Arv10] A. Arvanitaki, S. Dimopoulos, S. Dubovsky, N. Kaloper and J. March-Russel, Phys. Rev. D **81**, 123530 (2010).

[Asz03] S. Asztalos *et al.* [ADMX], "An Improved RF cavity search for halo axions," Phys. Rev. D **69** (2004), 011101 doi:10.1103/PhysRevD.69.011101 [arXiv:astro-ph/0310042 [astro-ph]].

[Aya14] A. Ayala, I. Domínguez, M. Giannotti, A. Mirizzi and O. Straniero, "Revisiting the bound on axion-photon coupling from Globular Clusters," Phys. Rev. Lett. **113** (2014) no.19, 191302 doi:10.1103/PhysRevLett.113.191302 [arXiv:1406.6053 [astro-ph.SR]].

[Aud03] G. Audi, A.H. Wapstra, C. Thibault, "The AME2003 atomic mass evaluation - (II). Tables, graphs and references," 2003. in2p3-00014186

[Au14] M. Arik, S. Aune, K. Barth, A. Belov, S. Borghi, *et al.*, "CAST solar axions by the cern axion solar telescope with ^{3}He buffer gas: Closing the hot dark matter gap," *Phys. Rev. Lett* **112** (2014) 091302, arXiv:1307.1985 [hep-ex].

[Bac04] J. N. Bahcall, A. M. Serenelli and S. Basu, "New solar opacities, abundances, helioseismology, and neutrino fluxes," Astrophys. J. Lett. **621** (2005), L85-L88 [arXiv:astro-ph/0412440 [astro-ph]].

[Bac92] J. N. Bahcall and M. H. Pinsonneault, "Standard solar models, with and without helium diffusion and the solar neutrino problem," Rev. Mod. Phys. **64** (1992), 885-926

[Bae09] H. Baer *et al.*, J. Cosmol. Astrophys. Phys. **0902**, 002 (2009).

[Bal14] R. Ballou *et al.*, "Latest Results of the OSQAR Photon Regeneration Experiment for Axion-Like Particle Search," [arXiv:1410.2566 [hep-ex]].

[Bar04] K. Barth, D. Delikaris, G. Passardi, M. Pezzetti, O. Pirotte, L. Stewart, B. Vullierme, L. Walckiers and K. Zioutas, "Commissioning and First Operation of the Cryogenics for the CERN Axion Solar Telescope (CAST)," AIP Conf. Proc. **710** (2004), 168-175

[Bat18] R. Battesti, *et al.* , "High magnetic fields for fundamental physics," Phys. Rept. **765-766** (2018), 1-39 [arXiv:1803.07547 [physics.ins-det]].

[Baul17] M. Bauer, M. Neubert and A. Thamm, "LHC as an Axion Factory: Probing an Axion Explanation for $(g-2)\mu$ with Exotic Higgs Decays," Phys. Rev. Lett.**119** (2017) no.3, 031802 doi:10.1103/PhysRevLett.119.031802 [arXiv:1704.08207 [hep-ph]].

[Cad11] D. Cadamuro and J. Redondo, "Cosmological bounds on pseudo Nambu-Goldstone bosons," JCAP **02** (2012), 032 [arXiv:1110.2895 [hep-ph]].

[Cic12] M. Cicoli, M. Goodsell and A. Ringwald, "The type IIB string axiverse and its low-energy phenomenology," JHEP **10** (2012), 146 [arXiv:1206.0819 [hep-th]].

[Cor07] C. Corianò and N. Irges, Phys. Lett. B **651**, 298 (2007).

[Cou03] S. Couvidat, S. Turck-Chieze and A. G. Kosovichev, "Solar seismic models and the neutrino predictions," Astrophys. J. **599** (2003), 1434-1448 [arXiv:astro-ph/0203107 [astro-ph]].

[Das04] S. Das, P. Jain, J. P. Ralston and R. Saha, "The dynamical mixing of light and pseudoscalar fields," Pramana **70**, 439 (2008) [arXiv:hep-ph/0410006 [hep-ph]].

[Del15] F. Della Valle, A. Ejlli, U. Gastaldi, G. Messineo, E. Milotti, R. Pengo, G. Ruoso and G. Zavattini, "The PVLAS experiment: measuring vacuum magnetic birefringence and dichroism with a birefringent FabryPerot cavity," Eur. Phys. J. C **76** (2016) no.1, 24 doi:10.1140/epjc/s10052-015-3869-8 [arXiv:1510.08052 [physics.optics]].

[Dic78] D. A. Dicus, E. W. Kolb, V. L. Teplitz and R. V. Wagoner, "Astrophysical Bounds on the Masses of Axions and Higgs Particles," Phys. Rev. D **18** (1978), 1829

[Dil00] L. Di Lella, A. Pilaftsis, G. Raffelt and K. Zioutas, "Search for solar Kaluza-Klein axions in theories of low scale quantum gravity," Phys. Rev. D **62** (2000), 125011 doi:10.1103/PhysRevD.62.125011 [arXiv:hep-ph/0006327 [hep-ph]].

[Dil20] L. Di Luzio, M. Giannotti, E. Nardi and L. Visinelli, "The landscape of QCD axion models," Phys. Rept. **870** (2020), 1-117 [arXiv:2003.01100 [hep-ph]].

[Din81] M. Dine, W. Fischler and M. Srednicki, "A Simple Solution to the Strong CP Problem with a Harmless Axion," Phys. Lett. **104B** (1981) 199.

[Dob14] A. Dobrynina, A. Kartavtsev and G. Raffelt, "Photon-photon dispersion of TeV gamma rays and its role for photon-ALP conversion," Phys. Rev. D **91** (2015), 083003 [arXiv:1412.4777 [astro-ph.HE]].

[Dol17] M. J. Dolan, T. Ferber, C. Hearty, F. Kahlhoefer and K. Schmidt-Hoberg, "Revised constraints and Belle II sensitivity for visible and invisible axion-like particles," JHEP **12**

(2017), 094 doi:10.1007/JHEP12(2017)094 [arXiv:1709.00009 [hep-ph]].

[Dzi95] H. Dzitko, S. Turck-Chièze, P. Delbourgo-Salvador, C. Lagrange, 1995, *Astrophysics Journal* 447, 428

[Ehre20] K. Ehret, M. Frede, S. Ghazaryan, M. Hildebrandt, E. A. Knabbe, D. Kracht, A. Lindner, J. List, T. Meier, N. Meyer, D. Notz, J. Redondo, A. Ringwald, G. Wiedemann and B. Willke, "New ALPS Results on Hidden-Sector Lightweights," Phys. Lett. B **689** (2010), 149-155 doi:10.1016/j.physletb.2010.04.066 [arXiv:1004.1313 [hep-ex]].

[Ell16] U. Ellwanger and S. Moretti, "Possible Explanation of the Electron Positron Anomaly at 17 MeV in 8Be Transitions Through a Light Pseudoscalar, JHEP **1611** (2016) 039 doi:10.1007/JHEP11(2016)039 [arXiv:1609.01669 [hep-ph]].

[Fla15] T. Flacke, C. Frugiuele, E. Fuchs, R. S. Gupta and G. Perez, "Phenomenology of relaxion-Higgs mixing," JHEP **06** (2017), 050 doi:10.1007/JHEP06(2017)050 [arXiv:1610.02025 [hep-ph]].

[Gal15] J. Galán *et al.*, "Exploring 0.110 eV axions with a new helioscope concept," JCAP **12** (2015), 012 [arXiv:1508.03006 [astro-ph.IM]].

[Gou90] D. O. Gough, M. J. Tgompson, "The effect of rotation and a buried magnetic field on stellar oscillations," MNRAS vol. 242 (1990)

[Gri06] D. Grin, G. Covone, J. P. Kneib, M. Kamionkowski, A. Blain and E. Jullo, "A Telescope Search for Decaying Relic Axions," Phys. Rev. D **75** (2007), 105018 doi:10.1103/PhysRevD.75.105018 [arXiv:astro-ph/0611502 [astro-ph]].

[Hal08] G.E. Hale, "On the Probable Existence of a magnetic field in Sun-Spots", *Astrophysical Journal*, Vol. **28** (1908)

[Hat14] D. H. Hathaway, `https://solarscience.msfc.nasa.gov/dynamo.shtml`, August 2014

[Ira11] I. Irastorza *et al.*, "Towards a new generation axion helioscope," JCAP **06** (2011), 013 doi:10.1088/1475-7516/2011/06/013 [arXiv:1103.5334 [hep-ex]].

[Ira18] I. G. Irastorza and J. Redondo, "New experimental approaches in the search for axion-like particles," Prog. Part. Nucl. Phys. **102**, 89-159 (2018) [arXiv:1801.08127 [hep-ph]].

[Kak93] M. Kaku, "Quantum Field Theory: A Modern Introduction", Oxford University Press (1993).

[Ino08] Y. Inoue, *et al*, *Phys. Lett.* **B** 536, 18 (2002).[arXiv:astro-ph/0204388]

[Kim08] J. E. Kim and G. Carosi, "Axions and the Strong CP Problem," Rev. Mod. Phys. **82**, 557-602 (2010) [arXiv:0807.3125 [hep-ph]].

[Jac75] J. D. Jackson, "Classical electrodynamics", New York: Wiley (1975)

[Kim86] J. E. Kim, "Light Pseudoscalars, Particle Physics and Cosmology," Phys. Rep. **150** (1987) 1.

[Jae17] J. Jaeckel, P. C. Malta and J. Redondo, "Decay photons from the axionlike particles burst of type II supernovae," Phys. Rev. D **98**, no.5, 055032 (2018) doi:10.1103/PhysRevD.98.055032 [arXiv:1702.02964 [hep-ph]].

[Kri16] M. Krief, A. Feigel and D. Gazit, "Solar opacity calculations using the super-transition-array method," Astrophys. J. **821** (2016) no.1, 45 [arXiv:1601.01930 [astro-ph.SR]].

[Lar19] J. Larmor, "How could a rotating body such as the Sun become a magnet?", *Rep. Brit. Assoc. Adv. Sci.*, **1919**, 159-160

[Laz92] D.M. Lazarus *et al.*, Phys. Rev. Lett. **69** (October, 1992) 2333

[Li15] D. Li, R. J. Creswick, F. T. Avignone and Y. Wang, "Theoretical Estimate of the Sensitivity of the CUORE Detector to Solar Axions," JCAP **10** (2015), 065 [arXiv:1507.00603 [astro-ph.CO]].

[Mar16] W. Marciano, A. Masiero, P. Paradisi and M. Passera, "Contributions of axionlike particles to lepton dipole moments," Phys. Rev. D **94** (2016) no.11, 115033 [arXiv:1607.01022 [hep-ph]].

[Mas06] E. Masso, "Axions and their relatives," Lect. Notes Phys. **741**, 83-94 (2008) [arXiv:hep-ph/0607215 [hep-ph]].

[Men19] J. T. Mendonça, J. D. Rodrigues and H. Terças, "Axion production in unstable magnetized plasmas," Phys. Rev. D **101**, no.5, 051701 (2020) [arXiv:1901.05910 [physics.plasm-ph]].

[Mil15] M. Millea, L. Knox and B. Fields, "New Bounds for Axions and Axion-Like Particles with keV-GeV Masses," Phys. Rev. D **92** (2015) no.2, 023010 [arXiv:1501.04097 [astro-ph.CO]].

[Mof78] H. K. Moffatt, "*Magnetic field generation in electrically conducting fluids,*", Cambridge University Press, 1978

[Mor98] S. Moryiama *et al.*, *Phys. Lett.* **69**, 2333 (1992). [arXiv:hep-ex/9805026]

[OH20] C. A. J. O'Hare, A. Caputo, A. J. Millar and E. Vitagliano, "Axion helioscopes as solar magnetometers," [arXiv:2006.10415 [astro-ph.CO]].

[Oue18] J. L. Ouellet *et al.*, "First Results from ABRACADABRA-10 cm: A Search for Sub-μeV Axion Dark Matter," Phys. Rev. Lett. **122** (2019) no.12, 121802 doi:10.1103/PhysRevLett.122.121802 [arXiv:1810.12257 [hep-ex]].

[Par55] E. N. Parker, "Hydromagnetic Dynamo Models," Astrophys. J. **122** (1955), 293

[Par79] E. N. Parker, "Cosmic magnetic fields: their origin and activity," Oxford: Clarendon Press, 1979.

[Pat16] C. Patrignani *et al.* [Particle Data Group], "Review of Particle Physics," Chin. Phys. C **40** (2016) no.10, 100001 doi:10.1088/1674-1137/40/10/100001

[Pay14] A. Payez, C. Evoli, T. Fischer, M. Giannotti, A. Mirizzi and A. Ringwald, "Revisiting the SN1987A gamma-ray limit on ultralight axion-like particles," JCAP **02** (2015), 006 doi:10.1088/1475-7516/2015/02/006 [arXiv:1410.3747 [astro-ph.HE]].

[Pec77a] R. D. Peccei and H. R. Quinn, "CP Conservation in the Presence of Instantons", Phys. Rev. Lett. **38** (1977) 1440.

[Pec77b] R. D. Peccei and H. R. Quinn, "Constraints Imposed by CP Conservation in the Presence of Instantons," Phys. Rev. D **16** (1977) 1791.

[Pec06] R. D. Peccei, "The Strong CP problem and axions", Lect. Notes Phys. **741** (2008) 3.

[Raf86] G. G. Raffelt, "ASTROPHYSICAL AXION BOUNDS DIMINISHED BY SCREENING EFFECTS," Phys. Rev. D **33** (1986), 897

[Raf88] G. Raffelt, L. Stodolsky, (1988) *Phys. Rev. D,* 37, 1237.

[Raf96] G. Raffelt, "Stars as Laboratories for Fundamental Physics," University of Chicago Press (1996).

[Red13] J. Redondo and G. Raffelt, "Solar constraints on hidden photons re-visited," JCAP **08** (2013), 034 [arXiv:1305.2920 [hep-ph]].

[Rey19] C. S. Reynolds, M. D. Marsh, H. R. Russell, A. C. Fabian, R. Smith, F. Tombesi and S. Veilleux, "Astrophysical limits on very light axion-like particles from Chandra grating spectroscopy of NGC 1275," doi:10.3847/1538-4357/ab6a0c [arXiv:1907.05475 [hep-ph]].

[Rin08] A. Ringwald, "From Axions to Other WISPs," [arXiv:0810.3106 [hep-th]].

[Ser09] A. Serenelli, S. Basu, J. W. Ferguson and M. Asplund, "New Solar Composition: The Problem With Solar Models Revisited," Astrophys. J. Lett. **705** (2009), L123-L127 [arXiv:0909.2668 [astro-ph.SR]].

[Shi80] M. A. Shifman, A. I. Vainshtein and V. I. Zakharov, "Can Confinement Ensure Natural CP Invariance of Strong Interactions?," Nucl. Phys. B **166** (1980) 493.

[Sch98] H. Schlattl, A. Weiss and G. Raffelt, "Helioseismological constraint on solar axion emission," Astropart. Phys. **10** (1999), 353-359 [arXiv:hep-ph/9807476 [hep-ph]].

[Sig92] G. Sigl and G. Raffelt, "General kinetic description of relativistic mixed neutrinos," Nucl. Phys. B **406** (1993), 423-451

[Sik83] P. Sikivie, "Experimental tests of the invisible axion," *Phys. Rev. Lett* **51** (1983) 1415.

[Sto86] L. Stodolsky, "On the Treatment of Neutrino Oscillations in a Thermal Environment," Phys. Rev. D **36** (1987), 2273

[Svr06] P. Svrcek and E. Witten, "Axions In String Theory," JHEP **06** (2006), 051 doi:10.1088/1126-6708/2006/06/051 [arXiv:hep-th/0605206 [hep-th]].

[Ter18] H. Terças, J. D. Rodrigues and J. T. Mendonça, "Axion-plasmon polaritons in strongly magnetized plasmas," Phys. Rev. Lett. **120**, no.18, 181803 (2018) [arXiv:1801.06254 [hep-ph]].

[Tur16] S. Turck-Chièze, "The Standard Solar Model and beyond," J. Phys. Conf. Ser. **665** (2016) no.1, 012078

[Tur01] S. Turck-Chieze, S. Couvidat, R. A. Garcia, A. G. Kosovichev, A. H. Gabriel, G. Berthomieu, J. Provost, A. S. Brun, J. Christensen-Dalsgaard, D. O. Gough, T. Roca-Cortes, I. W. Roxburgh and R. K. Ulrich, "Solar neutrino emission deduced from a seismic model," Astrophys. J. Lett. **555** (2001), L69-L73

[Tur96] N. Turok, Phys. Rev. Lett. **76**, 1015 (1996).

[Van88] K. van Bibber, P. M. McIntyre, D. E. Morris and G. G. Raffelt, "A Practical Laboratory Detector for Solar Axions," Phys. Rev. D **39** (1989), 2089

[Vin15] N. Vinyoles, A. Serenelli, F. L. Villante, S. Basu, J. Redondo and J. Isern, "New axion and hidden photon constraints from a solar data global fit," JCAP **10** (2015), 015 [arXiv:1501.01639 [astro-ph.SR]].

[Wei78] S. Weinberg, "A New Light Boson?," Phys. Rev. Lett. **40** (1978) 223.

[Wil78] F. Wilczek, "Problem of Strong p and t Invariance in the Presence of Instantons," Phys. Rev. Lett. **40** (1978) 279.

[Zio99] K. Zioutas *et al.*, "A decommissioned LHC model magnet as an axion telescope", *Nucl. Instrum. Meth.* **A425** (1999) 480489, arXiv:astro-ph/9801176.

[Zio04] K. Zioutas *et al.* [CAST], "First results from the CERN Axion Solar Telescope (CAST)," Phys. Rev. Lett. **94** (2005), 121301 [arXiv:hep-ex/0411033 [hep-ex]].

[Zio05] Y. Inoue, *et al.*,*Phys. Lett. B* **668**, 93 (2008) [arXiv:0806.2230].